AD-A131 366 EFFECTS OF RIGID INCLUSIONS ON WAVE PROPAGATION(U) 1/2
TEXAS UNIV AT AUSTIN GEOTECHNICAL ENGINEERING CENTER
C SUDDHIPRAKARN ET AL. MAR 83 GR83-3 AFOSR-TR-83-0656
UNCLASSIFIED AFOSR-80-0031 F/G 8/13 NL

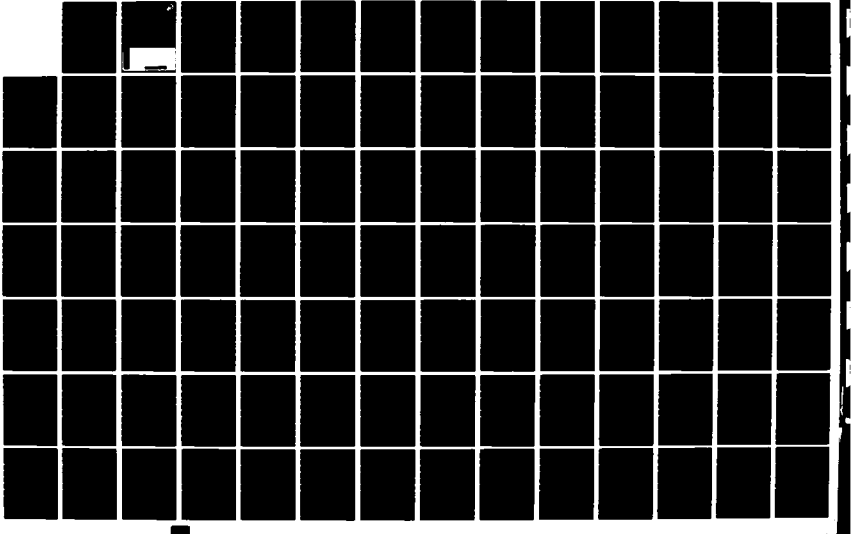

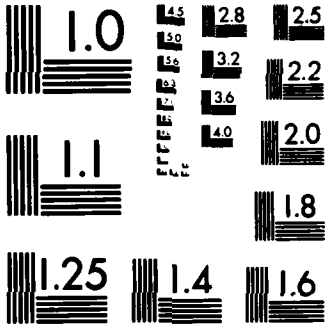

EFFECTS OF RIGID INCLUSIONS ON WAVE PROPAGATION

by
Chairat Suddhiprakarn

Supervised by
Jose M. Roesset
Kenneth H. Stokoe II

a report on research
sponsored by
United States Air Force
Office of Scientific Research
Bolling Air Force Base

Conditions of Reproduction

UNCLASSIFIED

SECURITY CLASSIFICATION OF THIS PAGE *(When Data Entered)*

REPORT DOCUMENTATION PAGE		READ INSTRUCTIONS BEFORE COMPLETING FORM
1. REPORT NUMBER AFOSR-TR- 83-0656	2. GOVT ACCESSION NO. AD A131366	3. RECIPIENT'S CATALOG NUMBER
4. TITLE *(and Subtitle)* EFFECTS OF RIGID INCLUSIONS ON WAVE PROPAGATION		5. TYPE OF REPORT & PERIOD COVERED INTERIM 6. PERFORMING ORG. REPORT NUMBER
7. AUTHOR(s) CHAIRAT SUDDHIPRAKARN JOSE M. ROESSET KENNETH H. STOKOE, II		8. CONTRACT OR GRANT NUMBER(s) AFOSR-80-0031
9. PERFORMING ORGANIZATION NAME AND ADDRESS UNIVERSITY OF TEXAS AT AUSTIN DEPARTMENT OF CIVIL ENGINEERING AUSTIN, TX 78712		10. PROGRAM ELEMENT, PROJECT, TASK AREA & WORK UNIT NUMBERS 61102F 2307/C1
11. CONTROLLING OFFICE NAME AND ADDRESS AIR FORCE OFFICE OF SCIENTIFIC RESEARCH/NA BOLLING AFB, DC 20332		12. REPORT DATE March 1983 13. NUMBER OF PAGES 109
14. MONITORING AGENCY NAME & ADDRESS*(if different from Controlling Office)*		15. SECURITY CLASS. (of this report) UNCLASSIFIED 15a. DECLASSIFICATION/DOWNGRADING SCHEDULE

16. DISTRIBUTION STATEMENT *(of this Report)*

Approved for Public Release; Distribution Unlimited.

17. DISTRIBUTION STATEMENT *(of the abstract entered in Block 20, if different from Report)*

18. SUPPLEMENTARY NOTES

19. KEY WORDS *(Continue on reverse side if necessary and identify by block number)*

WAVE PROPAGATION	INCLUSIONS
SHEAR WAVES	NON-HOMOGENEOUS MEDIA
SHEAR WAVE VELOCITY	SCATTERING OF WAVES
P-WAVES	FINITE ELEMENTS
P-WAVE VELOCITY	DYNAMIC ANALYSIS

20. ABSTRACT *(Continue on reverse side if necessary and identify by block number)*

The effect of rigid inclusions on the characteristics (amplitude and time of arrival) of shear and P-waves is investigated using a finite element model to discretize the region of interest and an explicit integration scheme. The effect of boundary conditions, type of excitation (point load versus distributed load) and wave length (or frequency of the excitation) are investigated and discussed.

DD FORM 1 JAN 73 1473 EDITION OF 1 NOV 65 IS OBSOLETE

UNCLASSIFIED

SECURITY CLASSIFICATION OF THIS PAGE *(When Data Entered)*

EFFECTS OF RIGID INCLUSIONS ON WAVE PROPAGATION

by

Chairat Suddhiprakarn

Supervised by

Jose M. Roesset

Kenneth H. Stokoe, II

a report on research
sponsored by
United States Air Force
Office of Scientific Research
Bolling Air Force Base

March, 1983

Geotechnical Engineering Report GR83-3
Geotechnical Engineering Center
Civil Engineering Department
The University of Texas at Austin
Austin, Texas

ACKNOWLEDGEMENTS

The work presented in this report is part of a research effort on wave propagation studies sponsored by the U.S. Air Force Office of Scientific Research (AFOSR), Bolling Air Force Base, Washington, D.C. under grant AFOSR 80-0031[illegible]. The author wishes to thank AFOSR and Major John J. Allen, the program manager, for their support.

The author is particularly indebted to Dr. Jose Roesset and Dr. Kenneth H. Stokoe, II for thier guidance and valuable suggestions, and finally to Ms. Sarah Clark for her excellent typing and aid in the completion of this report.

TABLE OF CONTENTS

LIST OF FIGURES

CHAPTER 1

INTRODUCTION

Stress wave propagation has long been a useful tool for studying the mechanical properties of various media, especially in the field of material science, geophysics, and engineering. Most applications in geotechnical engineering are oriented to the exploration of soil deposits and the determination of soil moduli by field and laboratory measurements of stress wave velocities. These soil moduli are used in dynamic soil structure interaction analyses ranging from small-strain problems, as associated with the vibrations of machine foundations, to larger strain problems, such as earthquake or blast loading. To simulate the situation in the field, knowledge of the dynamic properties of soils under different states of stress - isotropic, biaxial, and triaxial - is important. Unfortunately, most of the research results available have emphasized isotropic stress effects.

A research program was, therefore, undertaken to study the effects of the general state of stress on shear and compression wave velocities of soil at low levels of strain. The studies were conducted in a large scale triaxial testing device which is a cube constructed of reinforced steel, designed to hold a cubic soil sample measuring 7 ft (2.1 m) on each side. Rubber loading membranes are oriented along the three principal planes, between the soil and three mutually perpendicular walls of the cube. The membranes are hydraulically pressurized to attain an isotropic, biaxial, or triaxial state of stress. Compression or shear waves are generated along the principal axes through one of

three excitation ports located on the three walls of the cube which are not covered with membranes. Accelerometer packages are embedded in the soil along each principal axis of the cube to monitor the waves. Soil samples used to date have been dry sand. Details and results of the tests have been presented in Kopperman, et al (1982) and Knox, et al (1982).

While most of the effort during the first stage of the research project has been devoted to the design and construction of the triaxial cube, some work has also been performed implementing computer capabilities which could be used in the future for interpretation of the experimental data.

The first problem at hand was to determine the effect of th e much stiffer (almost rigid) accelerometer packages embedded in the sand on the characteristics of P-wave and S-wave propagating through the soil (scattering or filtering effect). Most of the effort in this work concentrated on shear waves because of the greater difficulty involved in these measurements. Two approaches were considered for the solution of this problem: a formulation based on the use of the boundary integral equation (or boundary element) method and a more classical discretization using finite elements.

The boundary integral equation method is particularly appropriate to study the filtering effect of one or more rigid inclusions on waves propagating through a full elastic space, since then only the boundaries of the inclusions must be discretized. For the particular case at hand, with three rigid inclusions along any principal axis (and considering only one principal axis), formulation of the

problem in the frequency domain requires the solution of a system of 54 equations with 54 unknowns for each frequency. The solution for a transient excitation can then be obtained using Fourier transforms.

For the actual case of the cube, by opposition to the full space, it would also be necessary to discretize its outer surface. A discretization appropriate for wavelengths of the order of 1 ft would lead to a system of 56,502 equations with 56,502 unknowns for each frequency. By taking advantage of symmetry and antisymmetry conditions, the number of degrees of freedom can be reduced to 23,574, but the two matrices associated with tractions and displacements are fully populated, which makes the solution prohibitively expensive.

If three-dimensional brick elements (with linear displacement expansion) are used, an appropriate discretization of the cube into finite elements for wavelengths of the order of 1 ft or larger requires a mesh size of 1.5 inches or 56 elements per side (1.5 inches is also the size of the rigid inclusions). This leads to a total of 175,616 elements or 185,193 joints, with three degrees of freedom per joint and a bandwidth of 9582. Solution of this problem would again be impractical by any method which requires assembling the total stiffness matrix or solving the coupled system of equations. It is possible, on the other hand, to solve it using an explicit integration scheme, such as the central difference formula, and marching out the solution in the time domain. While the time step of integration must be kept sufficiently small to guarantee stability and the solution is time consuming, the advantage of this approach is that it easily

allows incorporation of nonhomogeneous soil properties and evantually nonlinear soil behavior.

Because of these considerations, it was decided that the finite element formulation had definite advantages not only for the solution of the problem at hand but more importantly for future applications. By taking advantage of symmetry and antisymmetry, one fourth of the cube was discretized using 28 x 28 x 55 elements with dimensions of 1.5 x 1.5 x 1.5 inches. This makes the side of the cube equal to 6 ft 10.5 inches instead of the 7 ft assumed, but this small difference allows each one of the inclusions to be represented by a single rigid element. Even with these simplifactions, the memory capacity of the computer available at the University of Texas (CDC Dual Cyber 170/750) did not allow all degrees of freedom (141,288) to be stored in core. A computer program was implemented keeping in core at any time the degrees of freedom corresponding to two planes (2523 x 2 = 5046) and writing on disk those corresponding to one plane when the corresponding slice of finite elements had been processed, while reading in those of a new plane. Preliminary studies conducted to determine the smallest natural period and the required time step of integration indicated that some 90 to 100 steps were necessary to reproduce the arrival of the first shear wave to the central box. For this duration of response, the solution of the three-dimensional problem takes about three hours in the computer of the University of Texas, 50 percent of this time being associated with the transfer of data from primary to secondary memory and back.

Since only a small number of fully three-dimensional analyses were possible within the budget of the project, it was decided to implement also a two-dimensional (2-D), plane-strain solution which could be used for more extensive parametric studies. Two versions of this program were written: one taking again advantage of anti-symmetry and considering a mesh of 55 x 28 elements (3248 degrees of freedom), and the other with the complete square (55 x 55 elements or 5272 degrees of freedom). The smaller was used to verify the adequacy of the boundary conditions imposed on the larger. The two-dimensional finite element model is shown in Fig. 1.1.

Preliminary analyses were performed with the following conditions: all boundaries were fixed except for the small window area on the left face where a sinusoidal acceleration was specified with a frequency of 650 rad/sec corresponding to a wavelength of about 1 ft. The rigid inclusions had the same unit mass as the sand sample. The results of the studies, which were summarized in Stokoe, et al (1982), indicated that for the range of wavelengths of interest, while there is a small filtering effect, none of the basic characteristics of the wave (arrival time of the first shear wave and its shape) would be significantly affected by the presence of rigid inclusions of the size of the accelerometer boxes. Because both compression waves and shear waves are generated, the first shear wave arrival time is difficult to estimate accurately. It is easier to estimate the shear wave velocity from the time interval between arrivals of the waves at the various inclusions rather than from the time of first arrival at one location.

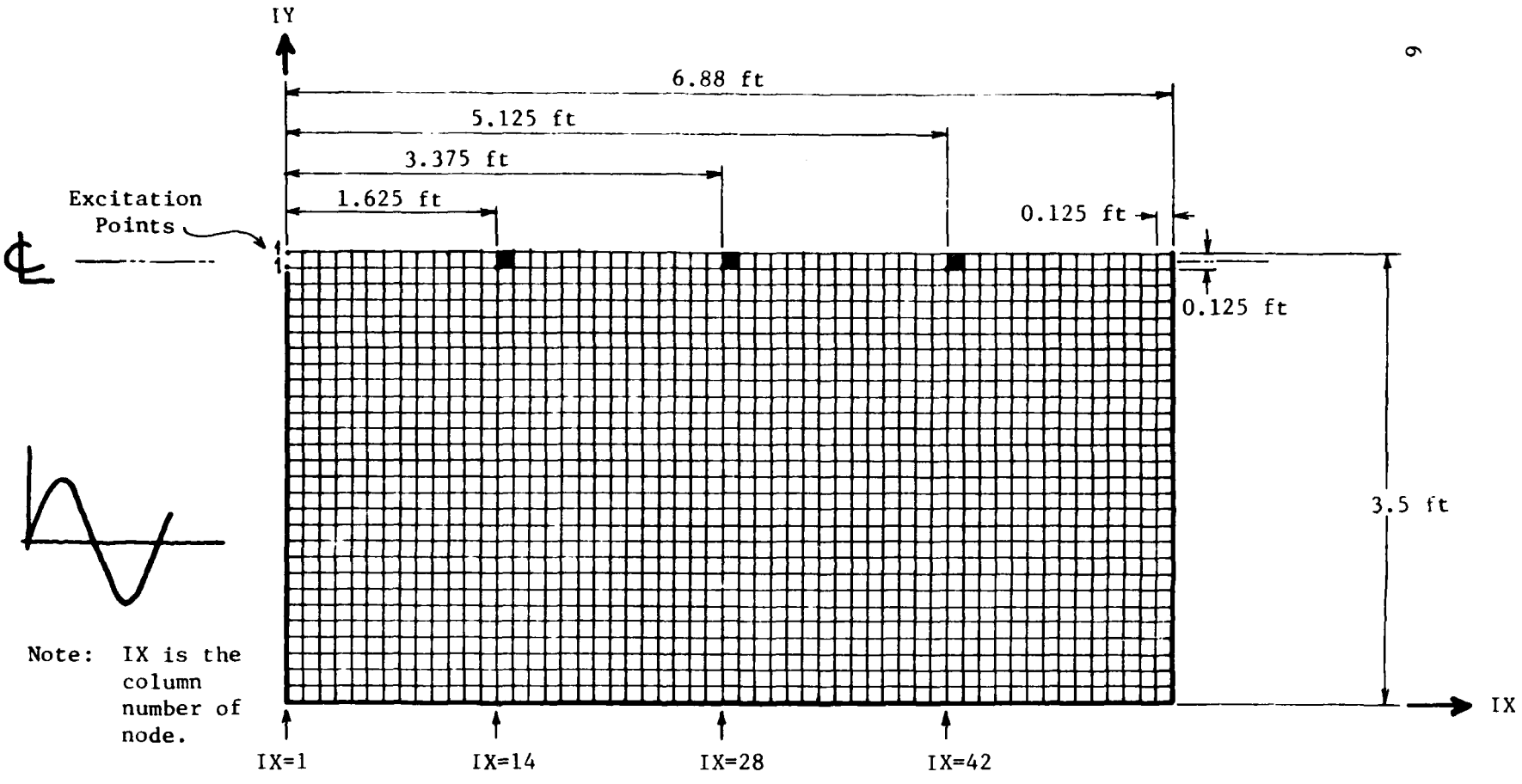

Fig. 1.1 - Two-Dimensional Finite Element Model

In all cases studied the results, in the form of accelerations versus time, showed some small motion in the direction associated with S-wave motion occurring substantially before the theoretical time of arrival of the S-wave (approximately at the P-wave arrival time). This is due primarily to the fact that the excitation is applied over a small area, simulating more closely a point source and a spherical wave front (cylindrical for the two-dimensional case) rather than a pure plane shear wave front. On the other hand the discrete finite element model and the numerical integration scheme will clearly introduce some errors, hopefully small, but difficult to quantify. The boundary conditions assumed on the faces of the cube may also have some effect on the type of waves that reach the accelerometer box.

It was decided therefore to investigate further these effects by considering different boundary conditions, different types of excitation and different wave lengths (or frequencies). In addition to the acceleration time histories considered in the initial studies, velocities and displacements were plotted in order to assess which one of these variables provided an easier means to identify initial wave arrival. The results of these additional studies, conducted with the two-dimensional, plane strain model, for reasons of economy, are presented in this report.

Chapter 2 presents the results relative to the effect of the boundary conditions applied on the faces of the cube. The effect of the type of excitation is studied in Chapter 3, and the effect of the frequency excitation, or wavelength, is reported in Chapter 4. Chapter 5 contains the conclusions of the study and recommendations for future work.

CHAPTER 2

EFFECT OF BOUNDARY CONDITIONS

2.1 INTRODUCTION

Two types of boundary conditions are considered in this chapter: (1) fixed boundaries, where all boundaries are assumed to be fixed except for the two central nodes (for 2-D case) on the left face of the cube, where a sinusoidal force (instead of an acceleration as in the previous report) is specified; and (2) free boundaries, where all boundaries are free to move and free of tractions (except, of course, for the point of excitation). Unfortunately, for this second case, the four boundaries can not all be free because the whole system could have a rigid body motion causing numerical problems. It was decided therefore to fix the boundary on the right side (far side in the path of wave propagation) because most of the waves of interest would arrive earlier than the reflected waves from this boundary.

The frequency of excitation used for these studies is 650 rad/sec, corresponding to a wavelength of approximately 1 ft. The rigid inclusions and soils have the same unit mass as before.

2.2 PRELIMINARY CONSIDERATIONS

All results in the last report were presented as time histories of the acceleration at three selected target points. These target points are at the lower left corner of the first, second, and third inclusion positions which are referred to in the text as location

IX = 14, IX = 28, and IX = 42, respectively (see Fig. 1.1). In this report, some results at the point of excitation will also be shown so that changes in the shape of the waves after travelling through the medium can be observed. The theoretical arrival times for plane shear and compressional waves to each target point are indicated in the figures by vertical lines marked with the letters 'S' and 'P', respectively.

In Fig. 2.1 the displacement, velocity and acceleration for a typical case are plotted on the same time scale. It can be seen, for this specific case, that beyond the time 0.04 sec, the results behave like classical harmonic motion, the acceleration, velocity and displacement being nearly sinusoidal curves with a constant phase difference between each. However, the earlier motion (before 0.04 sec in this case) is rather complex and irregular, starting at the theoretical time of arrival of the P-wave. This part of the motion is isolated for clarity for each one of the variables (displacement, velocity and acceleration) in Fig. 2.2. In the case of displacement, the time of arrival of the S-wave is only slightly ahead of the zero crossing point, when the positive motion starts. Points "a", corresponding to the zero crossing, or "b", corresponding to the time where the curve starts turning upwards are often used in experimental work to measure the arrival time of the S-wave. If the same approach were followed with the numerical results, the estimated shear wave velocity would be within five percent of the exact value.

When dealing with the velocity trace on the other hand, if point "d", corresponding to the zero crossing, were chosen the estimated shear wave velocity would be too high, with an error of 10 to 15 percent.

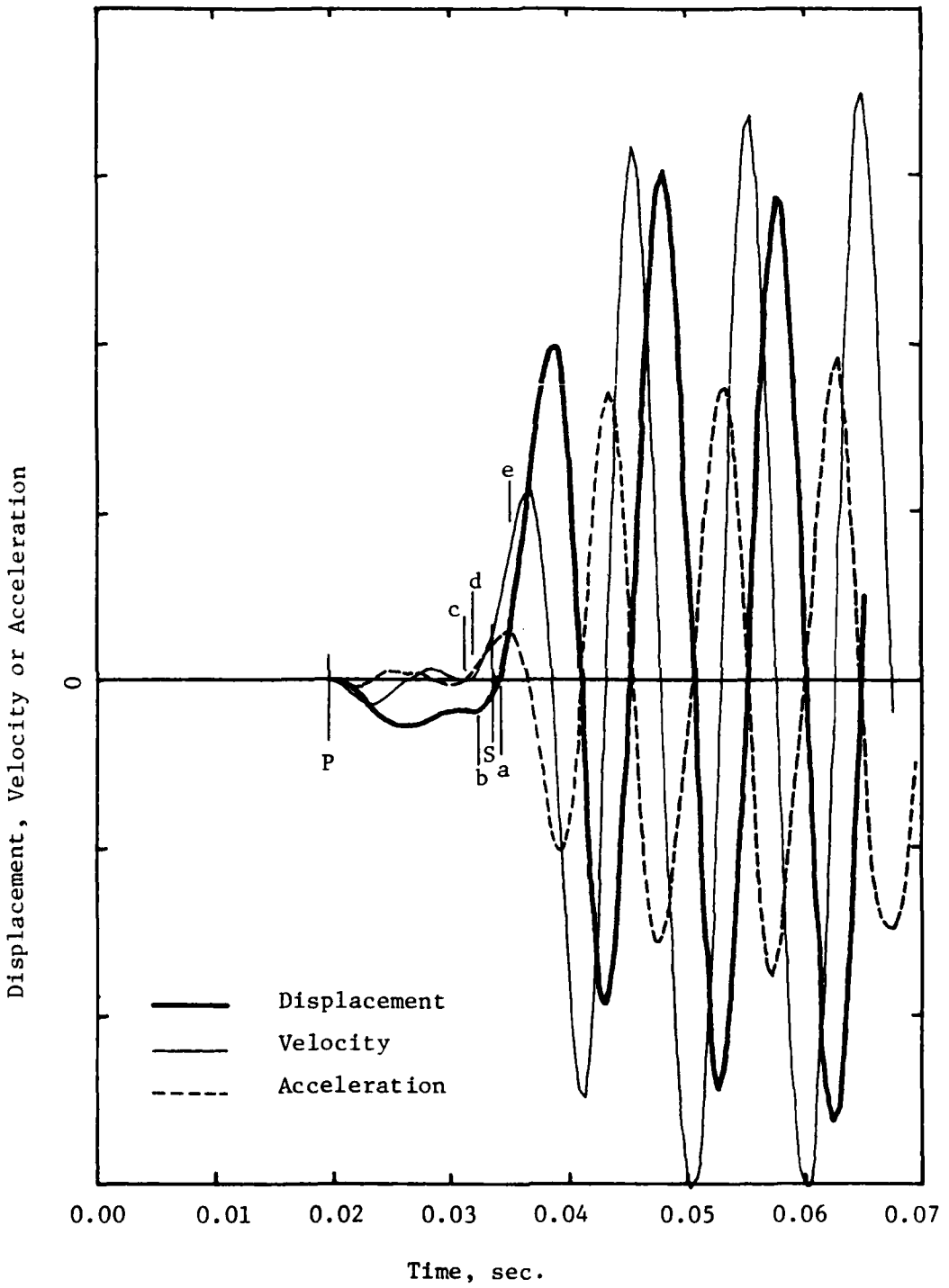

Fig. 2.1 - Displacement, Velocity, and Acceleration at IX=28. Free Boundaries. No Rigid Inclusions.

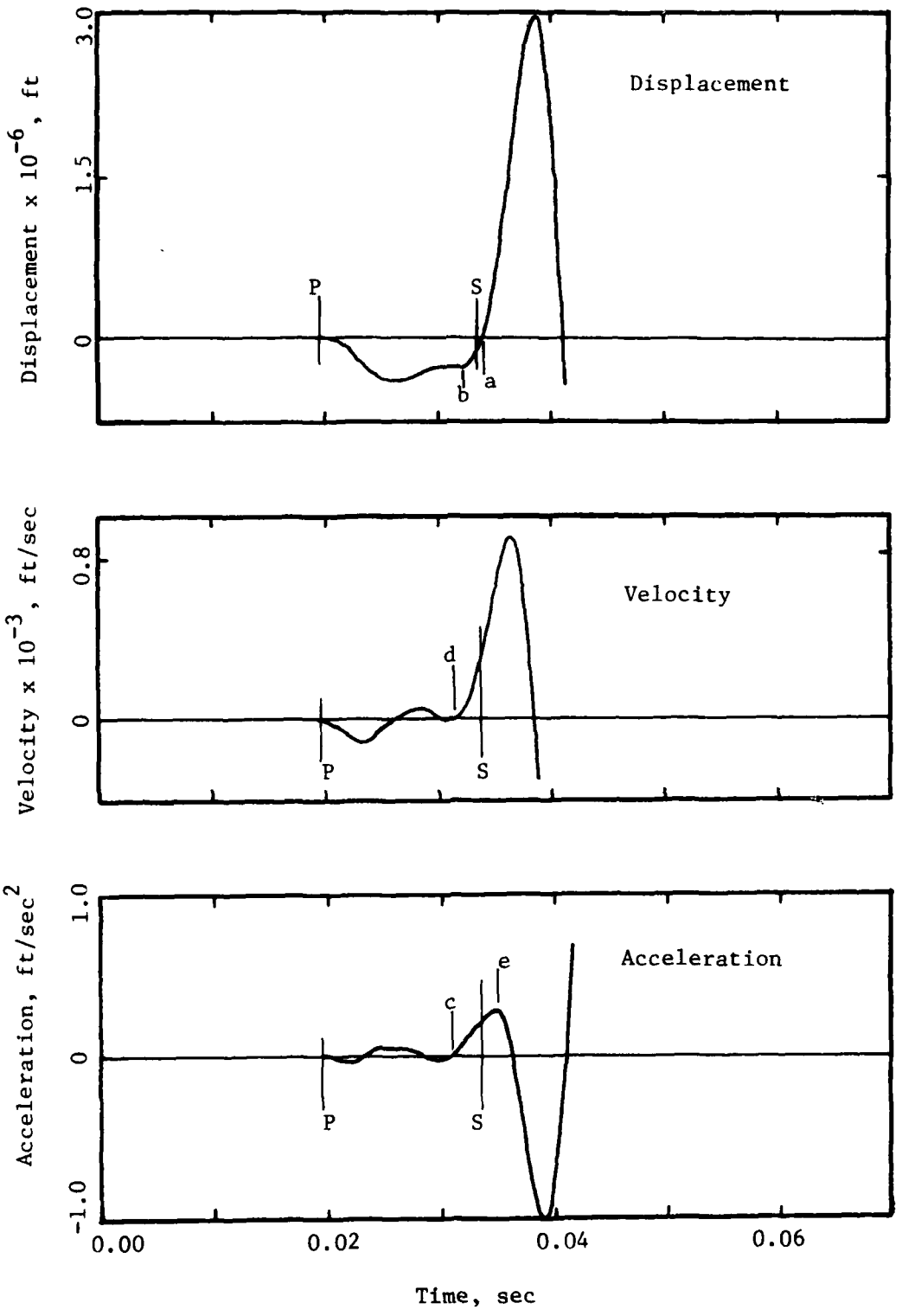

Fig. 2.2 - Details of the First Arrival of Shear Wave from Displacement, Velocity, and Acceleration Curves

The theoretical arrival time tends to be about one third up the ascending branch, coinciding approximately with the inflection point in this branch. This seems also to be consistent with experimental procedures used to pick the initial arrival time.

In the acceleration trace the time of arrival of the S-wave is higher up on the ascending branch and its best estimate would seem to be the time at which the first significant positive peak occurs (point "e"). Use of this point would yield a value of the wave velocity slightly too small, with an error of about 5 percent.

For the purposes of comparison, Fig. 2.3 shows the displacement, velocity and acceleration histories at the point of application of the sinusoidal force. It can be seen that the displacement starts with a slight delay due to the numerical solution (no correction was applied in the first time increment; thus, since the acceleration and velocity are zero at $t = 0$, the displacement is still zero at $t = \Delta t$). The time at which the displacement curve starts coincides approximately with the first peak in the acceleration curve and the inflection point in the ascending branch of the velocity trace.

These results tend to indicate that while there are some errors associated with the finite element discretization and the numerical integration scheme, the shear wave velocity can be estimated from the numerical results with reasonable accuracy (within 5 percent) if the appropriate points are selected in the time histories. These points will be different for the acceleration, velocity and displacement traces, and it would appear that the displacement curve

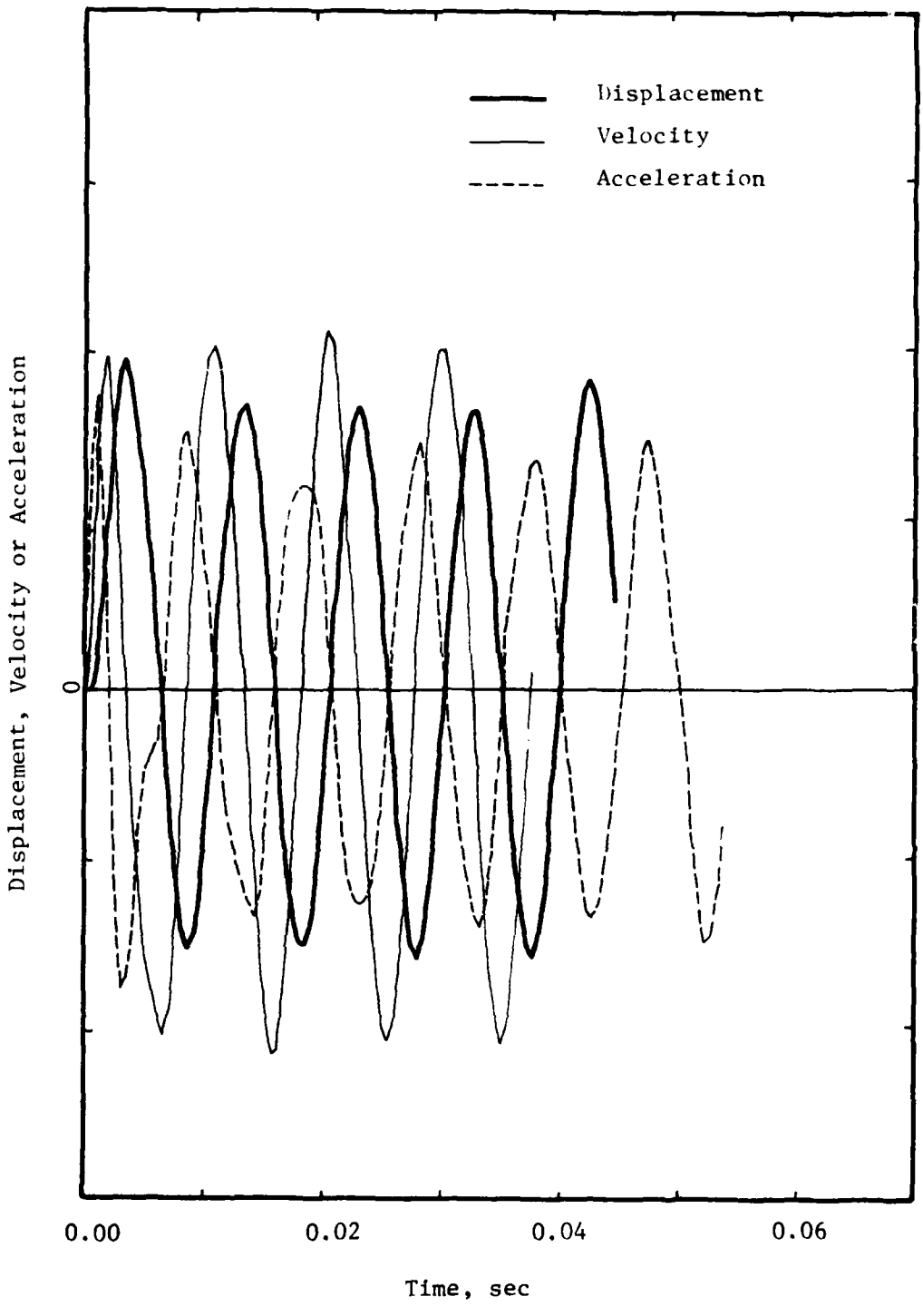

Fig. 2.3 - Displacement, Velocity, and Acceleration at the Point of Excitation. Free Boundaries. No Rigid Inclusions.

is the one that provides the clearest reference point. This conclusion seems logical if one takes into account that the numerical integration procedure used in the analyses computes directly the values of the displacements versus time, and that velocities and accelerations must then be obtained from the displacements. Since the velocity and accelerations are the first and second derivatives of the displacements, these time histories are less smooth.

2.3 EFFECT OF BOUNDARY CONDITIONS ON S-WAVES

Figures 2.4 to 2.6 show the time histories of displacements, velocities and accelerations at one of the points of application of the load for the cases of fixed and free boundaries and no rigid inclusions within the soil mass. In both cases the displacement curve starts slightly after the zero time. As pointed out earlier, this is due to the starting procedure in the numerical algorithm which forces a zero displacement at time Δt. This could be improved by applying a correction in the first step of integration (typically using a different formula for this step). All three figures show that the amplitudes of motion (displacement, velocity or acceleration) are similar for both types of boundaries. The results for the free boundaries are, however, smoother, which can be seen in the velocity and particularly in the acceleration traces. They also tend to lag behind the results of the fixed case.

Figures 2.7 to 2.9 and 2.10 to 2.12 show the corresponding results at the target points IX = 14 and IX = 28 (left lower corners of the positions of the first and second inclusions), respectively. The same

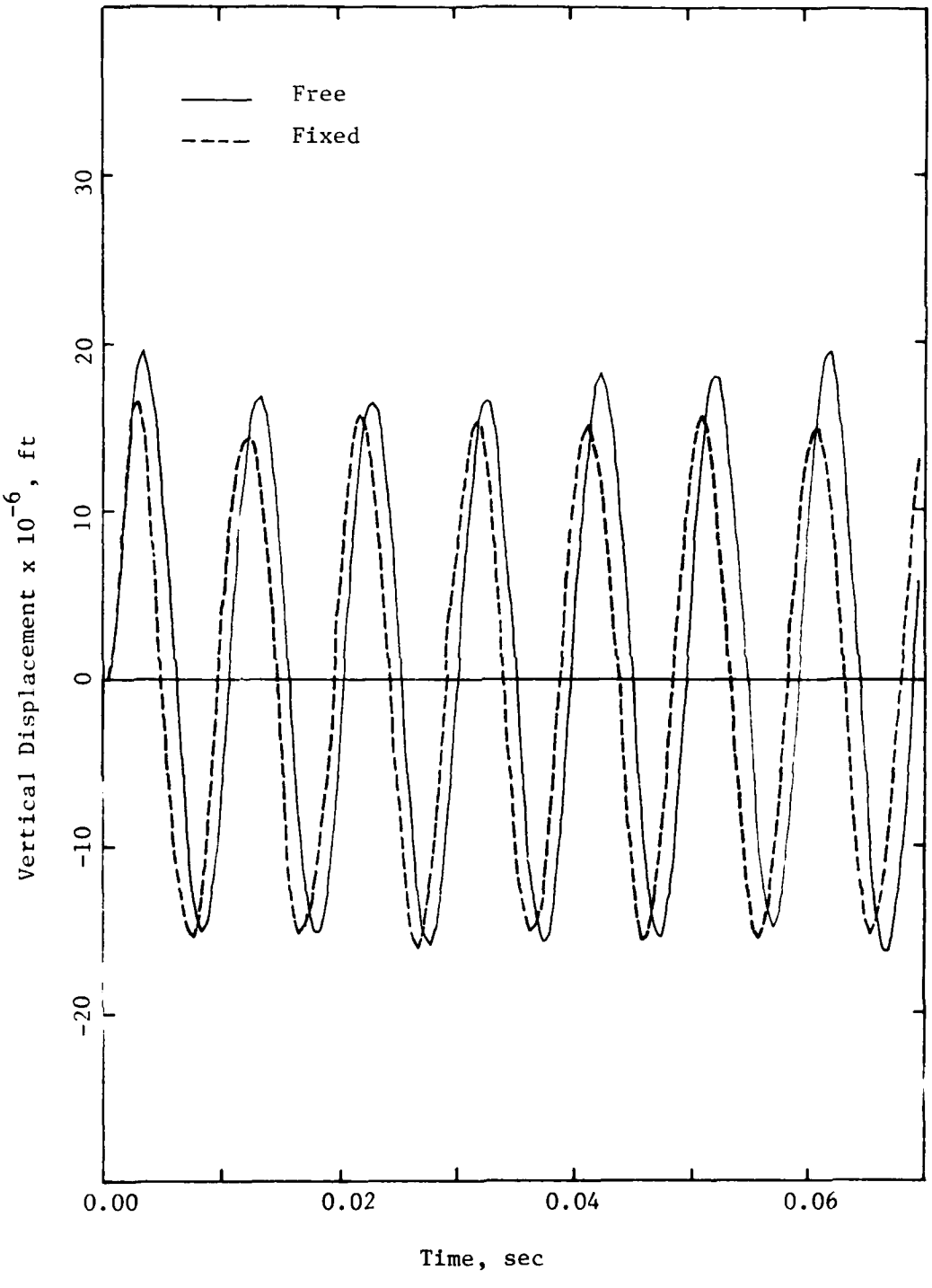

Fig. 2.4 - Vertical Displacements at the Point of Excitation. Fixed and Free Boundaries. No Rigid Inclusions.

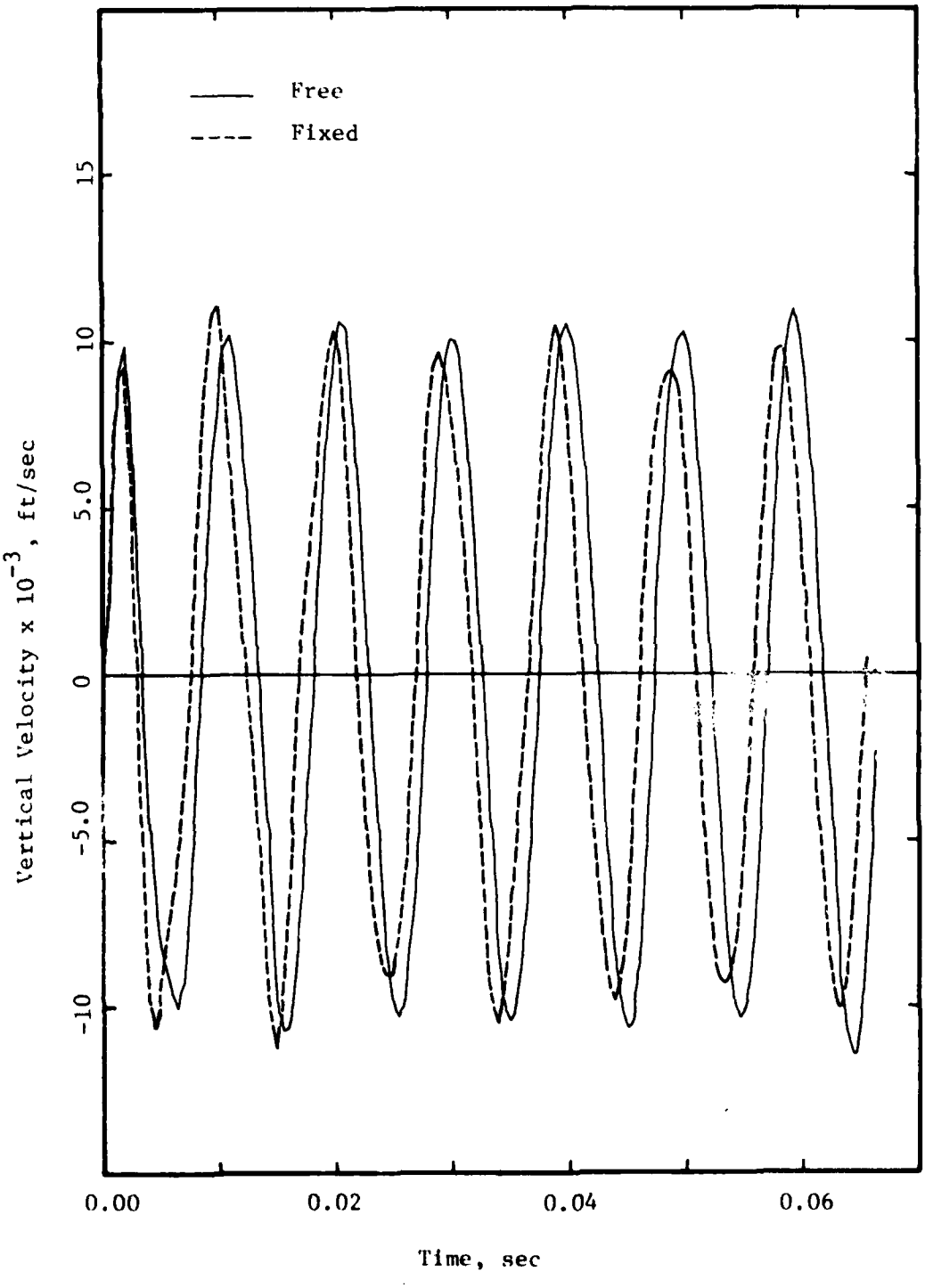

Fig. 2.5 - Vertical Velocities at the Point of Excitation. Fixed and Free Boundaries. No Rigid Inclusions.

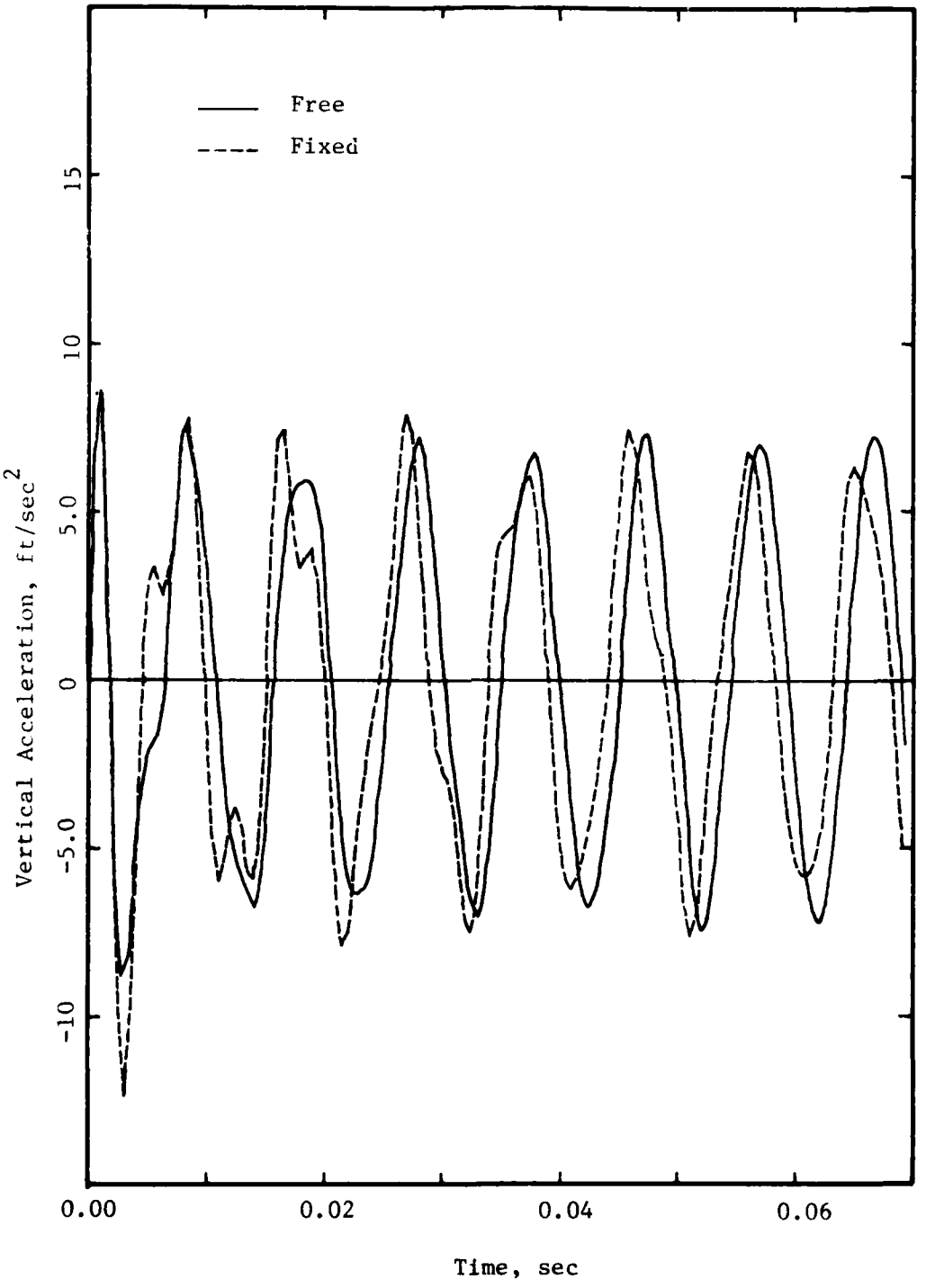

Fig. 2.6 - Vertical Accelerations at the Point of Excitation. Fixed and Free Boundaries. No Rigid Inclusions.

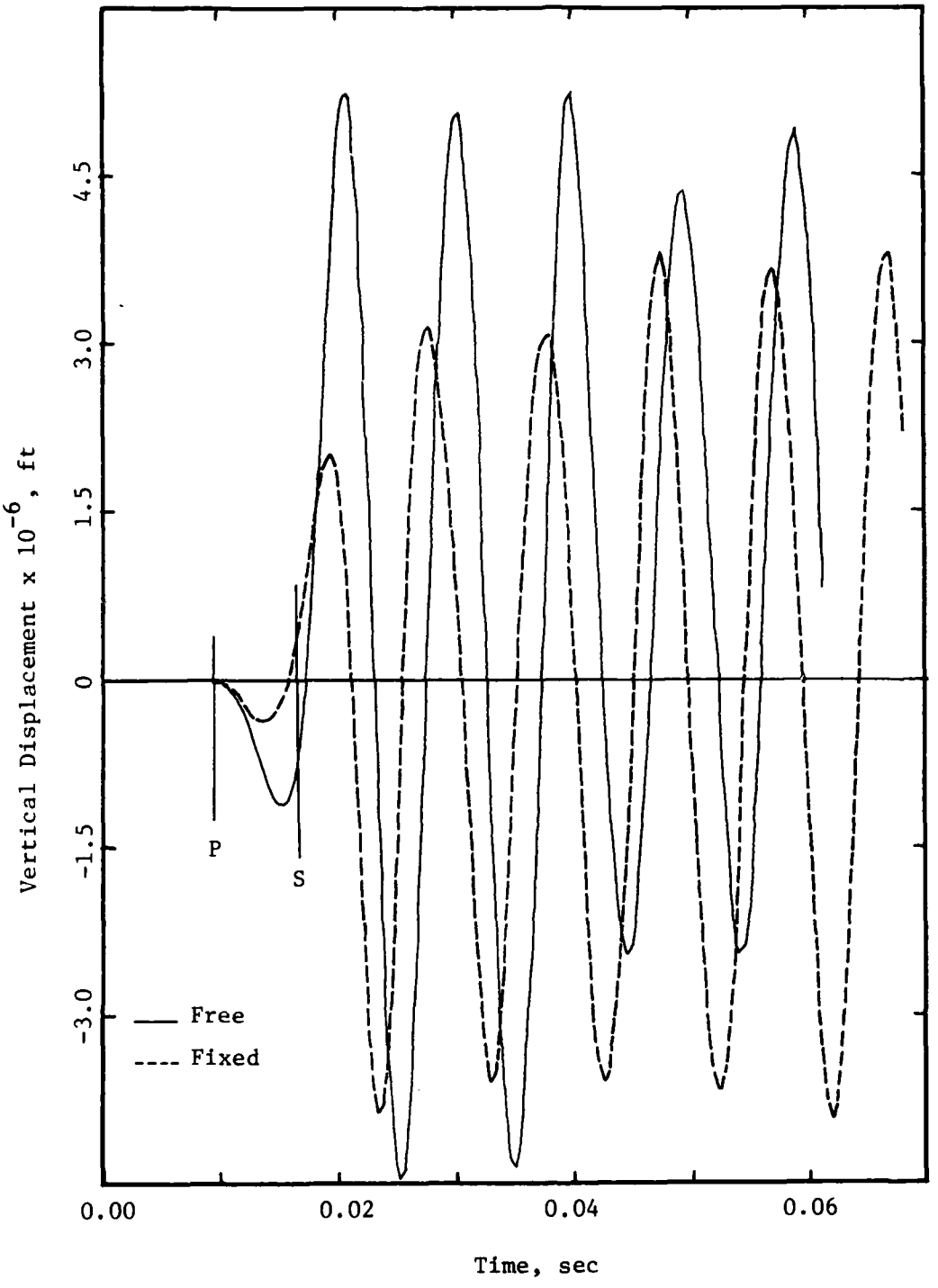

Fig. 2.7 - Vertical Displacements at IX=14. Fixed and Free Boundaries. No Rigid Inclusions.

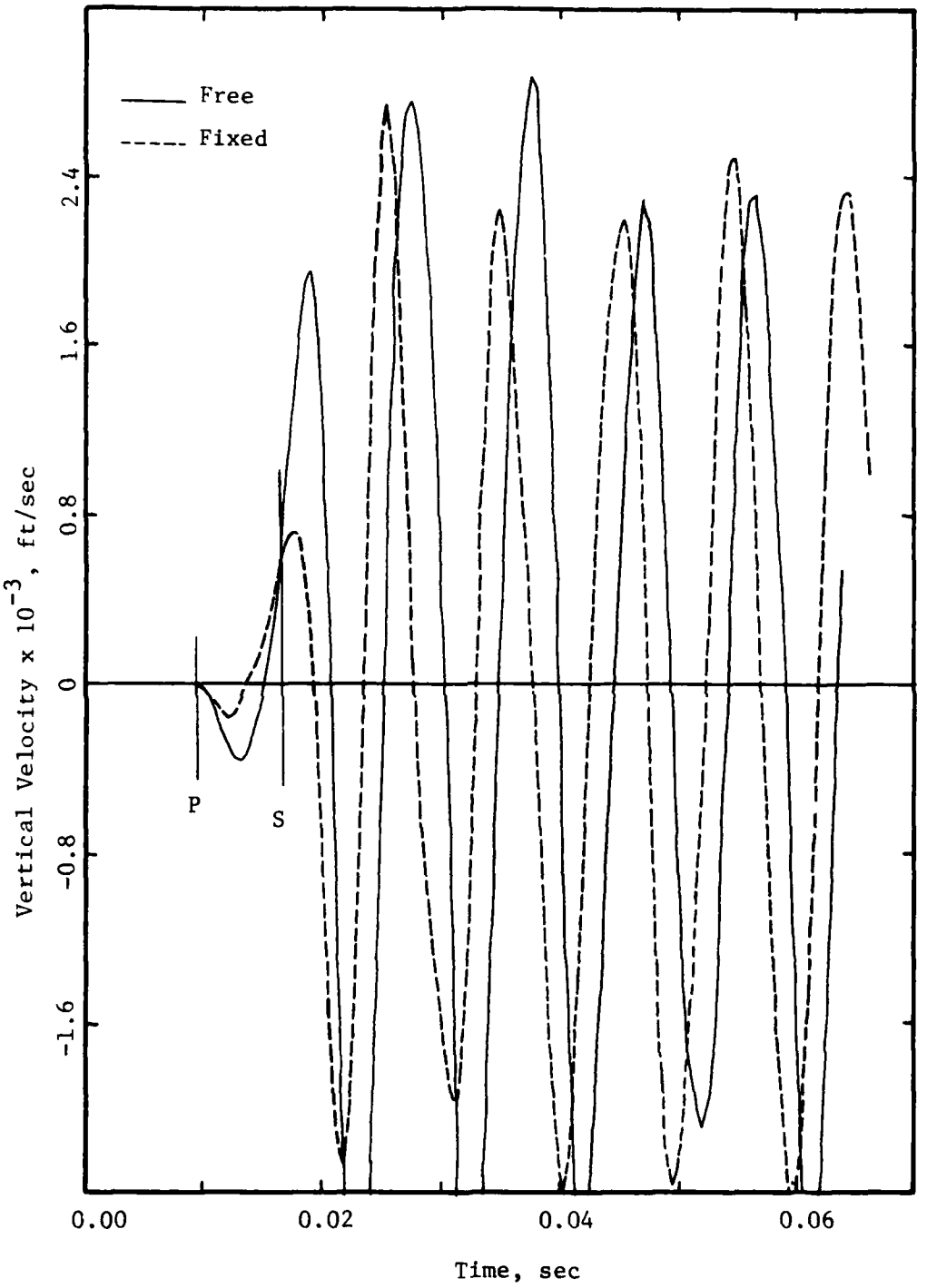

Fig. 2.8 - Vertical Velocities at IX=14. Fixed and Free Boundaries. No Rigid Inclusions.

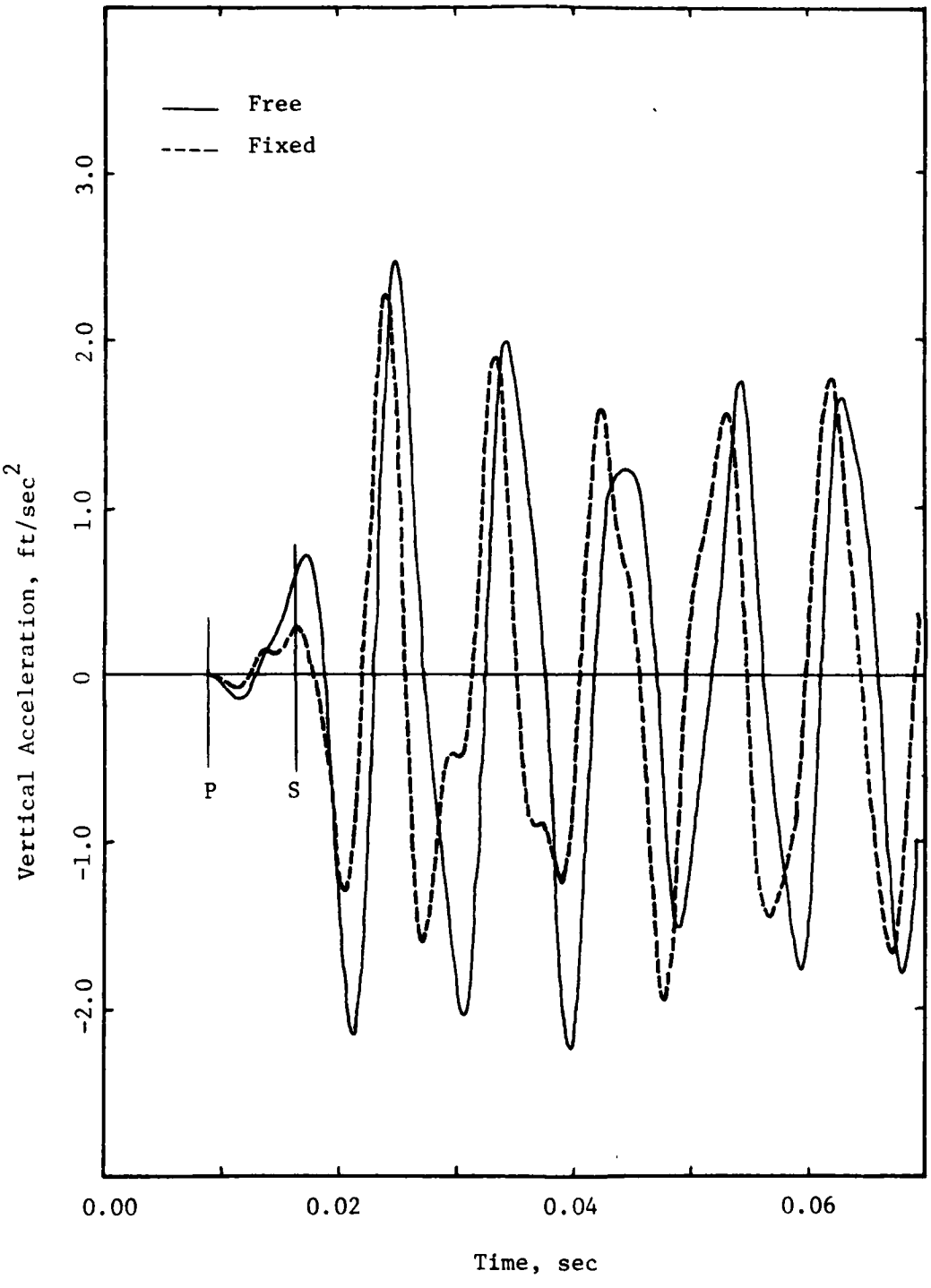

Fig. 2.9 - Vertical Accelerations at IX=14. Fixed and Free Boundaries. No Rigid Inclusions.

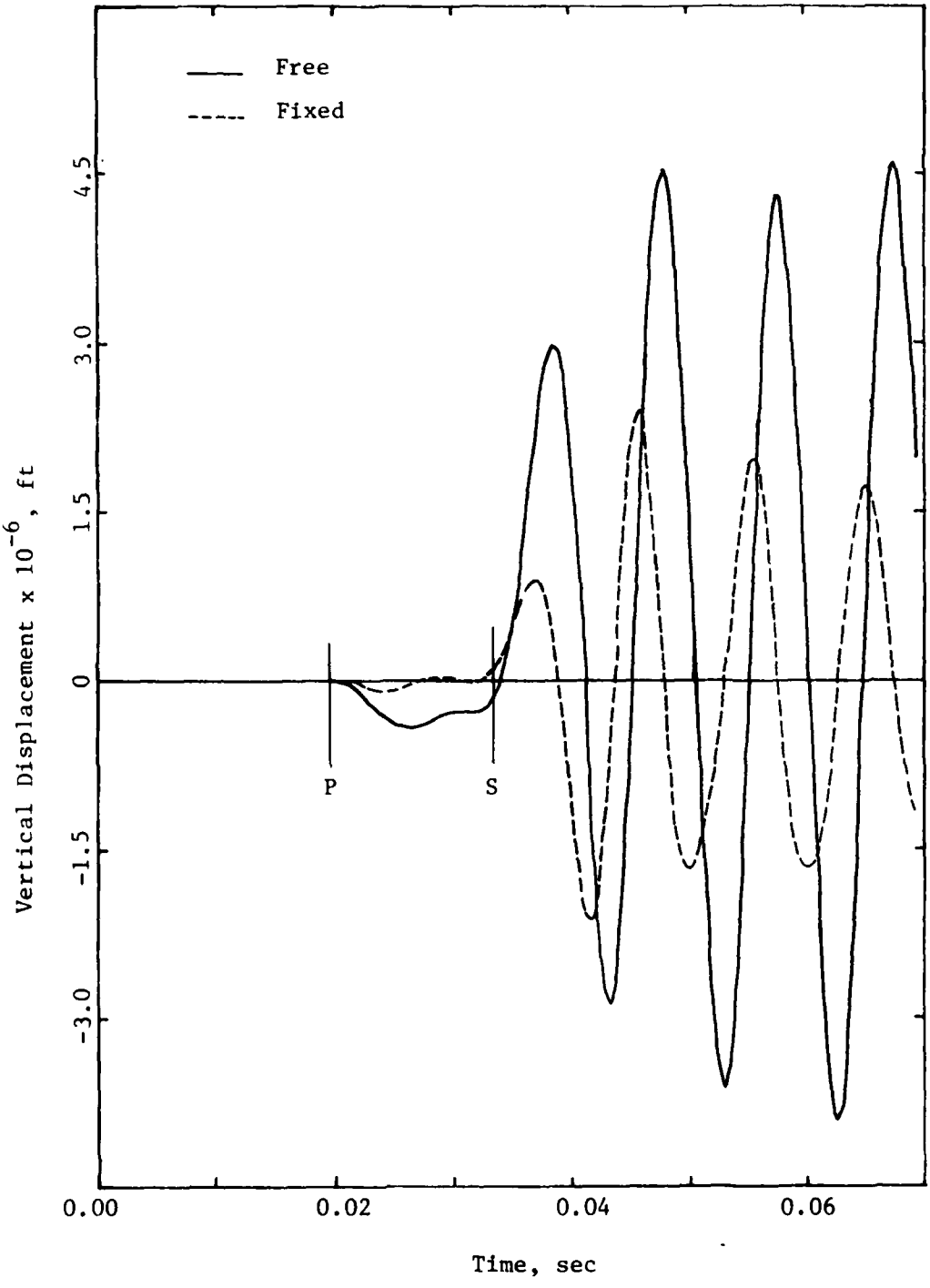

Fig. 2.10 - Vertical Displacements at IX=28. Fixed and Free Boundaries. No Rigid Inclusions.

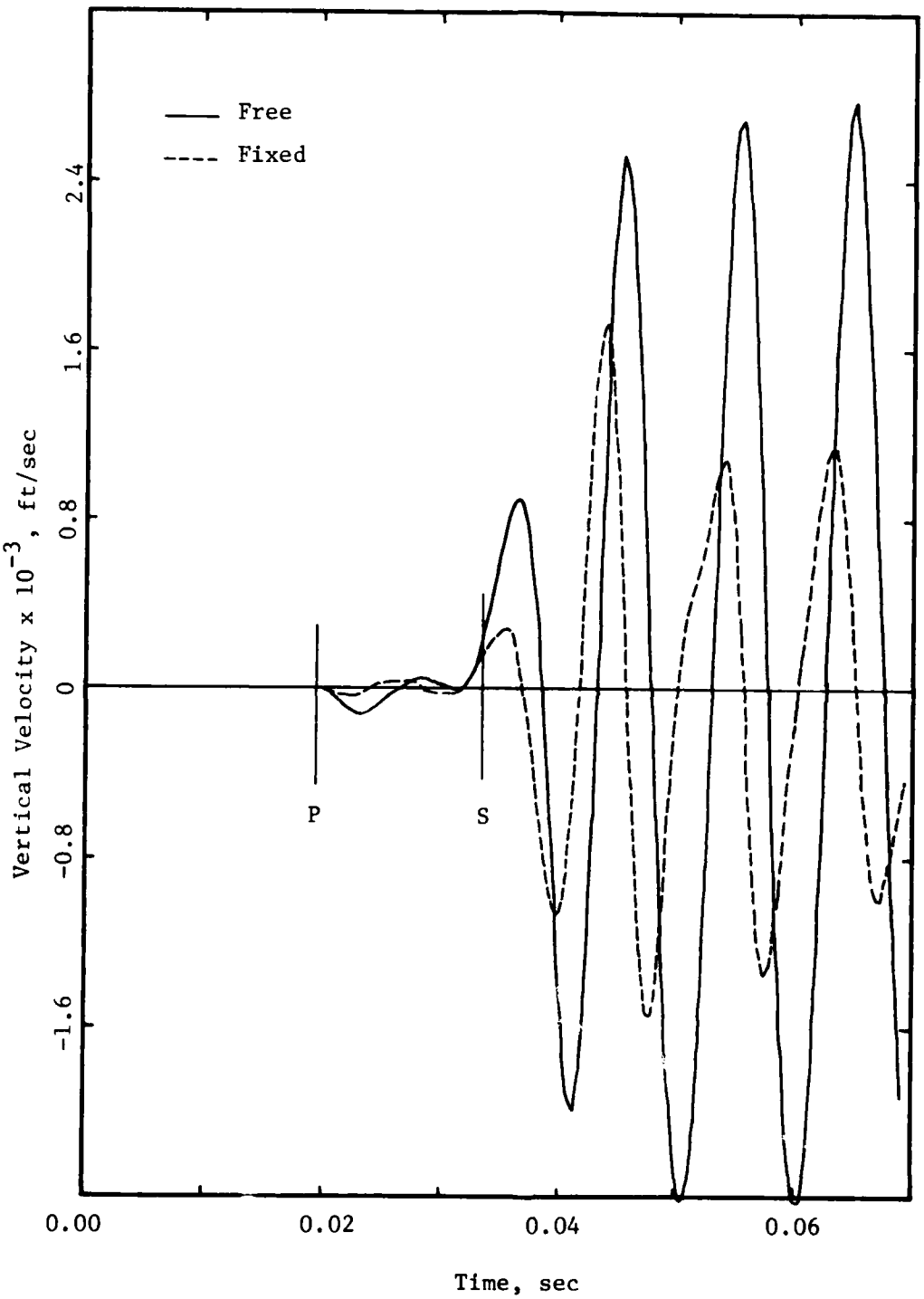

Fig. 2.11 - Vertical Velocities at IX=28. Fixed and Free Boundaries. No Rigid Inclusions.

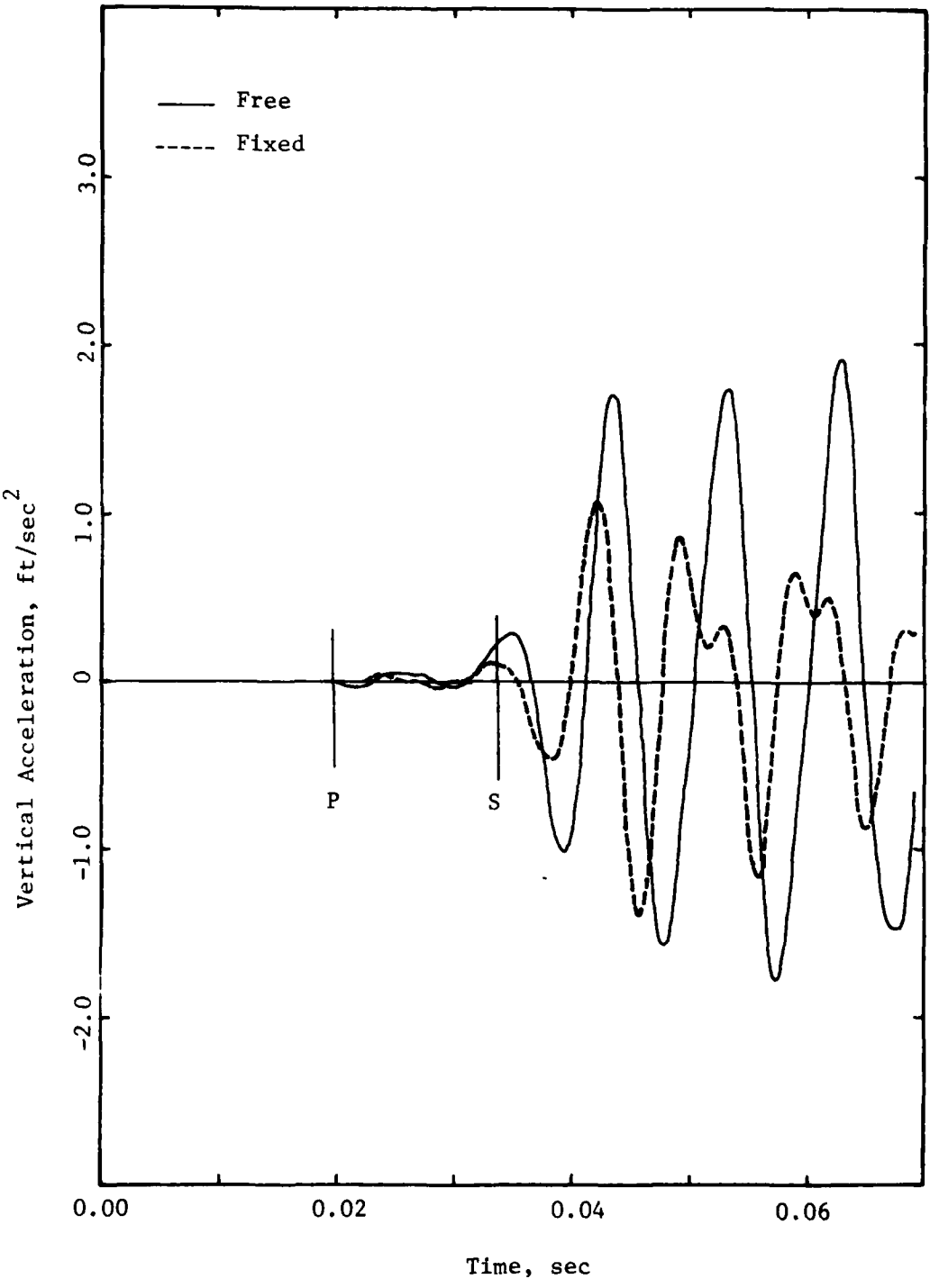

Fig. 2.12 - Vertical Accelerations at IX=28. Fixed and Free Boundaries. No Rigid Inclusions.

observations can be made, but in these cases, in addition, the motion for the fixed boundaries has clearly a smaller amplitude than that of the free model.

The corresponding results with three rigid inclusions are presented in Figures 2.13 to 2.15 (motion at excitation point), 2.16 to 2.18 (motion at IX = 14) and 2.19 to 2.21 (motion at IX = 28). The presence of these rigid inclusions does not produce any significant difference in the shape of the waves or in the effect of the boundary conditions, for the size of the inclusions and the wavelength considered.

Since the results for the free boundaries lag in all cases behind those corresponding to fixed boundaries, the shear wave velocity estimates based on the first arrival time would be smaller for the former case than for the latter. On the other hand, when interval arrival times between targets are used, by picking the corresponding points on the curves for each target position, the calculated shear wave velocities are about the same, irrespective of the boundary conditions. Figures 2.22 through 2.27 show interval arrival times when there are no inclusions and Figs. 2.28 through 2.33 show the corresponding results with three rigid inclusions. When the interval times are measured between the first S-wave peaks, calculated shear wave velocities have average values of 101.2 ft/sec for free boundaries and no inclusions, 102.4 ft/sec for free boundaries and three inclusions, and 97 and 97.5 ft/sec for fixed boundaries (no inclusions and three inclusions, respectively). The values for free boundaries tend to be, therefore, slightly higher than those for fixed boundaries, by opposition to the estimates based in initial arrival of the S-wave. Measuring interval travel times from the second peaks, a less desirable

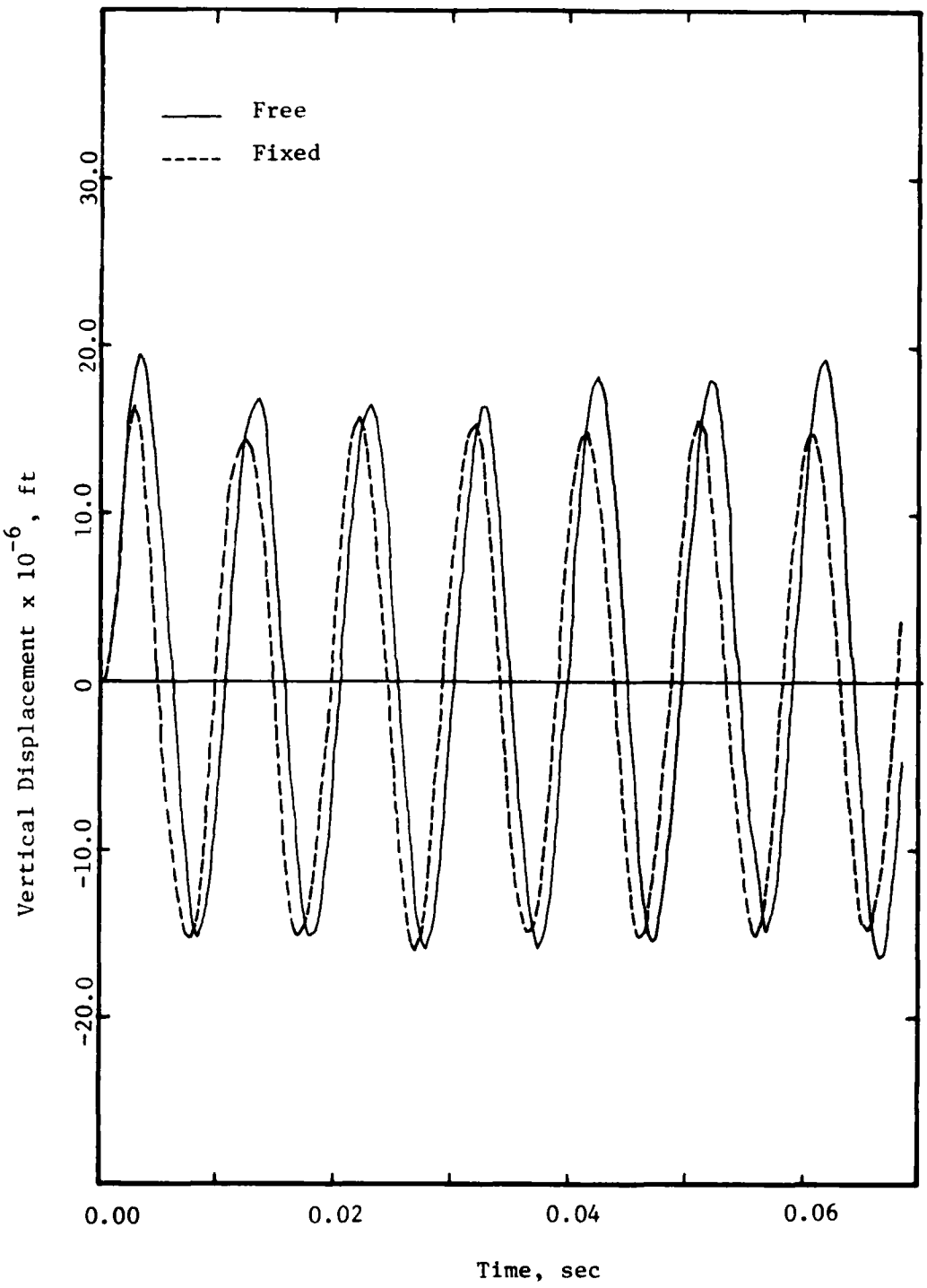

Fig. 2.13 - Vertical Displacements at the Point of Excitation. Fixed and Free Boundaries. Three Rigid Inclusions.

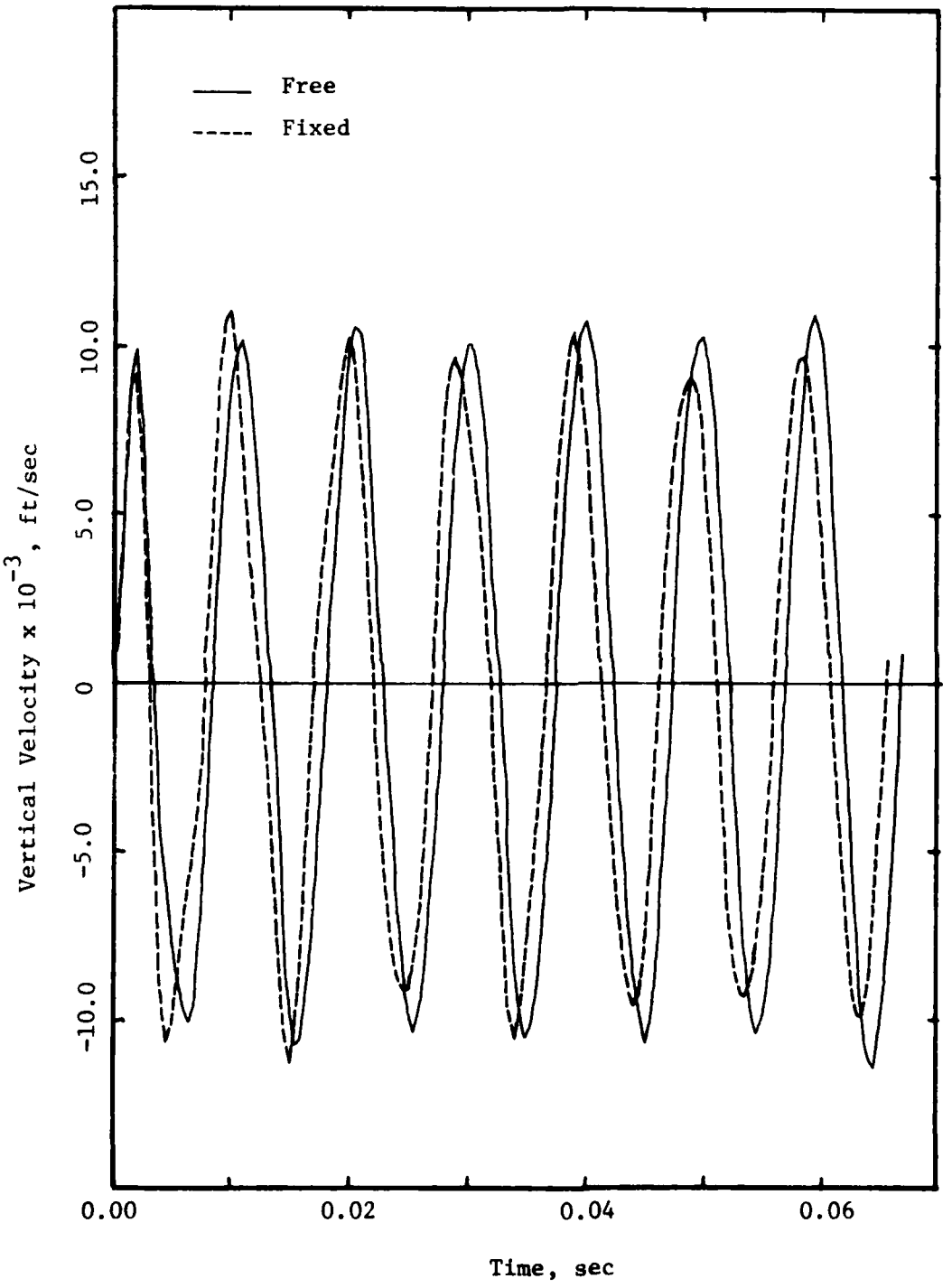

Fig. 2.14 - Vertical Velocities at the Point of Excitation. Fixed and Free Boundaries. Three Rigid Inclusions.

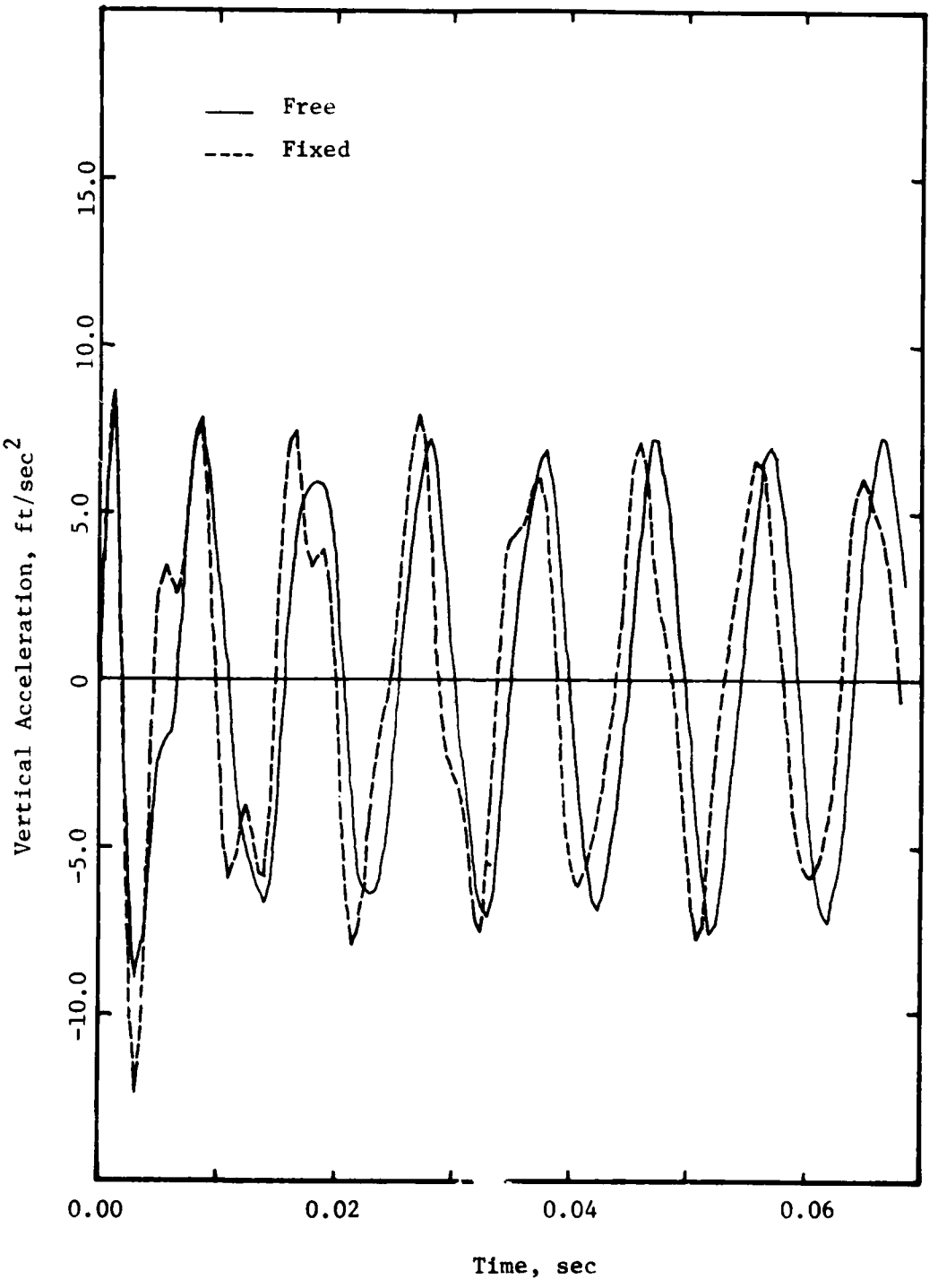

Fig. 2.15 - Vertical Accelerations at the Point of Excitation. Fixed and Free Boundaries. Three Rigid Inclusions.

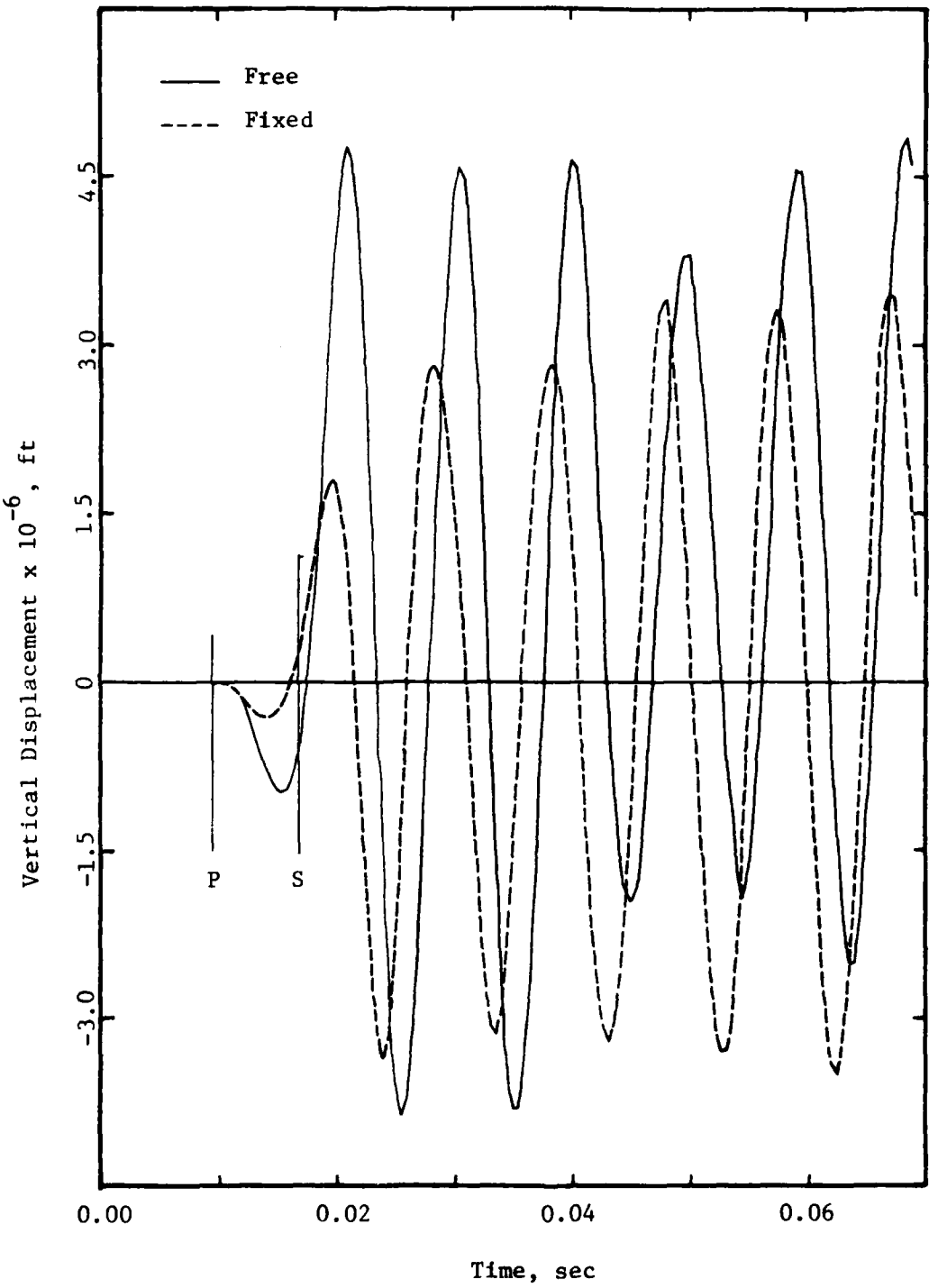

Fig. 2.16 - Vertical Displacements at IX=14. Fixed and Free Boundaries. Three Rigid Inclusions.

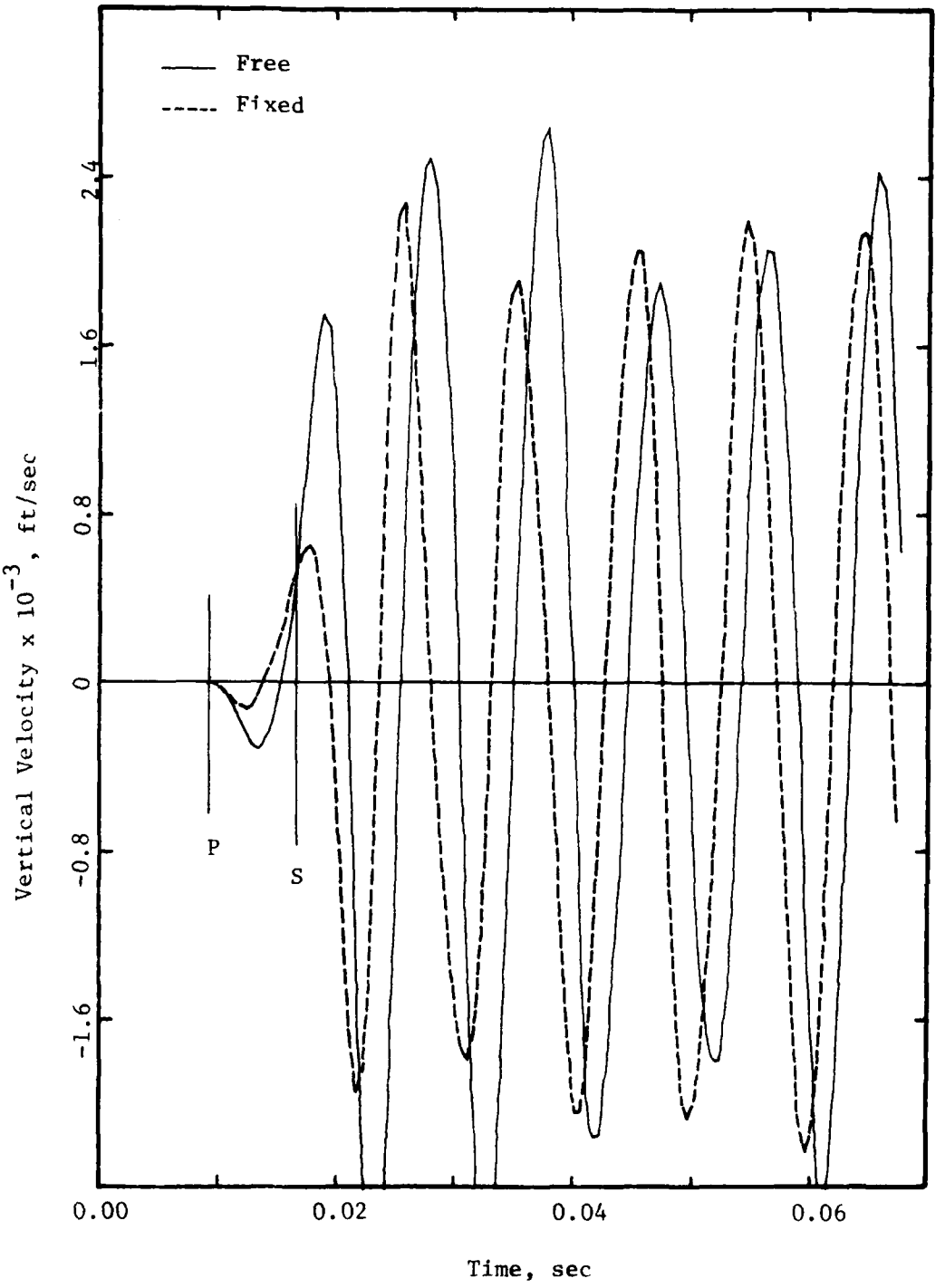

Fig. 2.17 - Vertical Velocity at IX=14. Fixed and Free Boundaries. Three Rigid Inclusions.

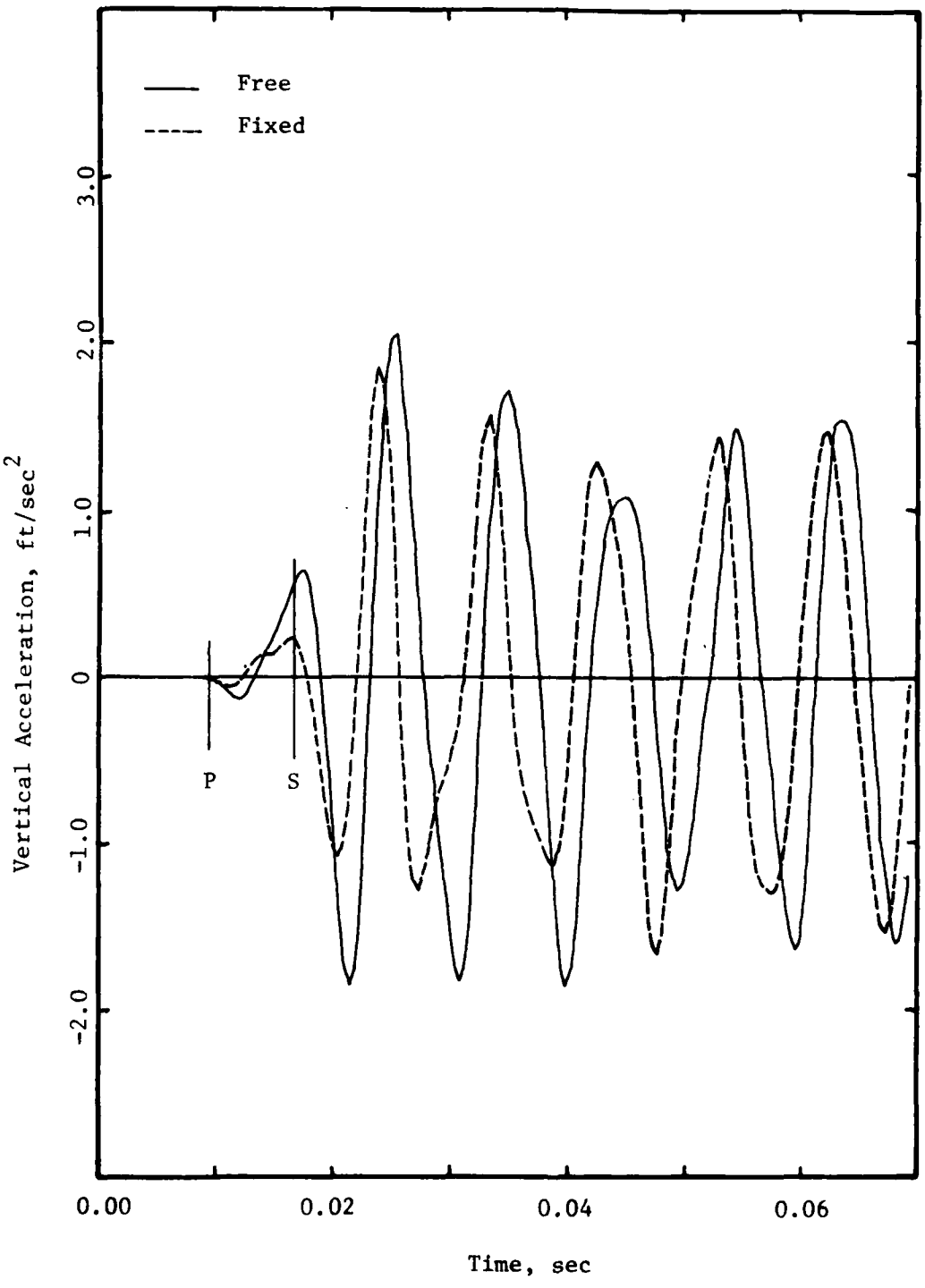

Fig. 2.18 - Vertical Accelerations at IX=14. Fixed and Free Boundaries. Three Rigid Inclusions.

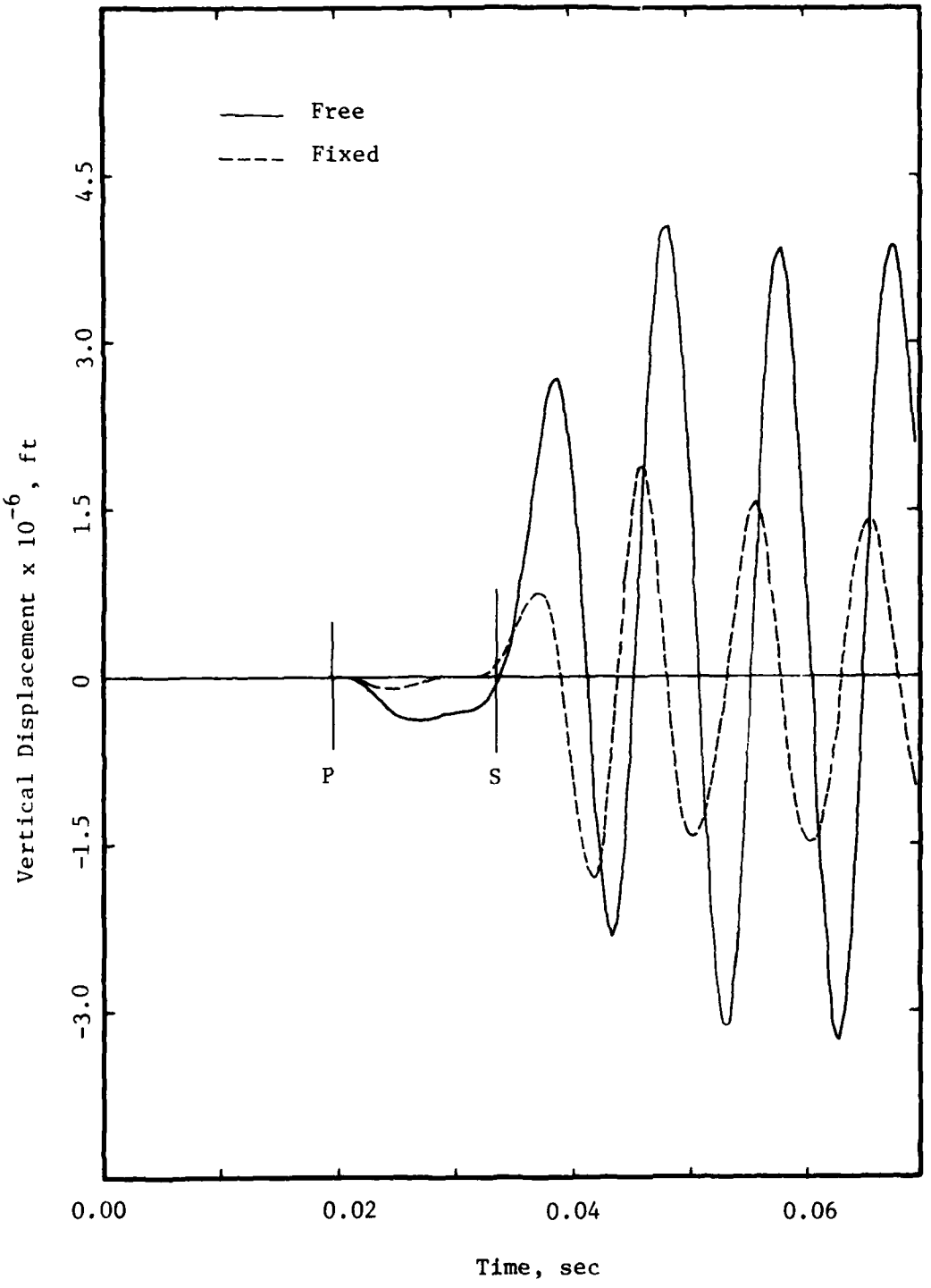

Fig. 2.19 - Vertical Displacements at IX=28. Fixed and Free Boundaries. Three Rigid Inclusions.

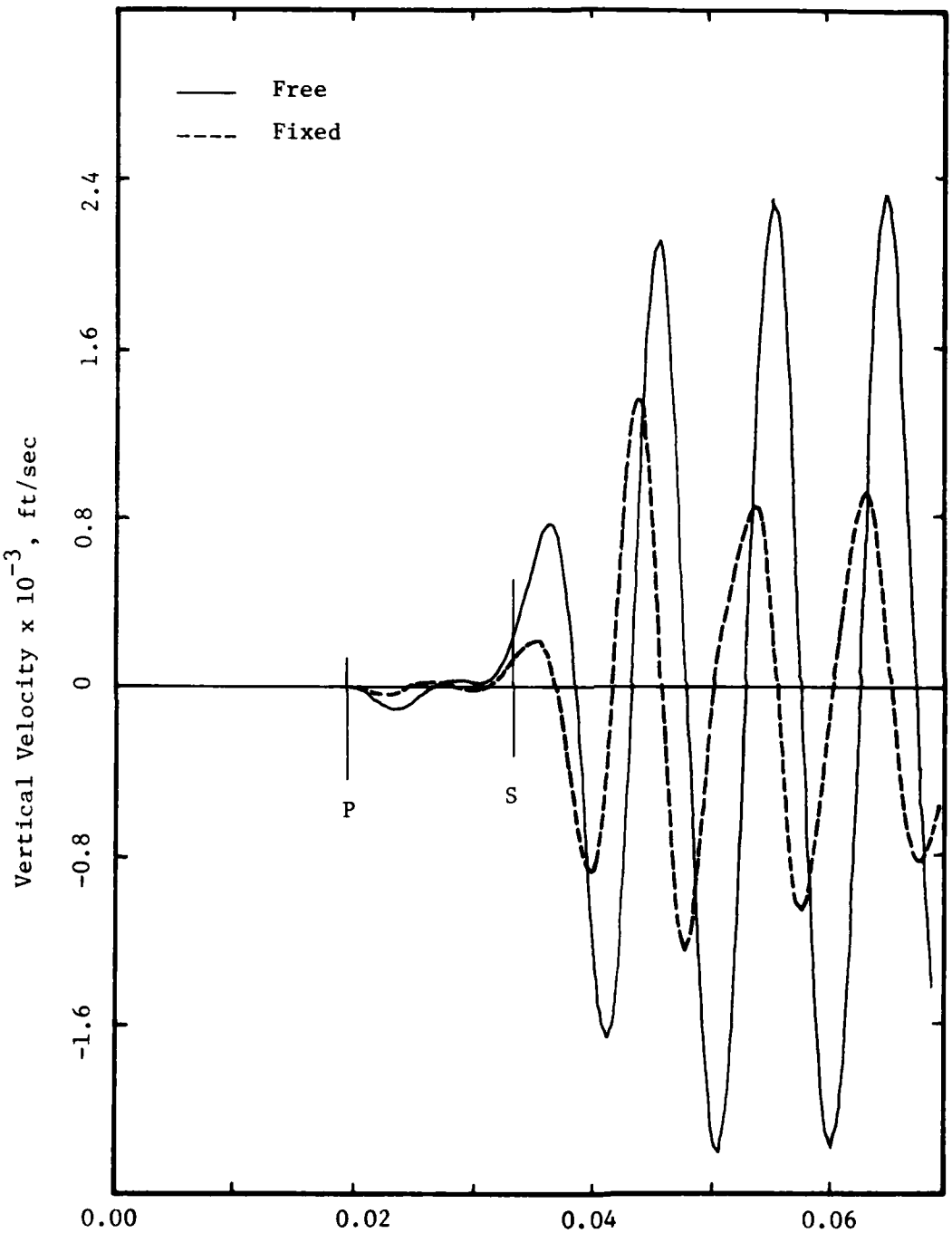

Fig. 2.20 - Vertical Velocities at IX=28. Fixed and Free Boundaries. Three Rigid Inclusions.

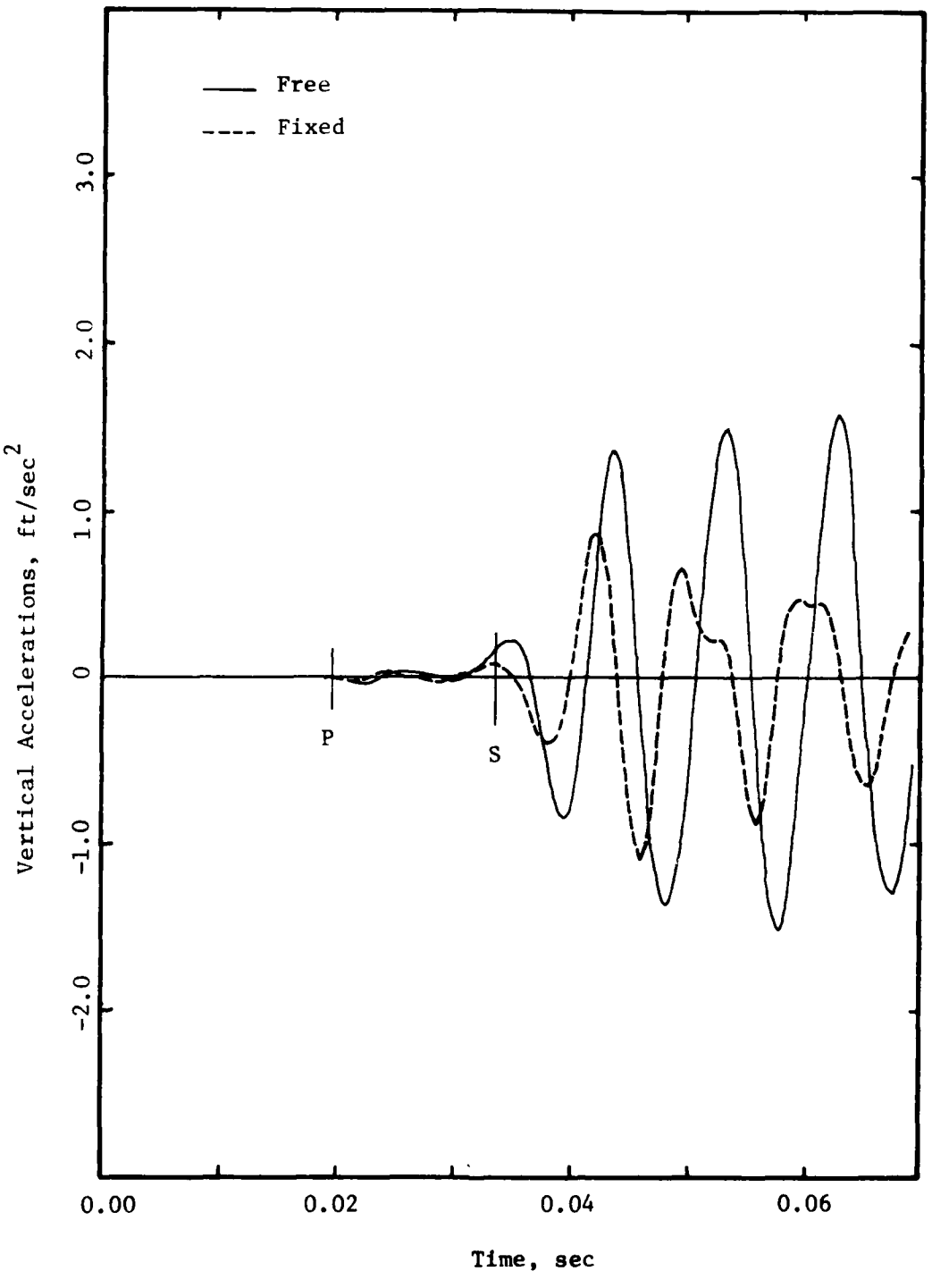

Fig. 2.21 - Vertical Accelerations at IX=28. Fixed and Free Boundaries. Three Rigid Inclusions.

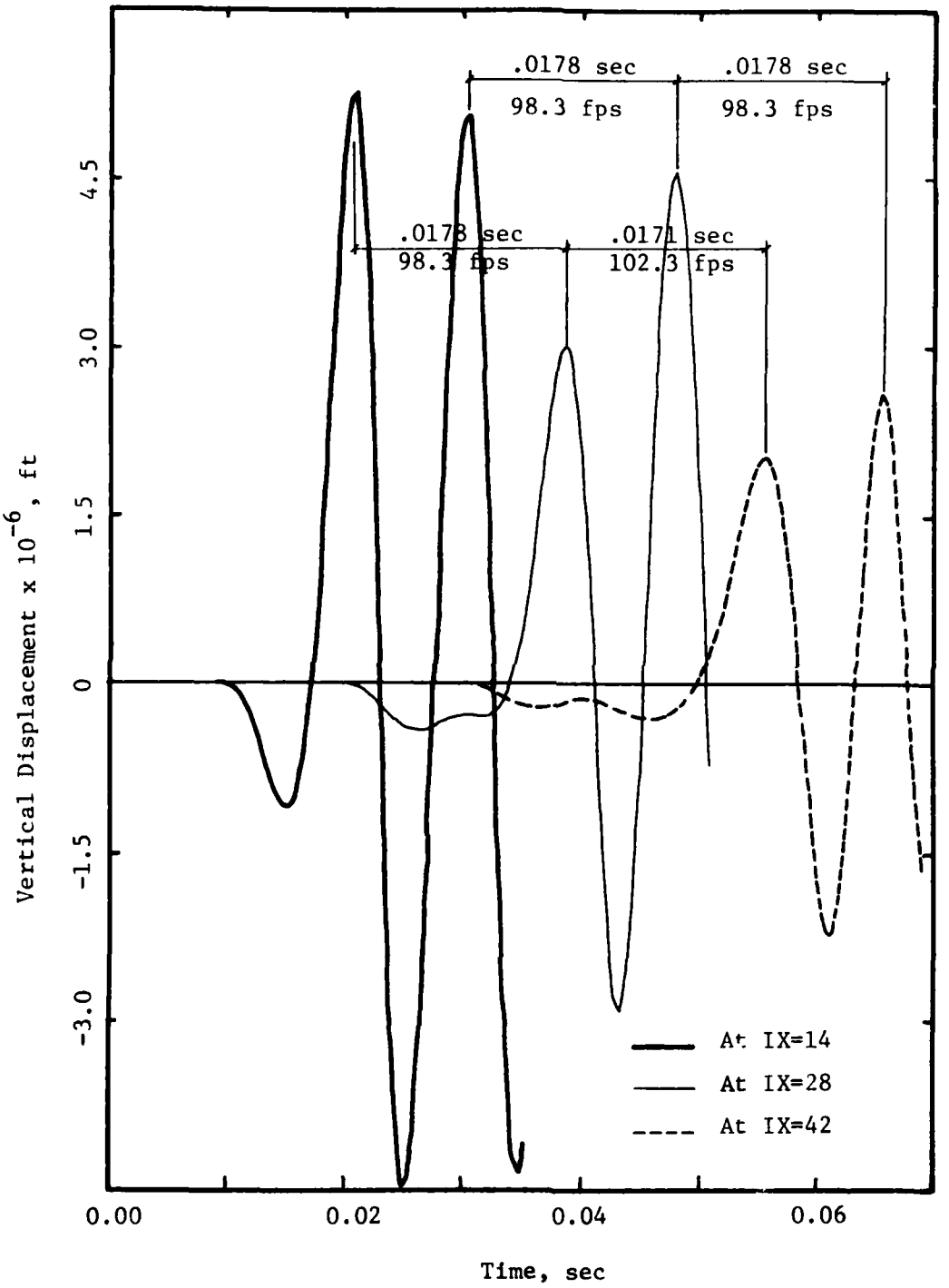

Fig. 2.22 - Inter-arrival Times and Corresponding Shear Wave Velocities from Displacement Curves. Free Boundaries. No Rigid Inclusions.

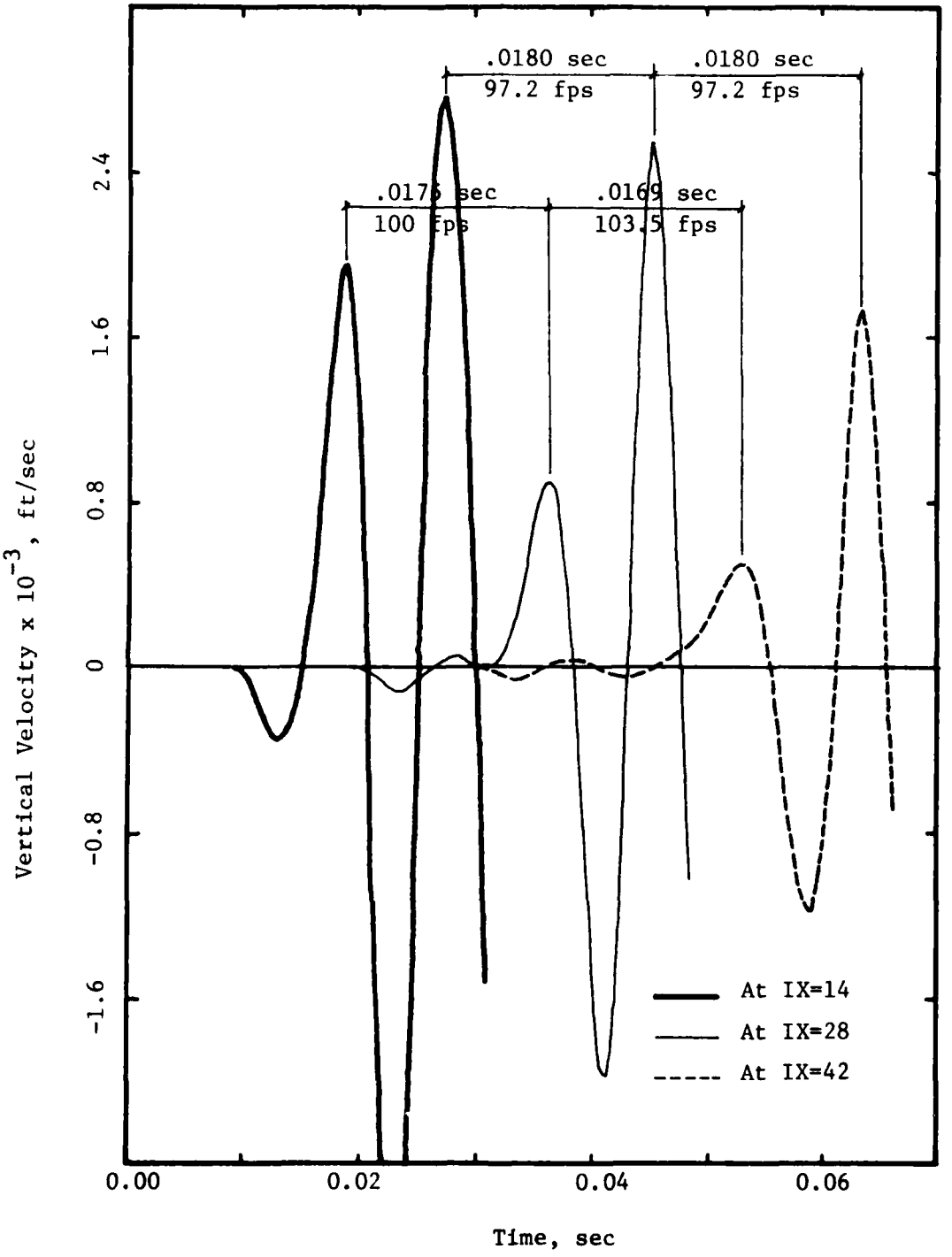

Fig. 2.23 - Inter-arrival Times and Corresponding Shear Wave Velocities from Velocity Curves. Free Boundaries. No Rigid Inclusions.

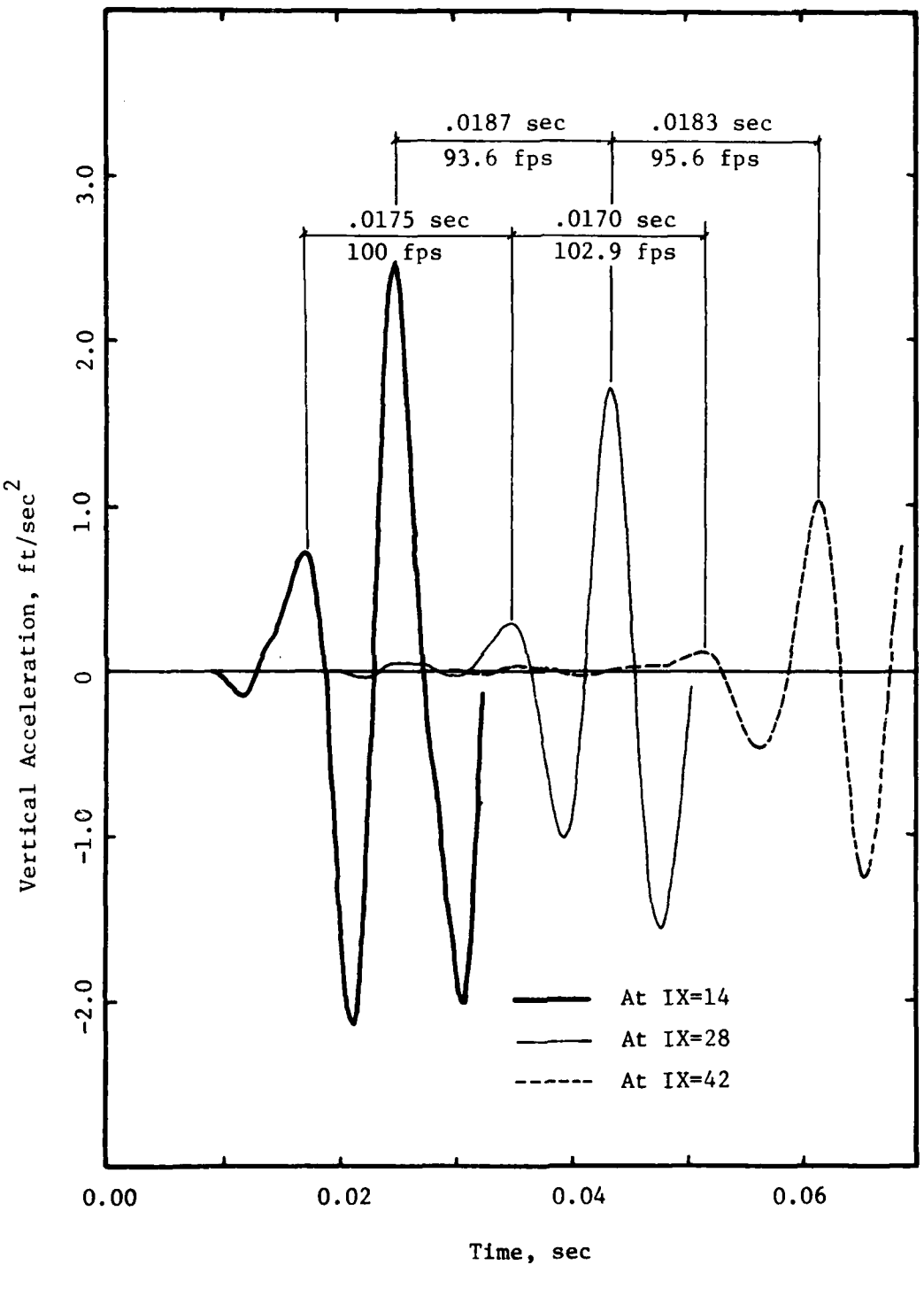

Fig. 2.24 - Inter-arrival Times and Corresponding Shear Wave Velocities from Acceleration Curves. Free Boundaries. No Rigid Inclusions.

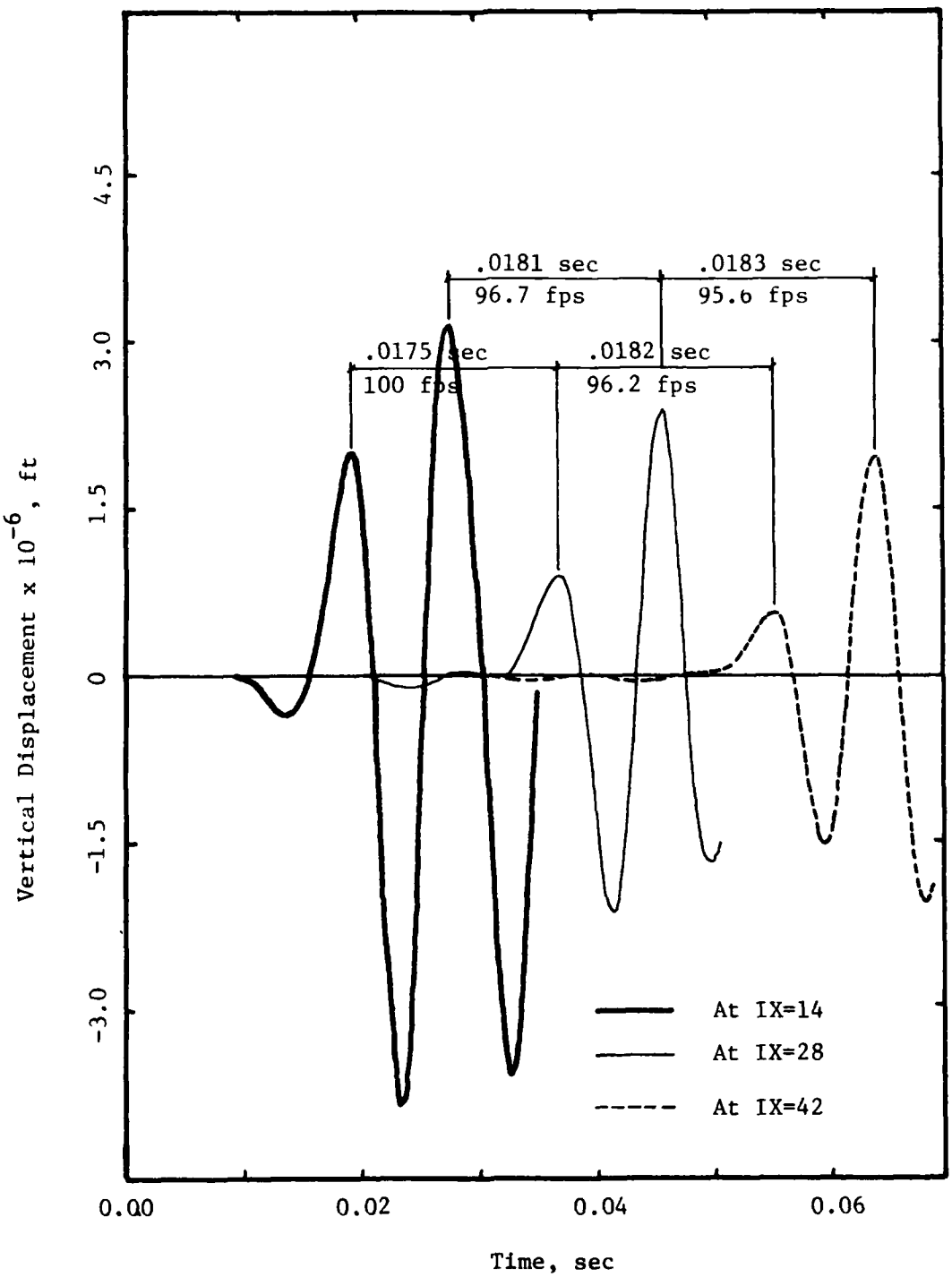

Fig. 2.25 - Inter-arrival Times and Corresponding Shear Wave Velocities from Displacement Curves. Fixed Boundaries. No Rigid Inclusions.

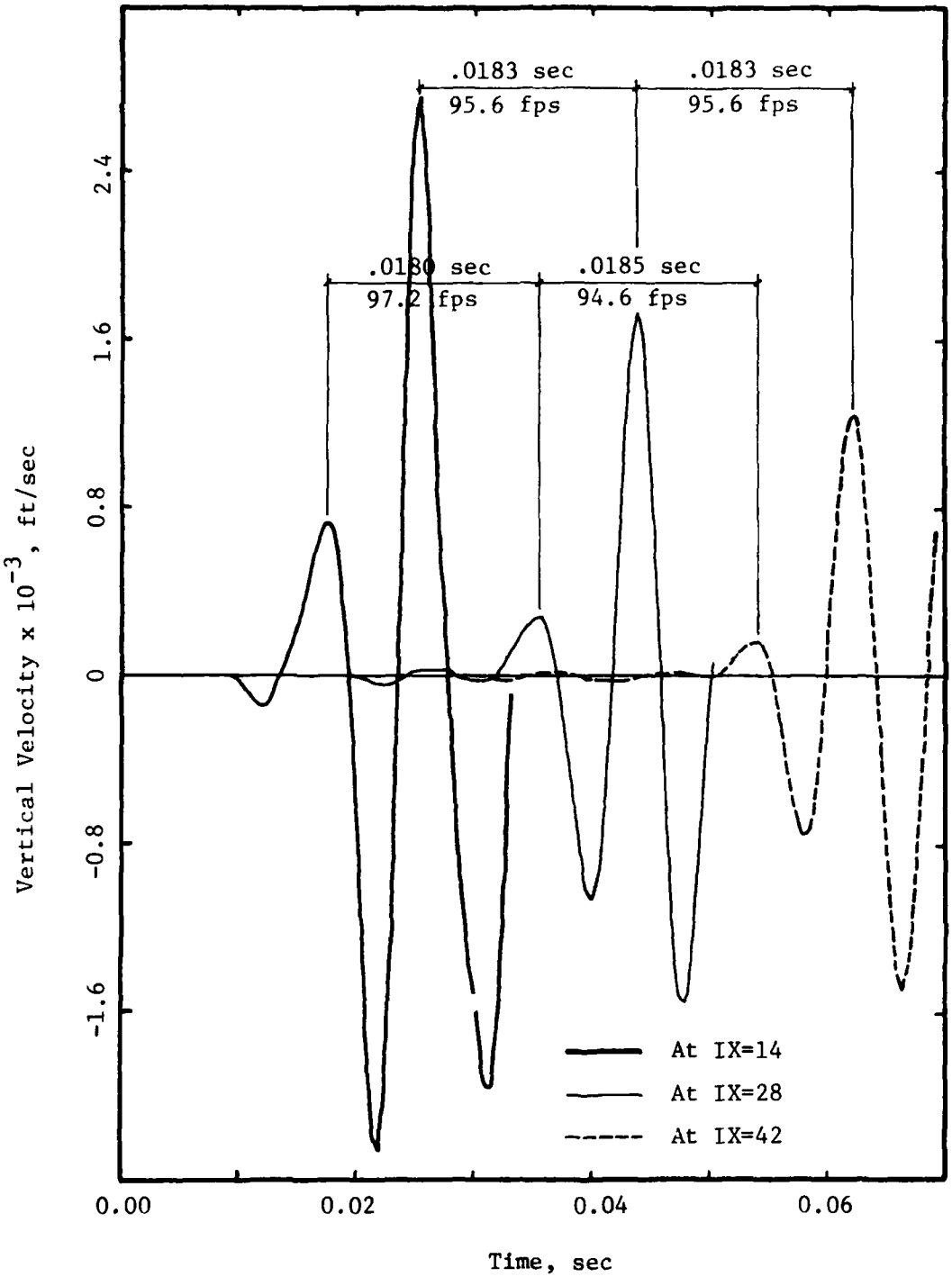

Fig. 2.26 - Inter-arrival Times and Corresponding Shear Wave Velocities from Velocity Curve. Fixed Boundaries. No Ridig Inclusions.

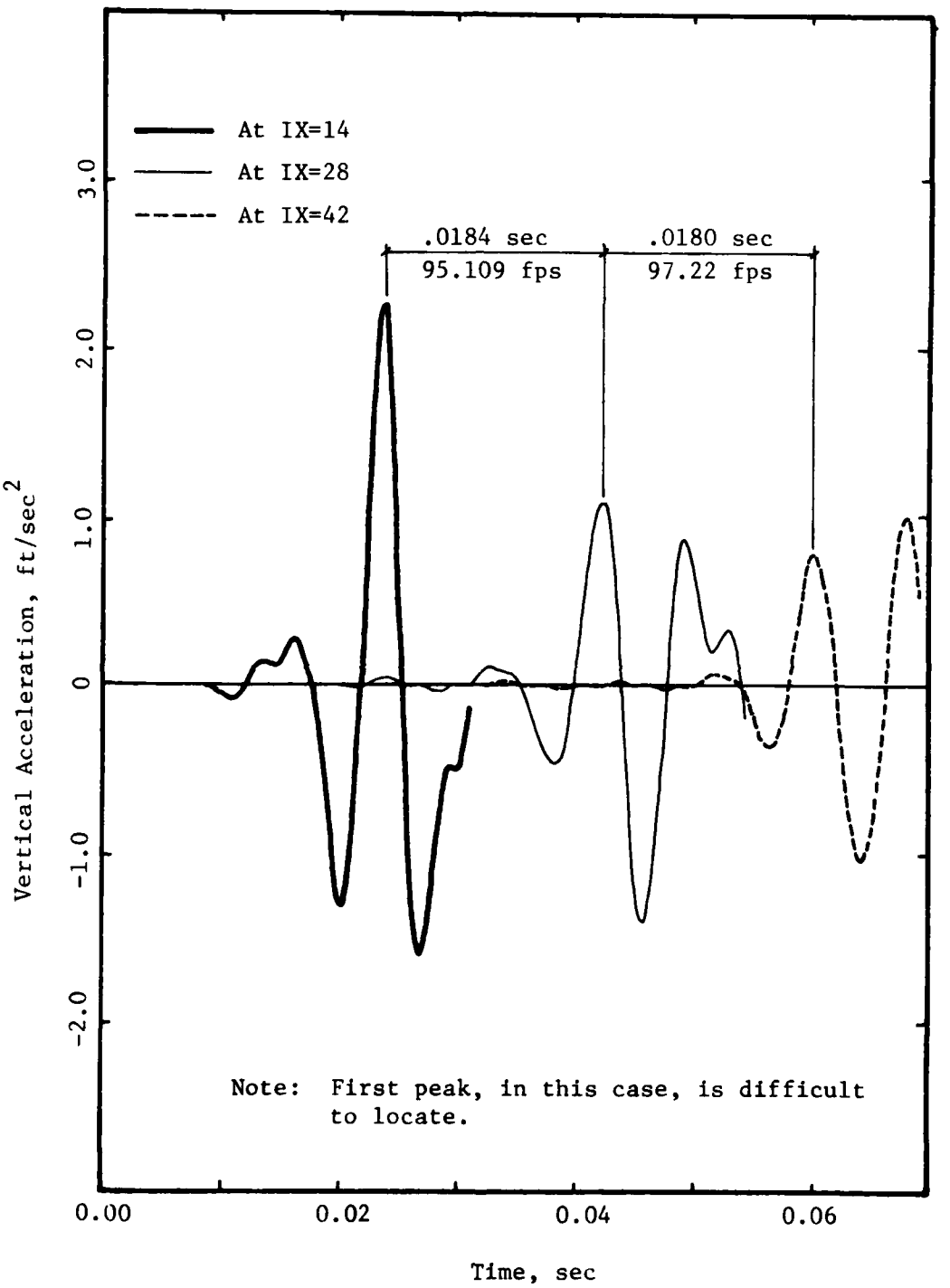

Fig. 2.27 - Inter-arrival Times and Corresponding Shear Wave Velocities from Acceleration Curve. Fixed Boundaries. No Rigid Inclusions.

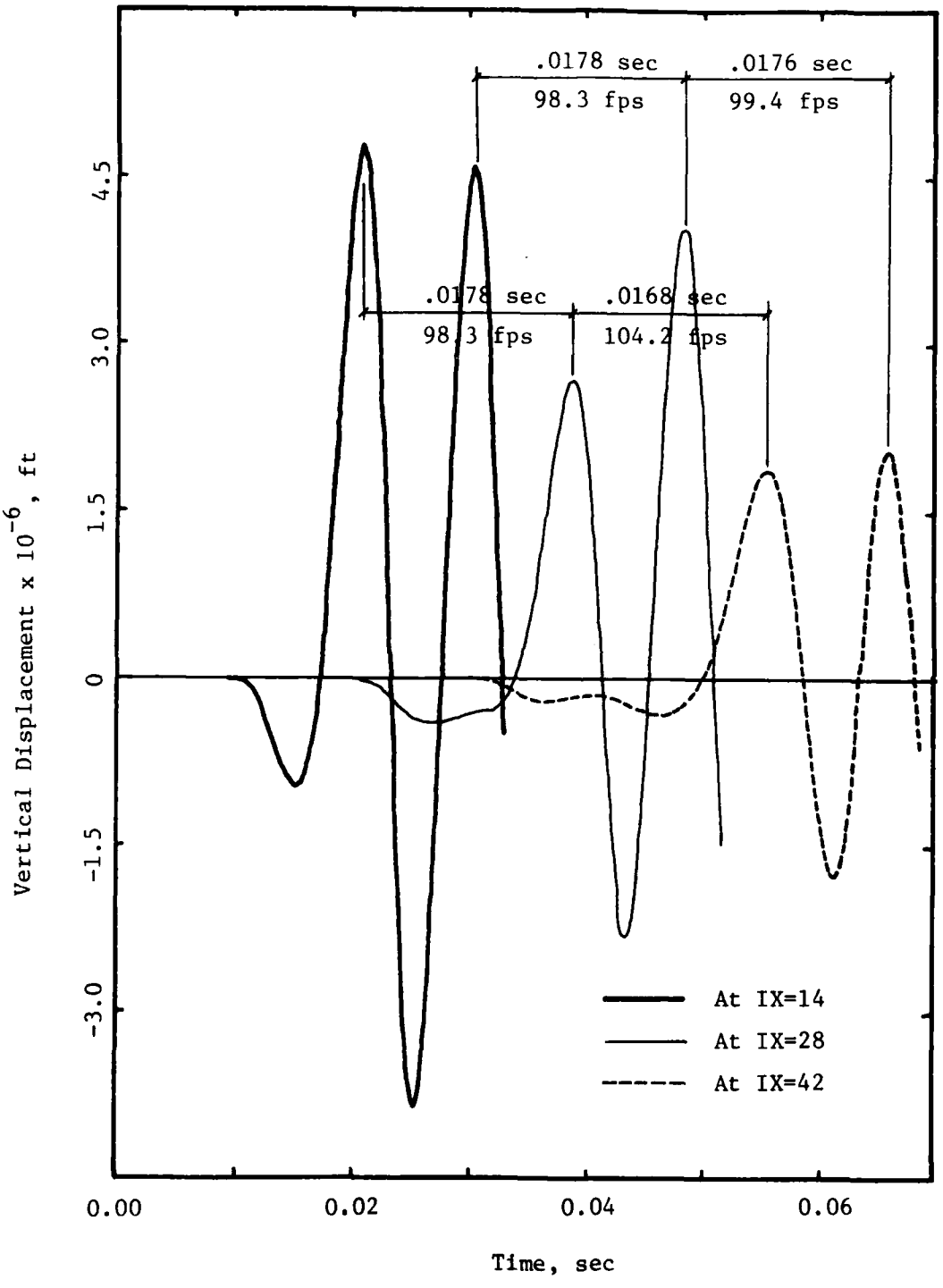

Fig. 2.28 - Inter-arrival Times and Corresponding Shear Wave Velocities from Displacement Curve. Free Boundaries. Three Rigid Inclusions.

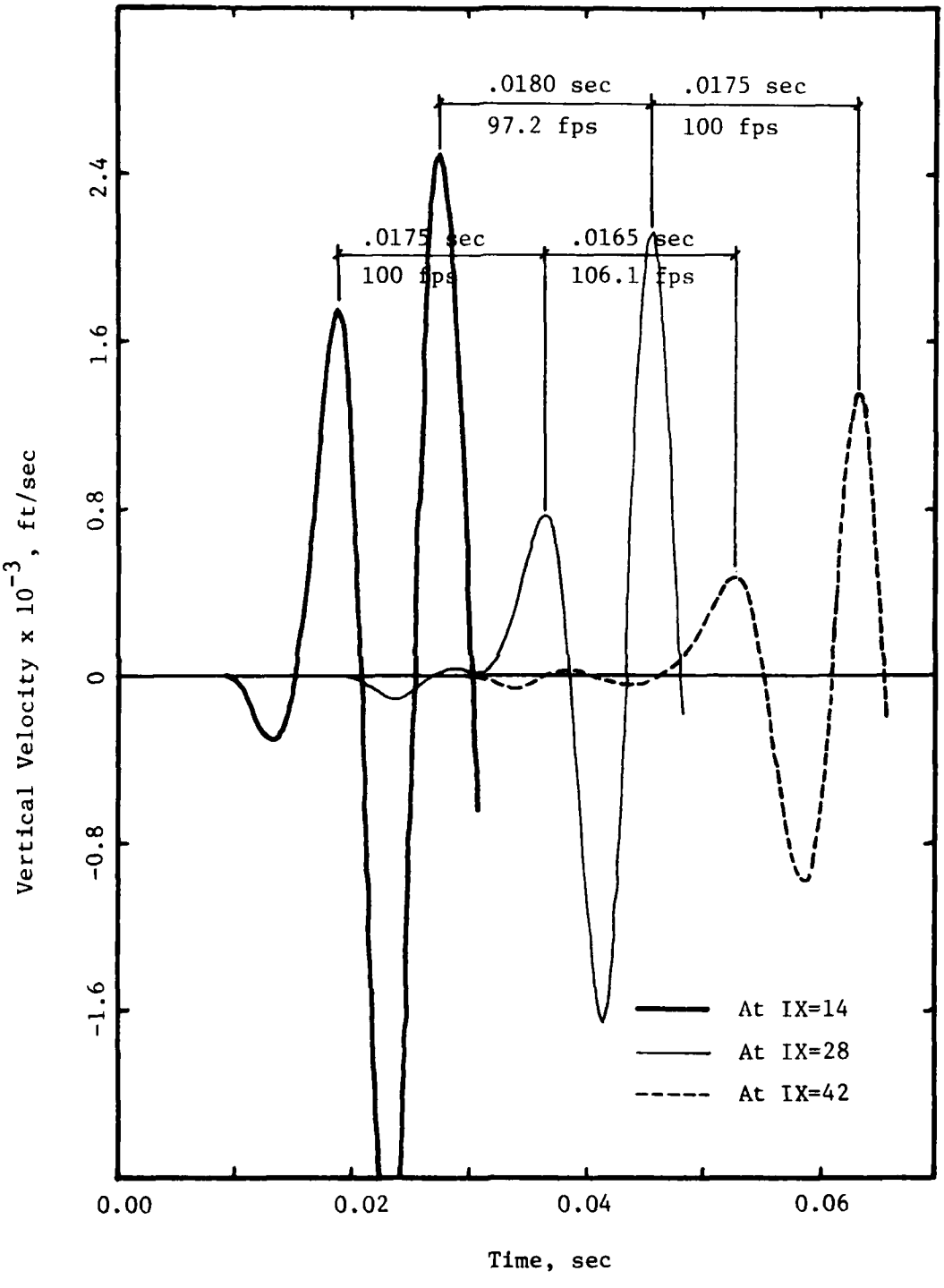

Fig. 2.29 - Inter-arrival Times and Corresponding Shear Wave Velocities from Velocity Curves. Free Boundaries. Three Rigid Inclusions.

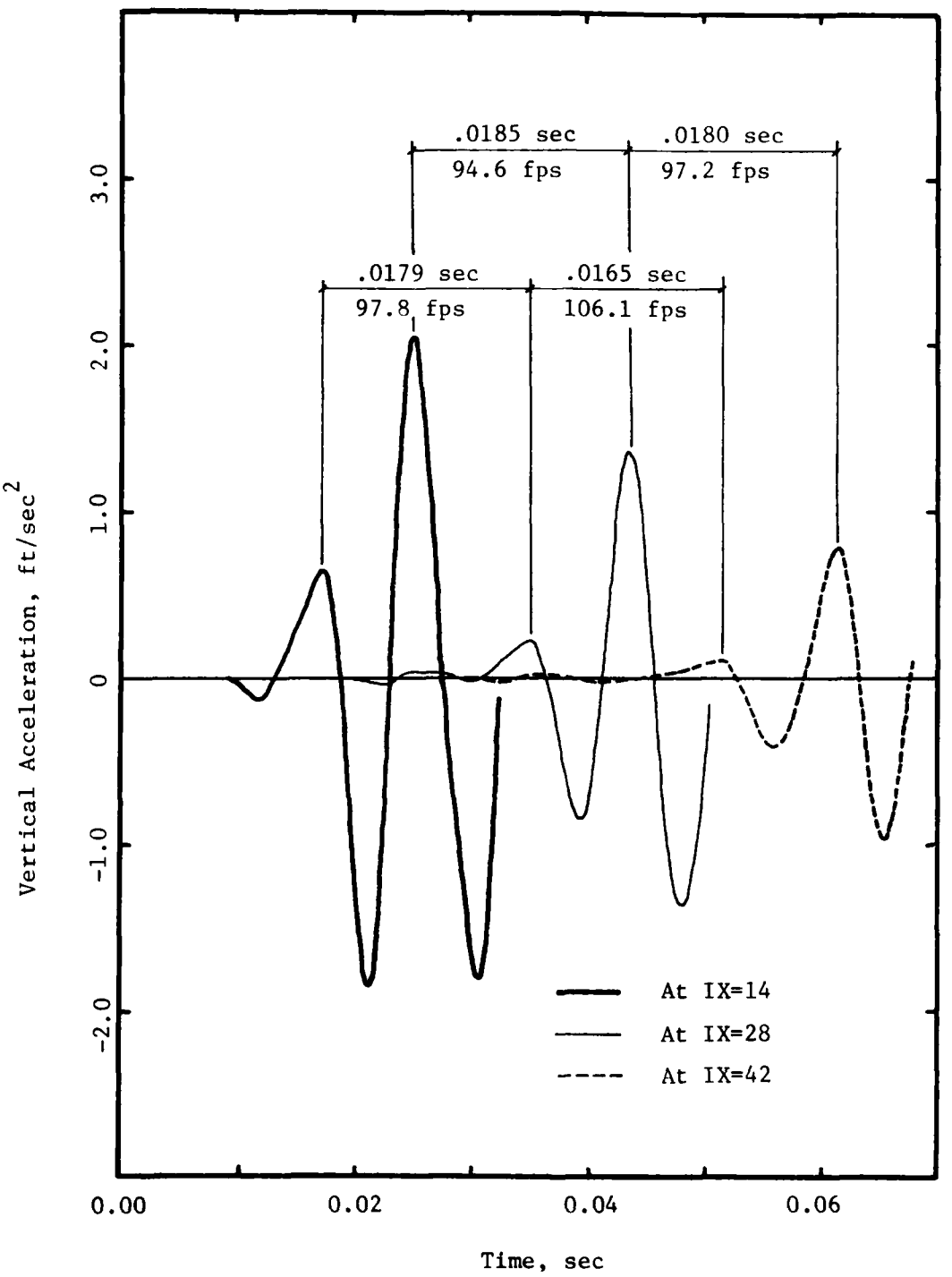

Fig. 2.30 - Inter-arrival Times and Corresponding Shear Wave Velocities from Accelerati n Curves. Free Boundaries. Three Rigid Inclusions.

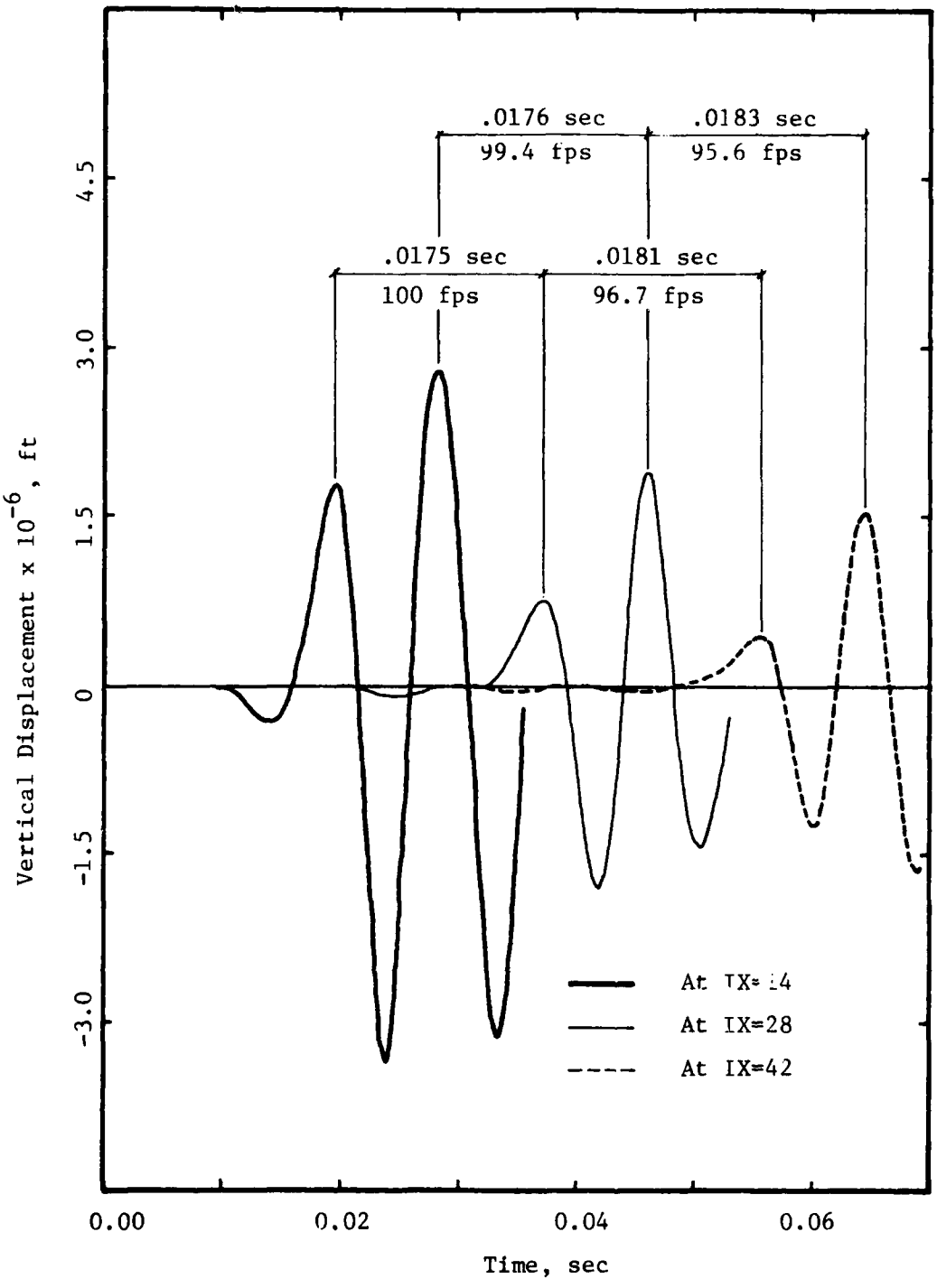

Fig. 2.31 - Inter-arrival Times and Corresponding Shear Wave Velocities from Displacement Curves. Fixed Boundaries. Three Rigid Inclusions.

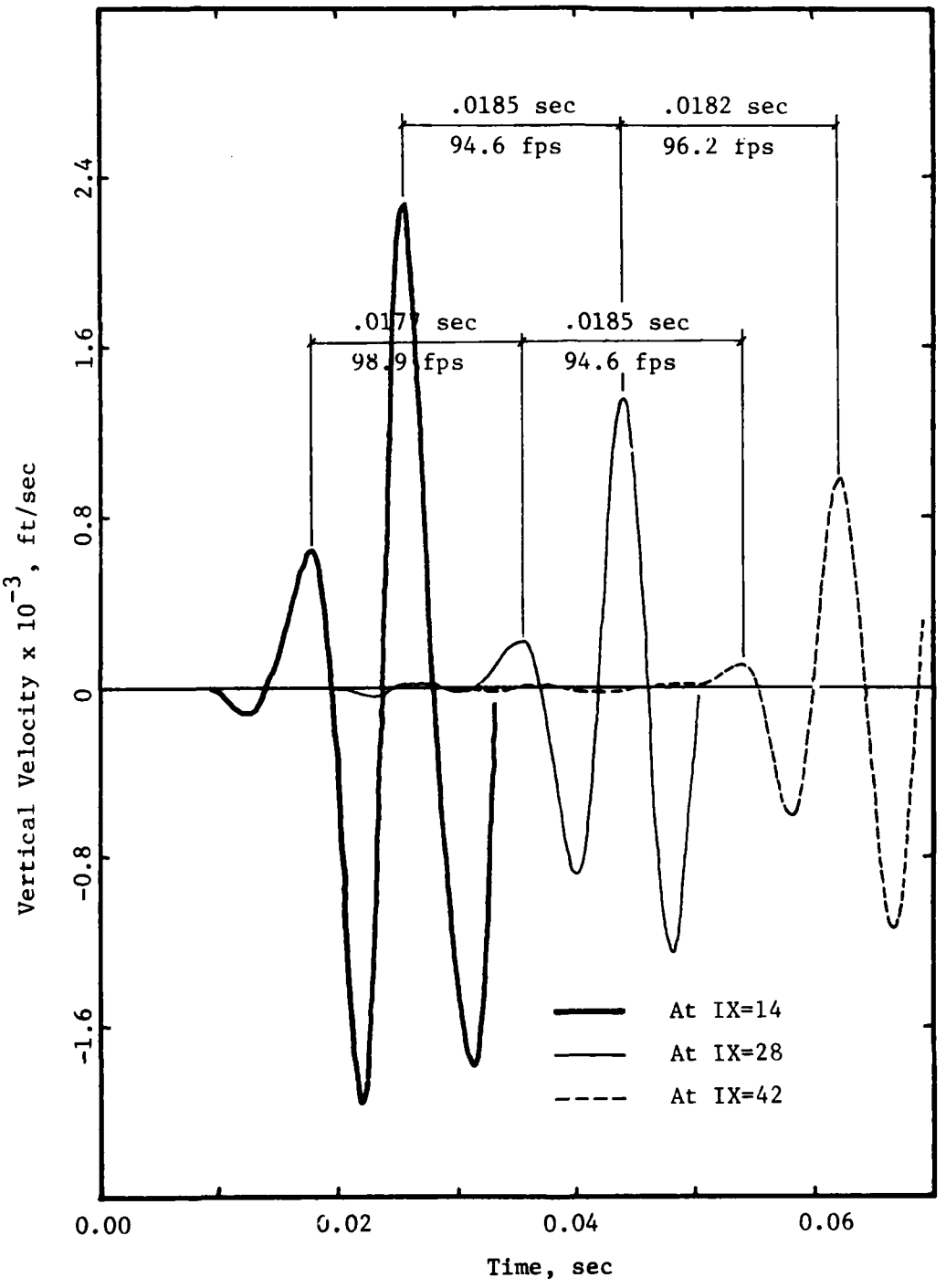

Fig. 2.32 - Inter-arrival Times and Corresponding Shear Wave Velocities from Velocity Curves. Fixed Boundaries. Three Rigid Inclusions.

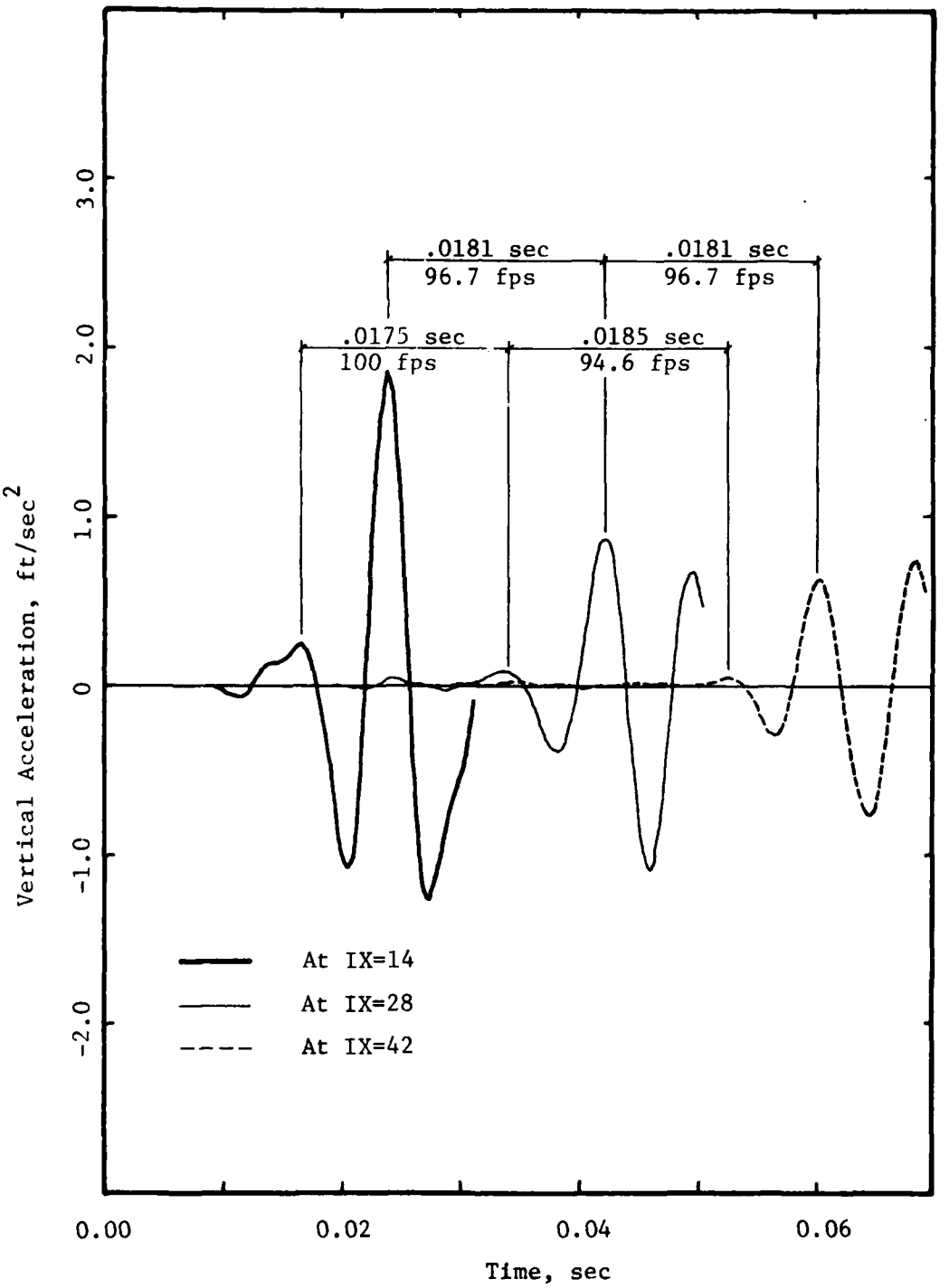

Fig. 2.33 - Inter-arrival Times and Corresponding Shear Wave Velocities from Acceleration Curves. Fixed Boundaries. Three Rigid Inclusions.

solution, since it involves a longer time of integration, the corresponding values are 96.7, 97.7, 96 and 96.5 ft/sec, respectively. These values are consistently smaller and less accurate (the actual shear wave velocity of the soil used in the analyses was 100 feet per second). It can also be noticed that the presence of the inclusions increases the value of the calculated shear wave velocity by about one percent at most.

Figures 2.34 to 2.36 illustrate better the effect of the rigid inclusions for the case of free boundaries and Figs. 2.37 to 2.39 for fixed boundaries. It can be seen that the shapes are practically the same for no inclusions, one inclusi n or three inclusions. Changes in the arrival times or position of the peaks are very small leading to differences in the estimated wave velocites of the order of one percent The main effect of the inclusions is a smoothing of the curves, particularly noticeable in the acceleration traces of the fixed boundary case, and a small reduction in amplitude (filtering). There is a reduction with a placement of a single inclusion at the center and an additional one with the placement of the other two inclusions. The filtering effect seems to be of the same nature and magnitude for both sets of boundary conditions.

2.4 EFFECT OF BOUNDARY CONDITIONS ON P-WAVES

Most of the studies conducted assumed a vertical, shear type excitation, since it was felt that determination of the shear wave velocity might present more problems than that of the P-wave. A number of cases were considered, however, with a horizontal, compressional type force which would generate primarily P-waves.

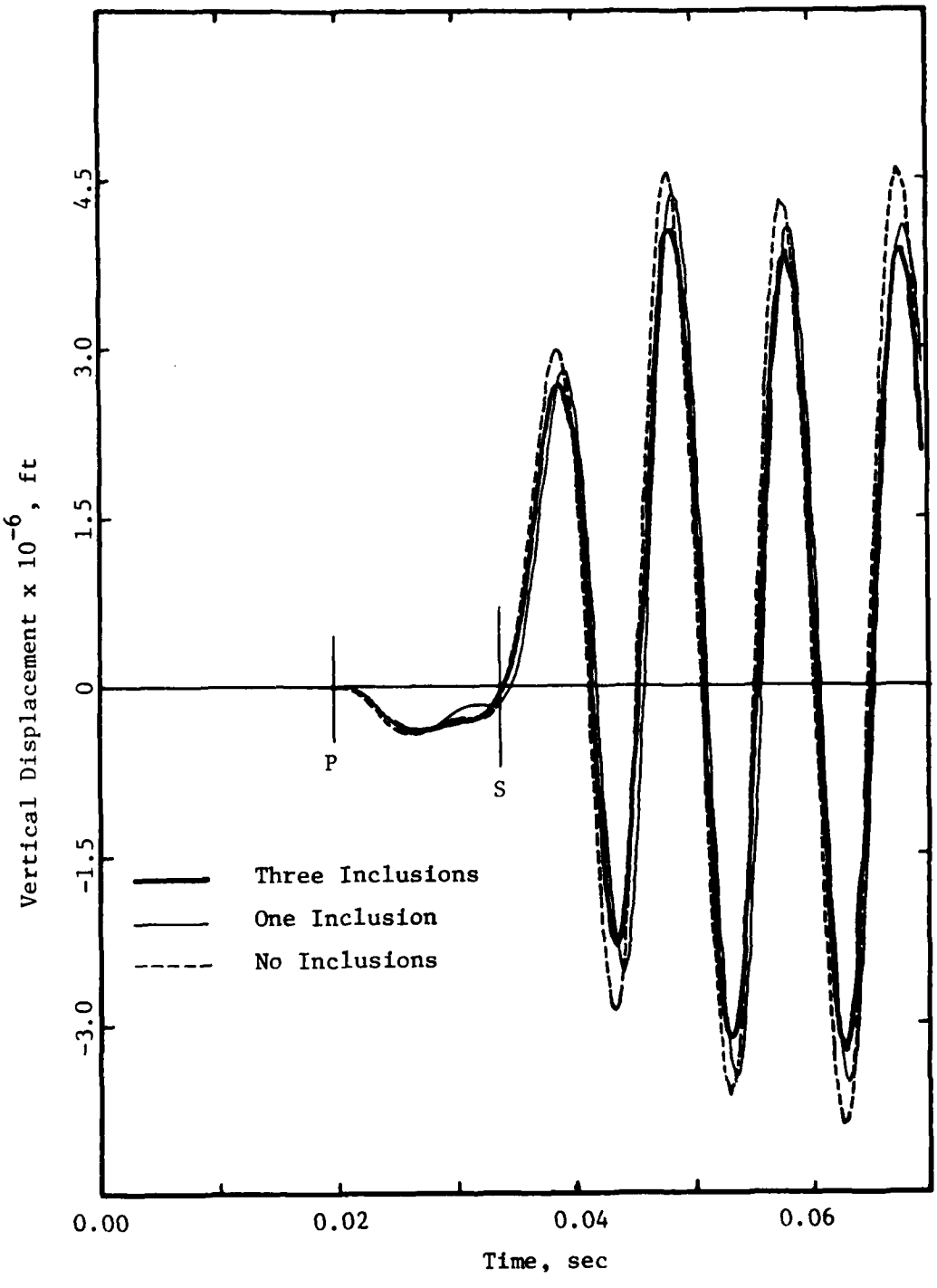

Fig. 2.34 - Free Field and Inclusion Displacements. Free Boundaries.

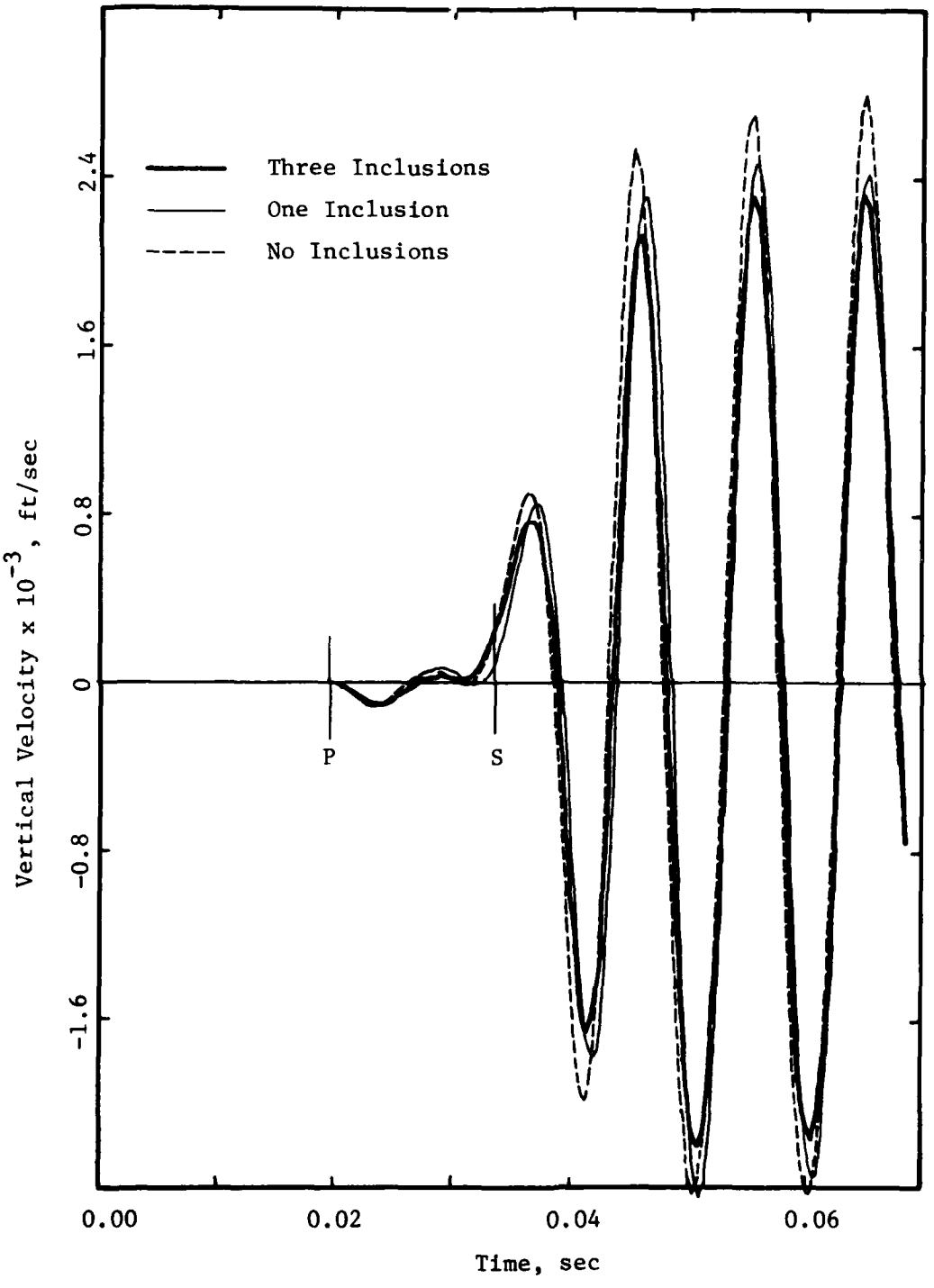

Fig. 2.35 - Free Field and Inclusion Velocities. Free Boundaries.

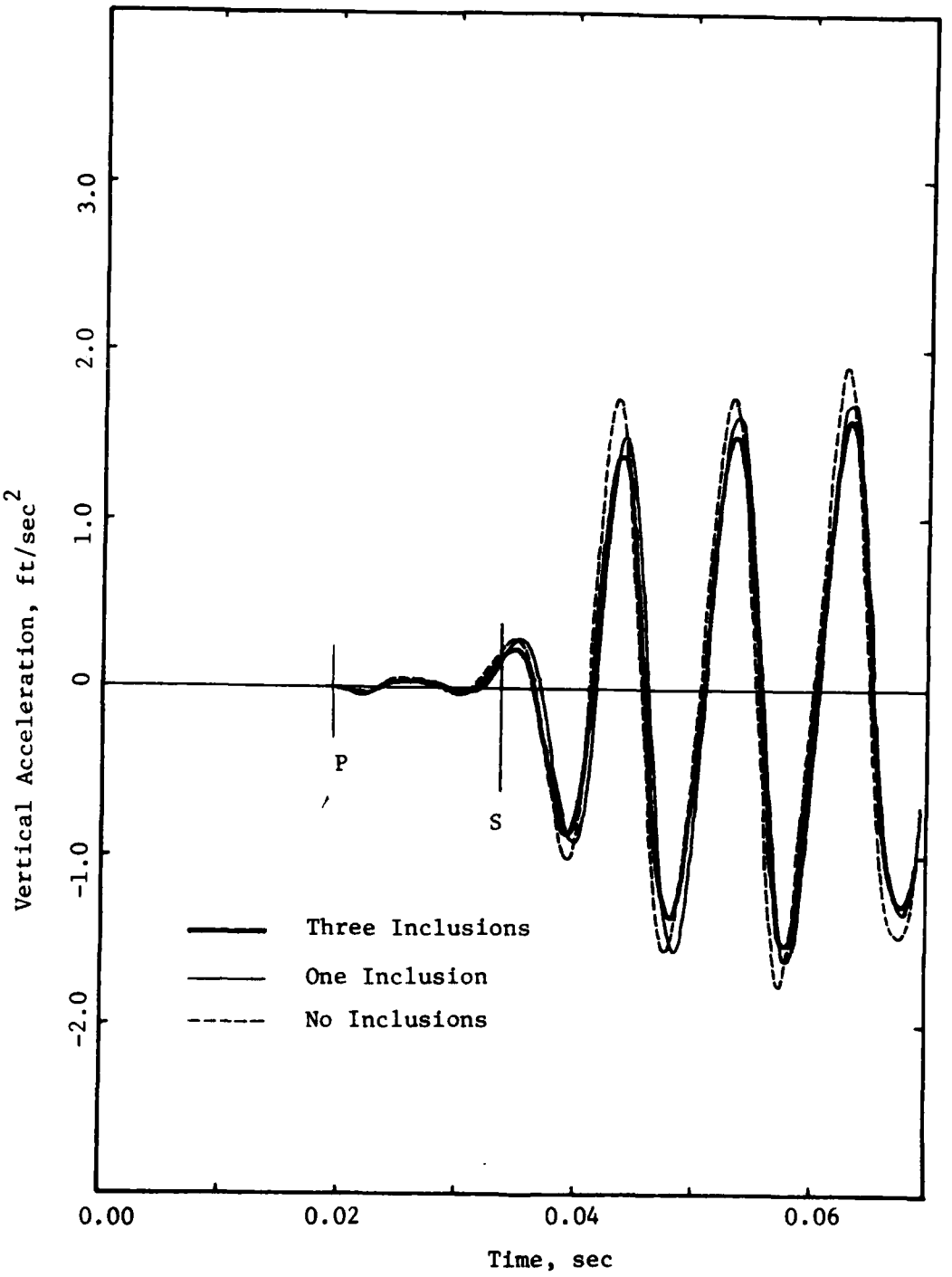

Fig. 2.36 - Free Field and Inclusion Accelerations. Free Boundaries.

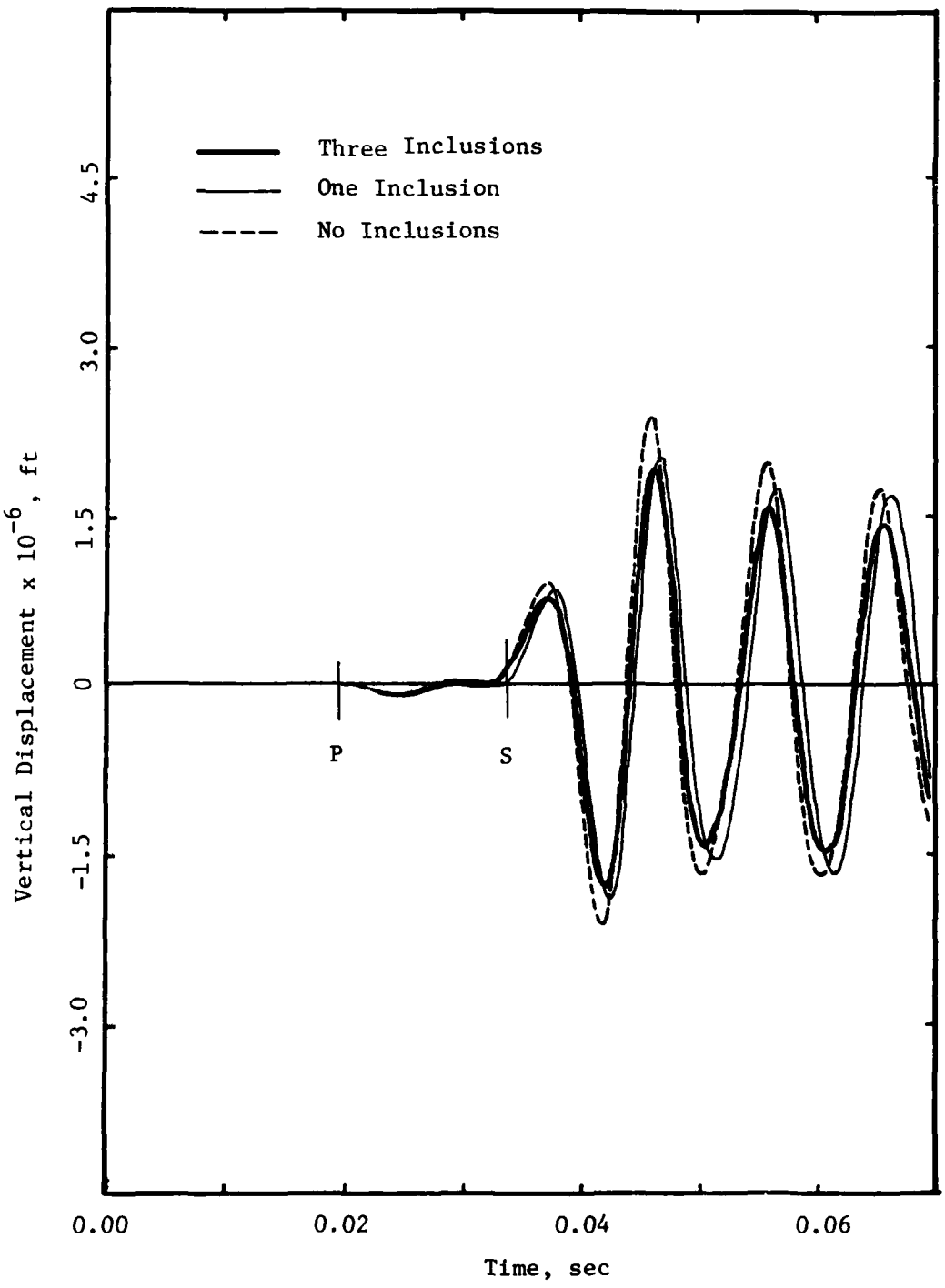

Fig. 2.37 - Free Field and Inclusion Displacement. Fixed Boundaries.

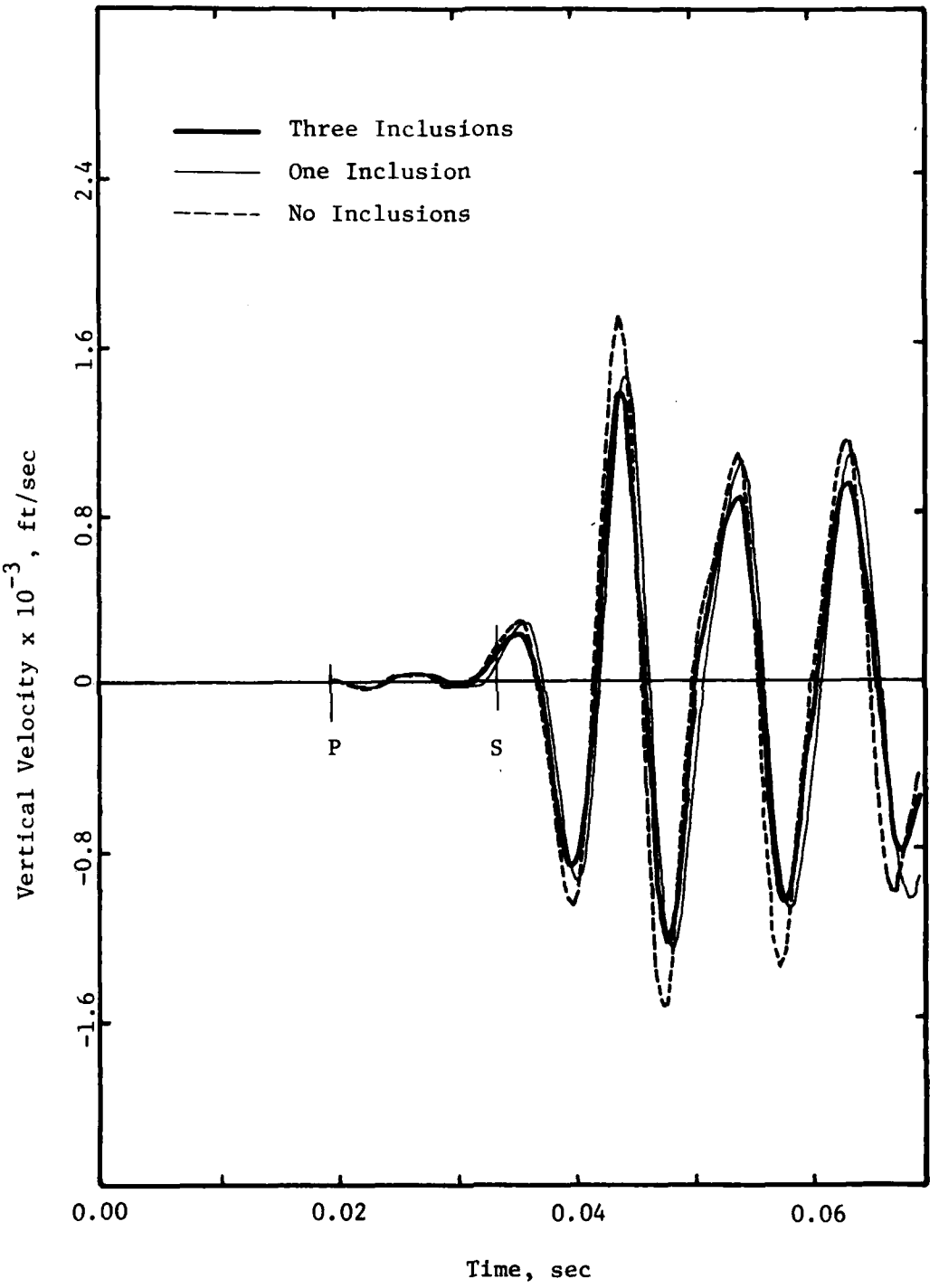

Fig. 2.38 - Free Field and Inclusion Velocities. Fixed Boundaries.

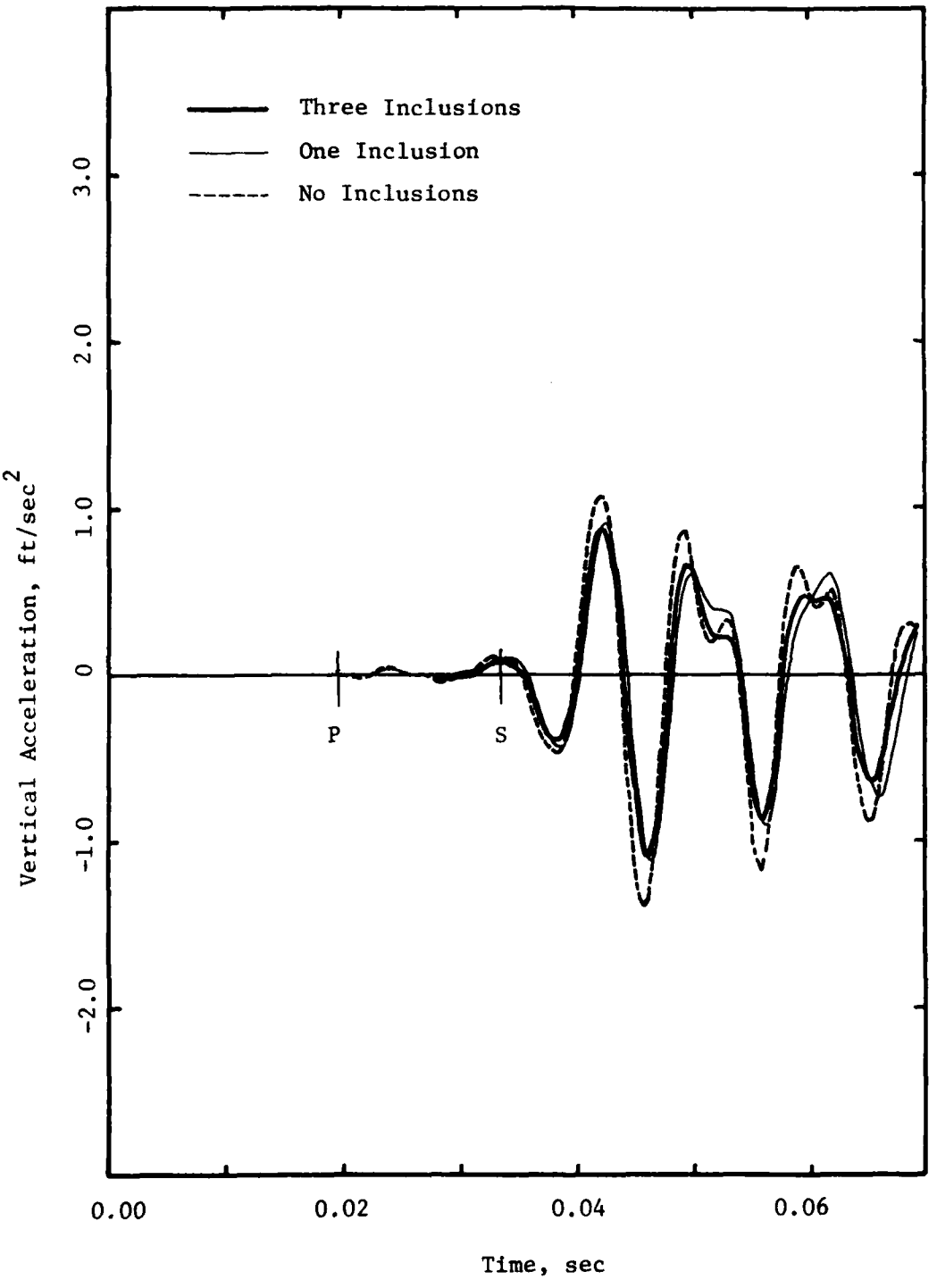

Fig. 2.39 - Free Field and Inclusion Accelerations. Fixed Boundaries.

Figures 2.40 to 2.42 show the time histories of the horizontal displacement, velocity and acceleration at target point IX28 (left corner of the middle inclusion), when there are no inclusions, for free and fixed boundaries. The motion starts now only slightly ahead of the theoretical arrival time, with a well defined beginning. All three (or six) curves start with a small positive curvature which can be attributed to the integration scheme. If the displacement curves were rounded at the start to make them approach more closely a half sinusoid, the theoretical arrival time of the P-wave would be predicted very well. For the velocity curves, on the other hand, the arrival time would correspond again more closely to the inflection point on the ascending branch, while for the acceleration it is just slightly ahead of the first peak. As in the case of S-waves, the first time of arrival would be easier to estimate from the displacement traces, which are smoother curves.

The motions for the model with free boundaries lag again behind those for fixed boundaries, except at the start where they are almost identical. On the other hand the amplitudes of motion are larger for fixed boundaries, contrary to what was observed for a shear type excitation.

The effect of the rigid inclusions is illustrated in Figs. 2.43 to 2.45, where the results for the cases of no inclusions, one inclusion and three inclusions are directly compared for the solution with free boundaries. The main effect is again a filtering of higher frequency components, particularly in the acceleration trace (Fig. 2.45) and a reduction in the amplitudes of motion.

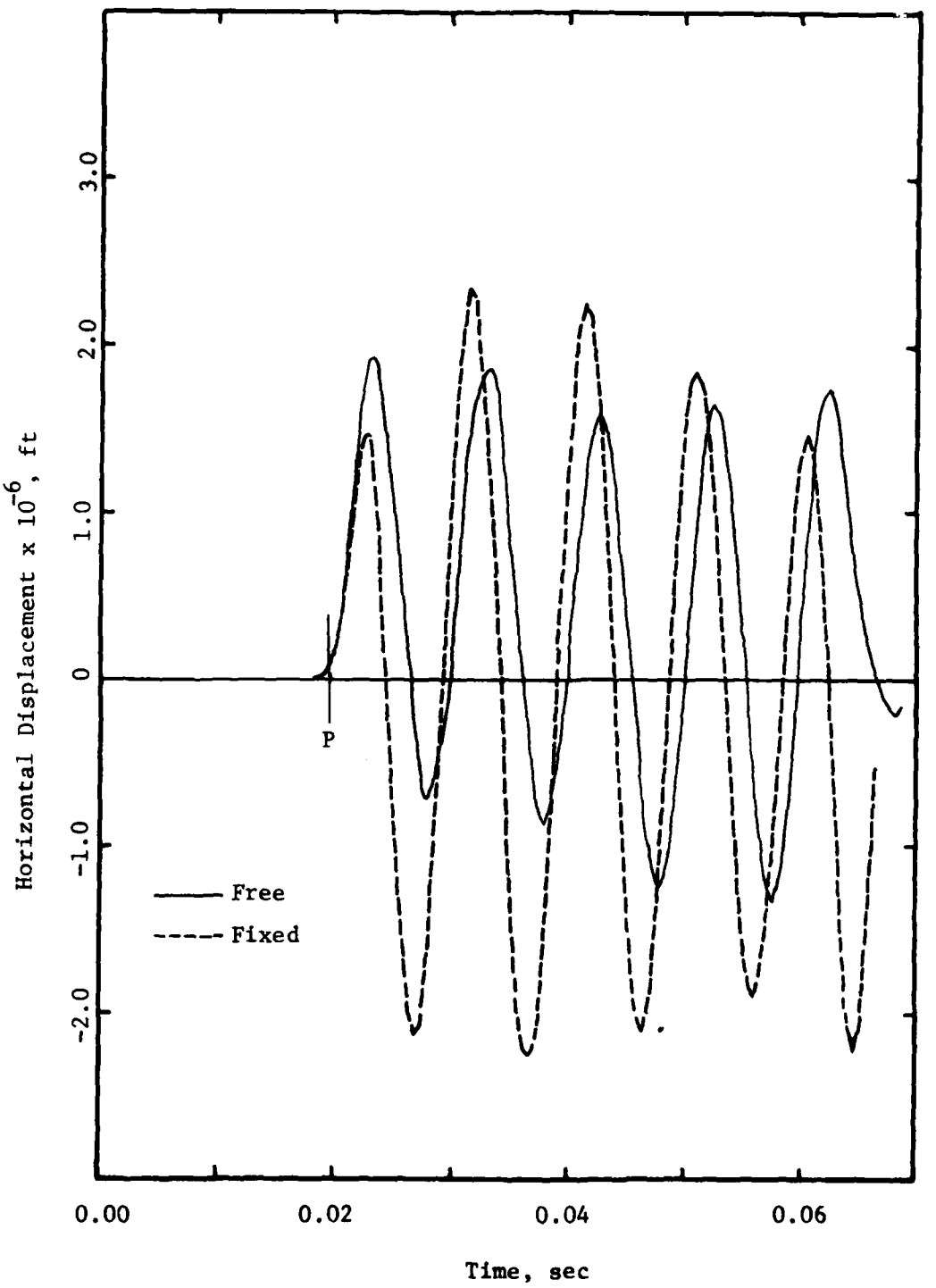

Fig. 2.40 - Horizontal Displacements at IX=28. Fixed and Free Boundaries. No Rigid Inclusions. P-wave.

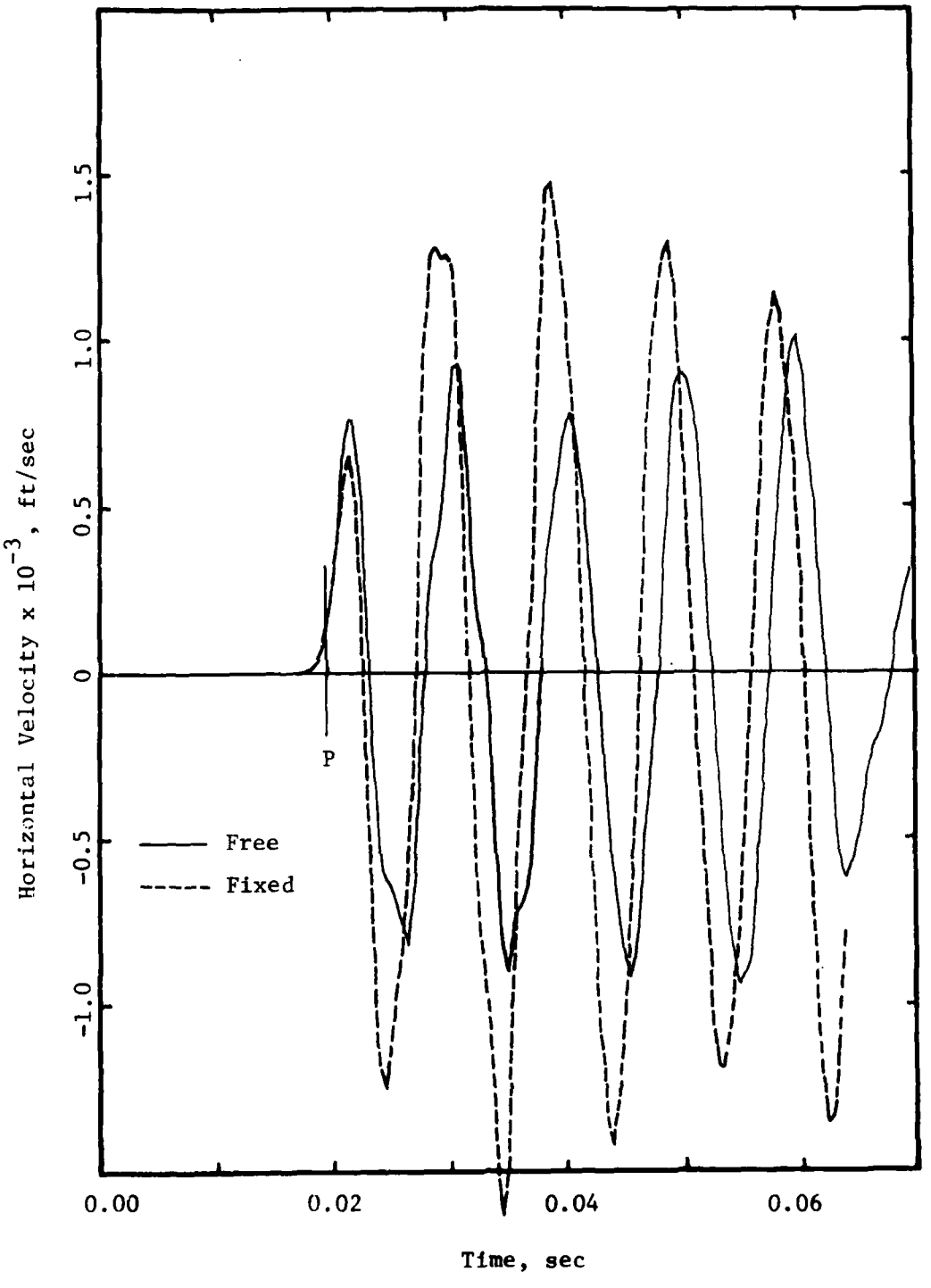

Fig. 2.41 - Horizontal Velocities at IX=28. Fixed and Free Boundaries. No Rigid Inclusions. P-wave.

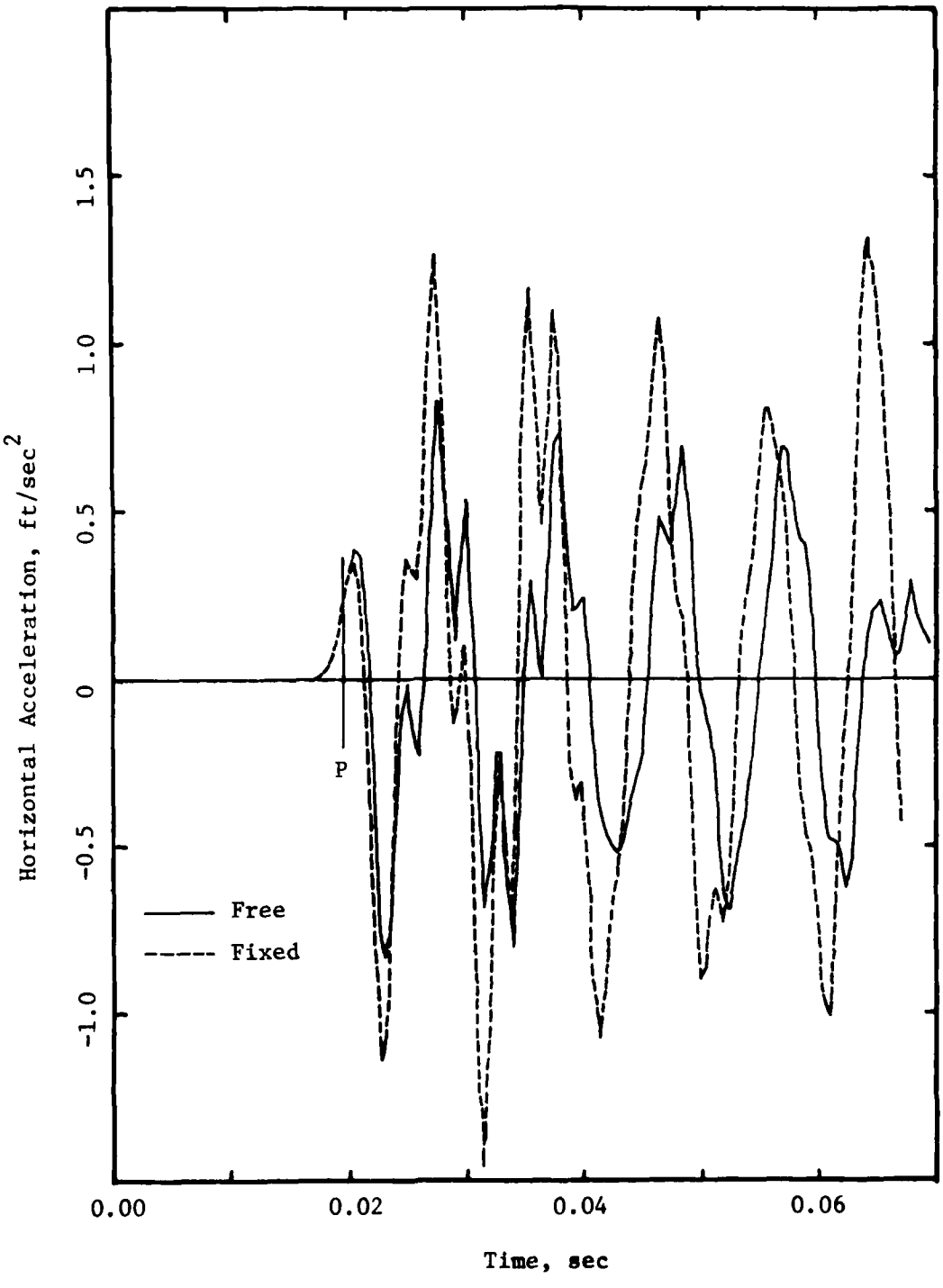

Fig. 2.42 - Horizontal Accelerations at IX=28. Fixed and Free Boundaries. No Rigid Inclusions. P-wave.

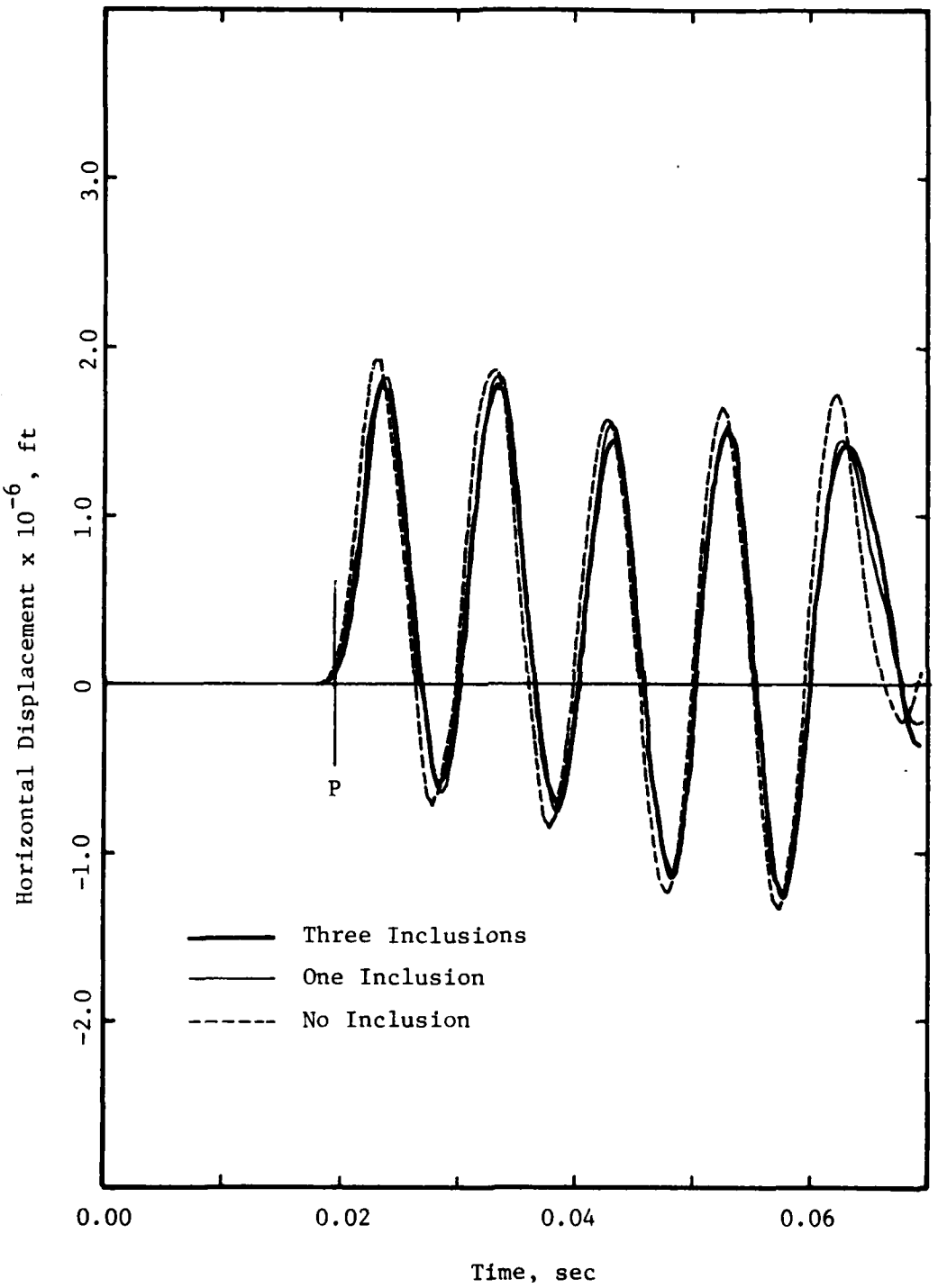

Fig. 2.43 - Free Field and Inclusion Displacement. Free Boundaries. P-wave.

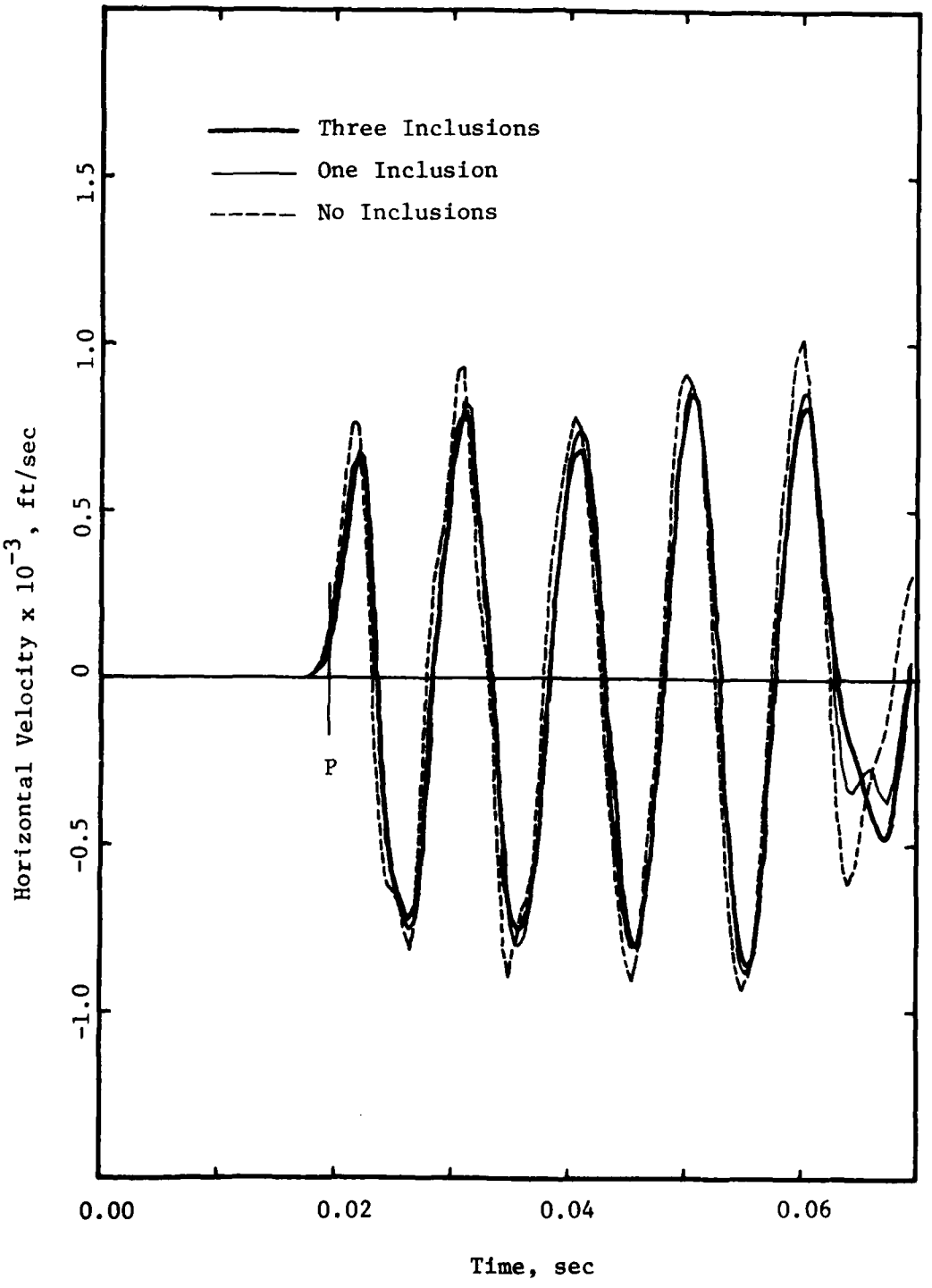

Fig. 2.44 - Free Field and Inclusion Velocities. Free Boundaries. P-wave.

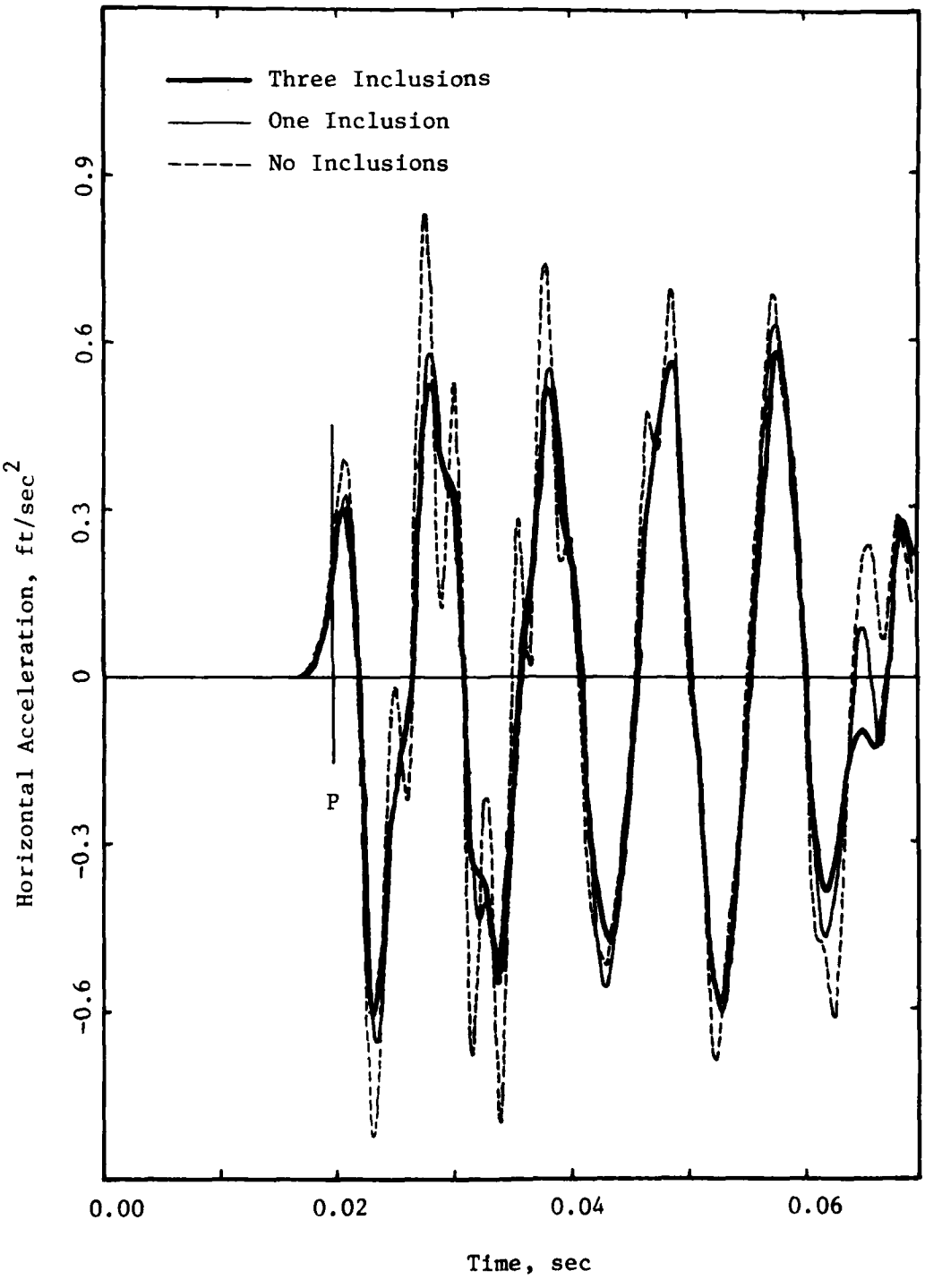

Fig. 2.45 - Free Field and Inclusion Accelerations. Free Boundaries. P-wave.

CHAPTER 3

EFFECT OF TYPE OF EXCITATION

3.1 INTRODUCTION

As mentioned in Chapter 1, most studies were conducted attempting to simulate the conditions existing in the cube during the experimental work. As a result the loads were applied over a small area, simulating more closely a point source and a spherical wave front (cylindrical for the two-dimensional model) than a plane wave. Under these conditions vertical motions due to a vertical, shear type excitation, were starting at the time of arrival of the P-waves. To determine to what extent this was due to the type of excitation, and reproduced therefore the physical reality, or to noise introduced by the discretization and the integration scheme, additional studies were conducted changing the type of excitation. Three different situations were considered: one in which the point excitation was replaced by equal forces at all points on the left boundary simulating a uniformly distributed harmonic force; a second one with still a point load but preventing the horizontal displacement of all nodes; and a third one with the distributed load and the same constraints on the nodal displacements. The results for each one of these models are discussed in the following sections. In all cases the free boundary conditions were applied,and it was assumed that there were no inclusions.

3.2 UNIFORMLY DISTRIBUTED EXCITATION

The model used in this case was the same discussed in Chapter 2 for free boundaries, the only difference being in the applied loads.

The nodal forces were scaled down so as to have the same magnitude of total load.

Figures 3.1 and 3.2 compare the time histories of accelerations at the target points IX14 and IX28 for the point load and the distributed force. It can be seen that with the distributed excitation the small motion that started at the time of arrival of the P-wave no longer exists. The motion starts still a little early, with a positive curvature, but if the curve were to be rounded to approximate a half sinusoid, the starting point would almost coincide with the theoretical time of arrival of the S-wave (in spite of the fact that these are acceleration traces). The motion is nearly a perfect sinusoid with constant amplitude, particularly for the second target point. The amplitude of motion is smaller than for the case of a concentrated load, as could be expected, and the peaks are slightly out of phase, occurring later for the distributed load.

3.3 POINT EXCITATION WITH NO HORIZONTAL DISPLACEMENTS

In this second case the point excitation is again used but all nodes are forced to move in vertical planes (vertical lines actually) to simulate the kind of motion that would take place under a plane shear wave travelling in the horizontal direction.

Figures 3.3 and 3.4 show again the vertical accelerations at the target points IX14 and IX28, for this case and the standard solution of Chapter 2. It can be seen that when horizontal displacements are prevented the motion no longer starts at the time of arrival of the P-waves. It starts, however, substantially before the theoretical

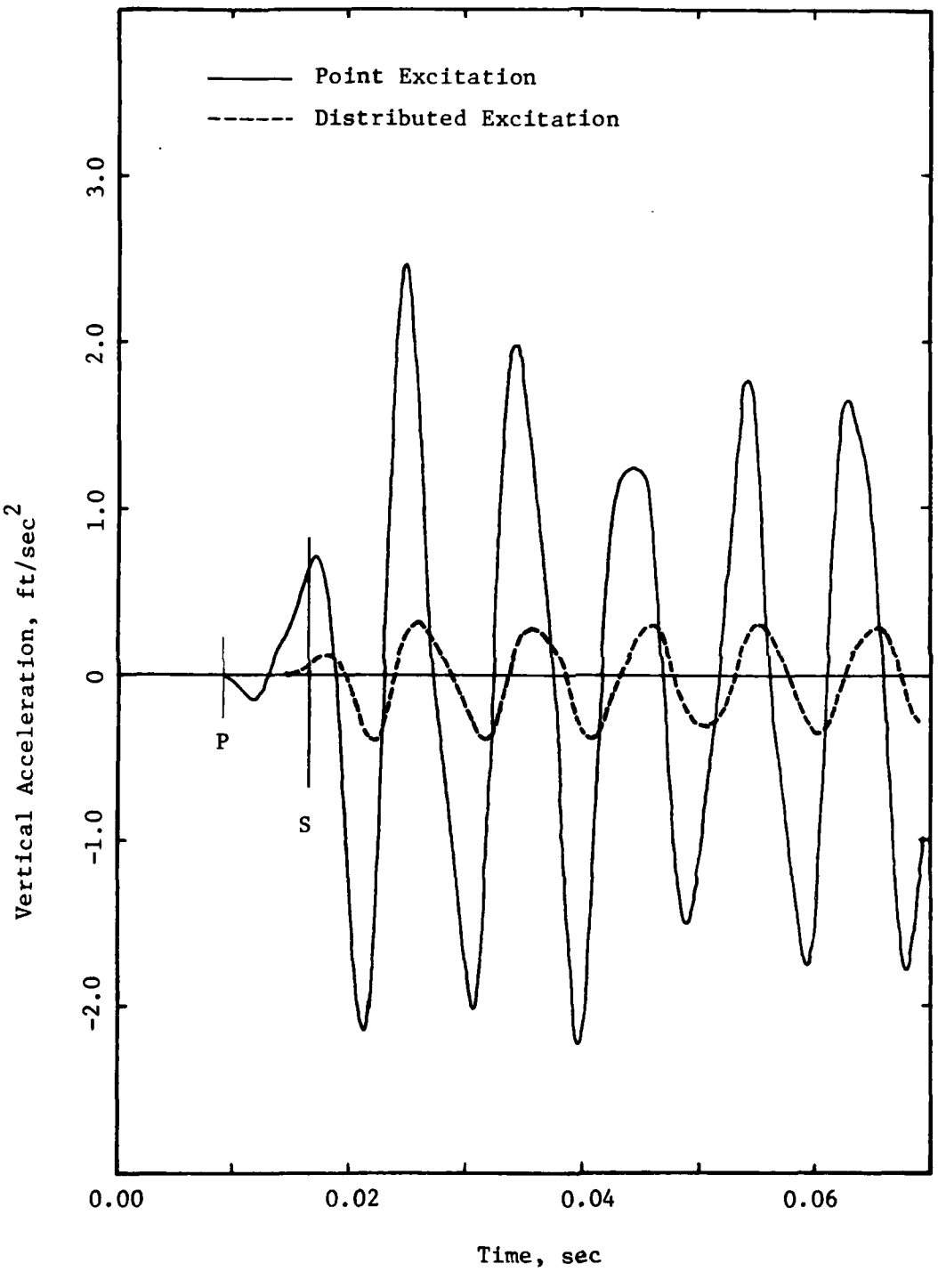

Fig. 3.1 - Vertical Accelerations at IX=14. Point Excitation and Uniformly Distributed Excitation.

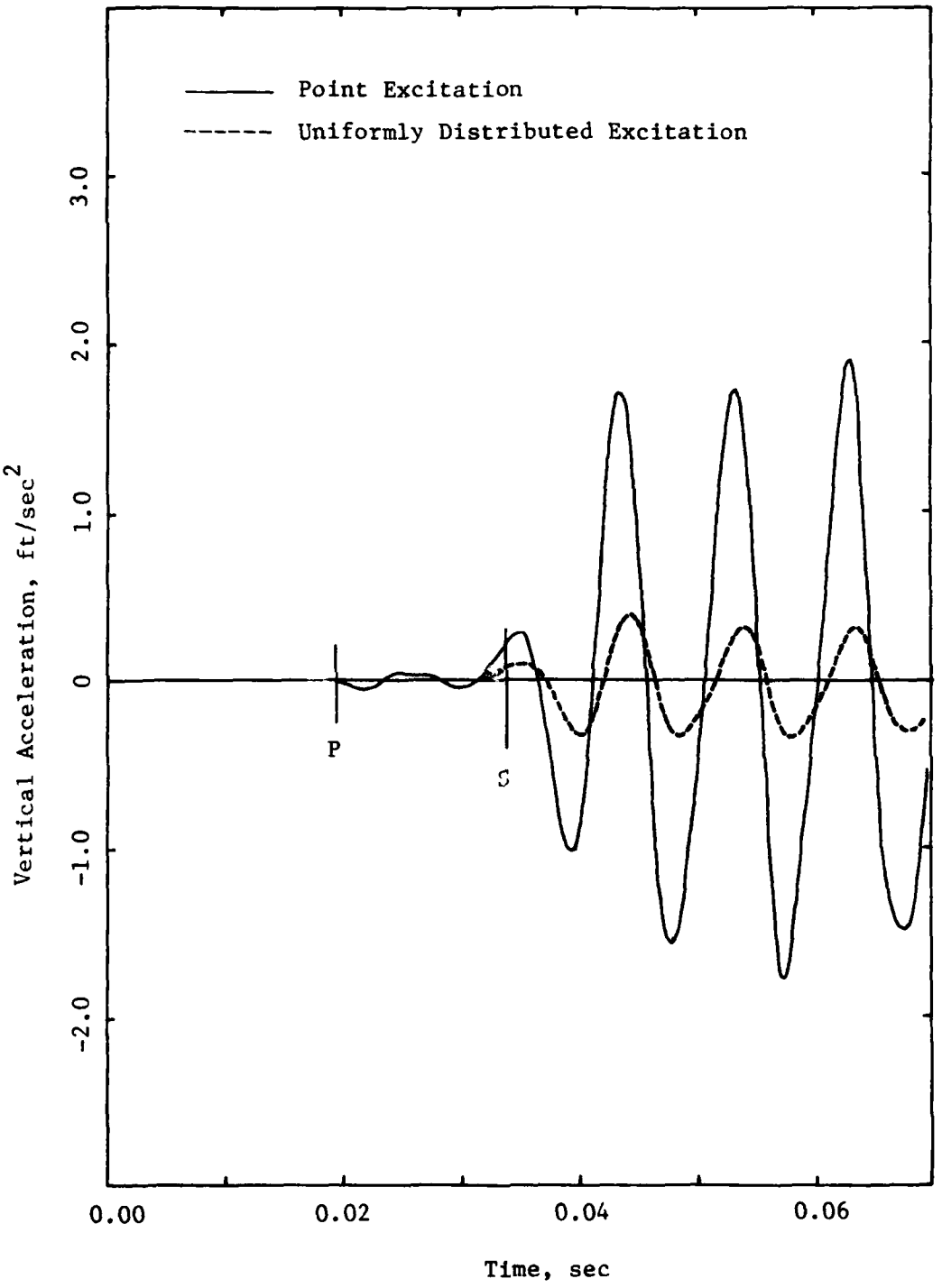

Fig. 3.2 - Vertical Accelerations at IX=28. Point Excitation and Uniformly Distributed Excitation.

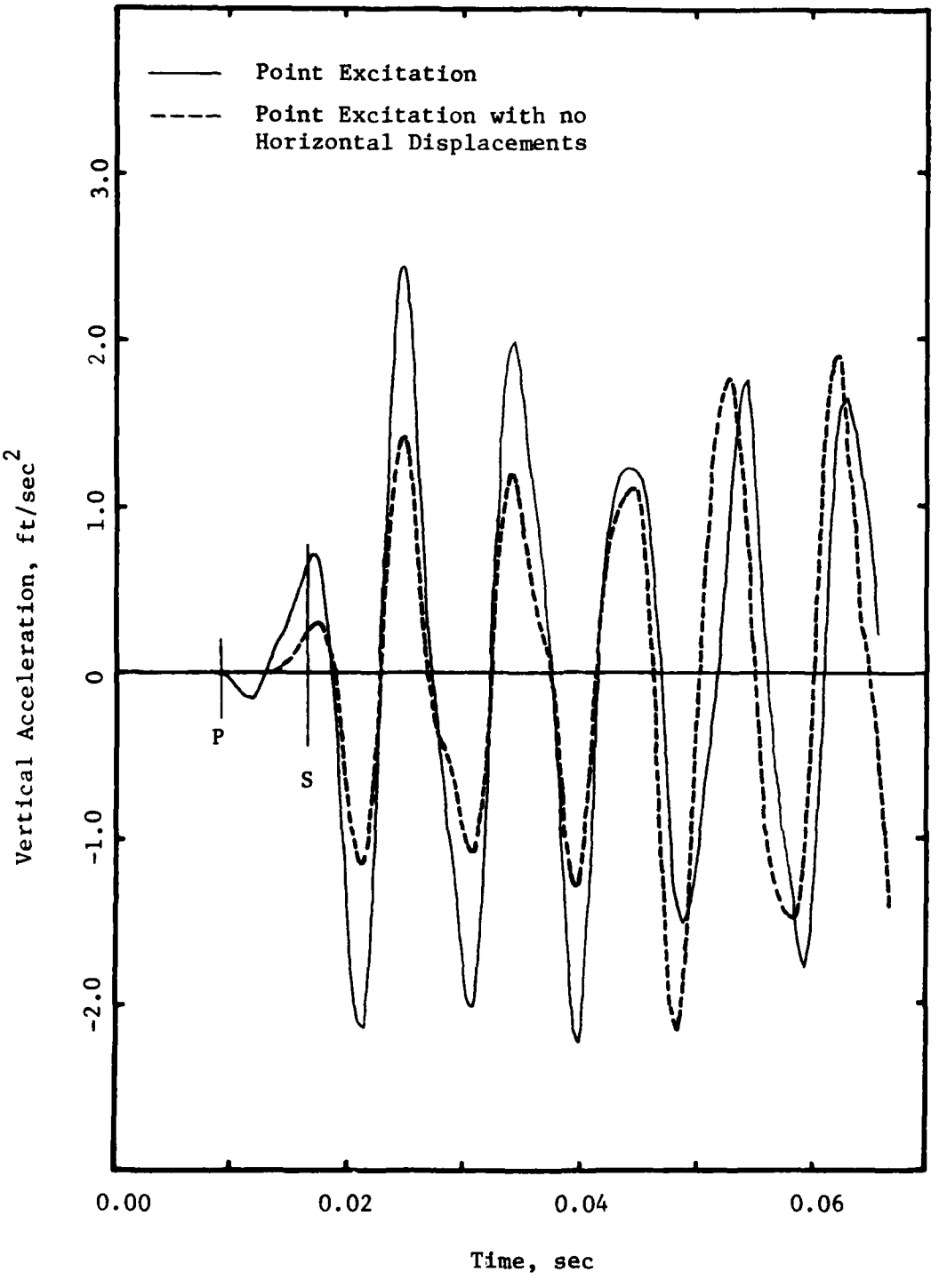

Fig. 3.3 - Vertical Accelerations at IX=14. Point Excitation with and without Restrains on Horizontal Movement.

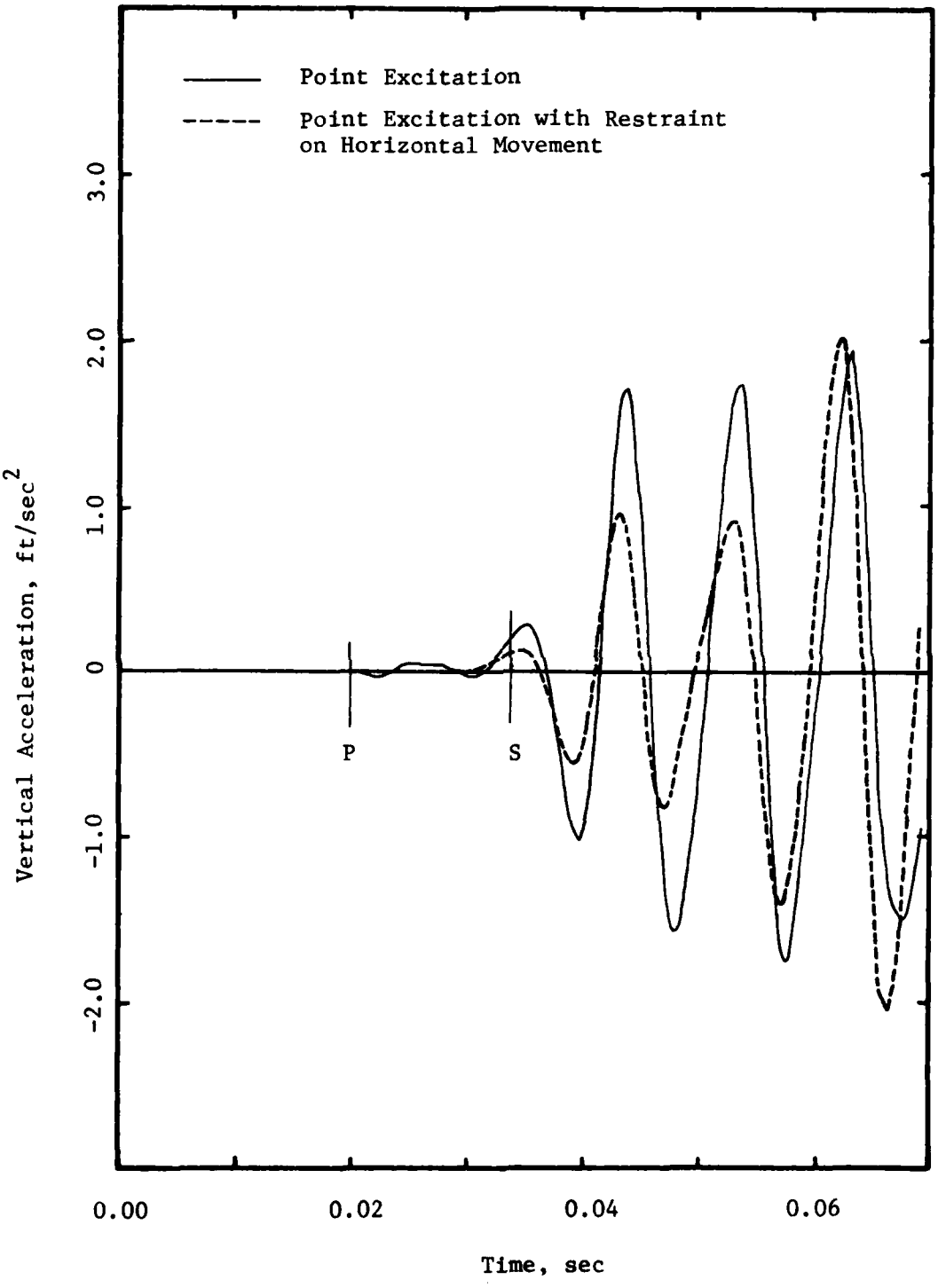

Fig. 3.4 - Vertical Accelerations at IX=28. Point Excitation With and Without Restrains on Horizontal Movements.

S-wave arrival time. For the first few cycles the motion is nearly in phase with the results without displacement constraints. As a consequence the theoretical time of arrival of the S-wave is still relatively close to the first peak. For later cycles the constrained solution is slightly ahead of the standard one, but their amplitudes tend to be more similar.

Preventing horizontal displacements but applying still a concentrated force does not eliminate enirely volumetric deformations. The motions are not as smooth and regular as for the case of a distributed force.

3.4 UNIFORM LOAD WITH NO HORIZONTAL DISPLACEMENTS

The changes introduced in the model in the previous two sections were combined, using a uniformly distributed excitation on the left face (instead of a point force) and preventing at the same time the hroizontal displacements of all the nodes. The reuslts are shown in Figs. 3.5 and 3.6 and are almost identical to those obtained in Section 3.2 (uniform load but no displacement constraints). The motion resembles again a sinusoidal curve with uniform amplitude and starts only slightly ahead of the theoretical time. Figure 3.7 compares the results at IX28 with those of Section 3.2 indicating that the enforcement of only vertical displacements has very little effect when the applied loads are uniformly distributed over the left face (it should have no effect at all for a pure plane shear wave travelling in the horizontal direction).

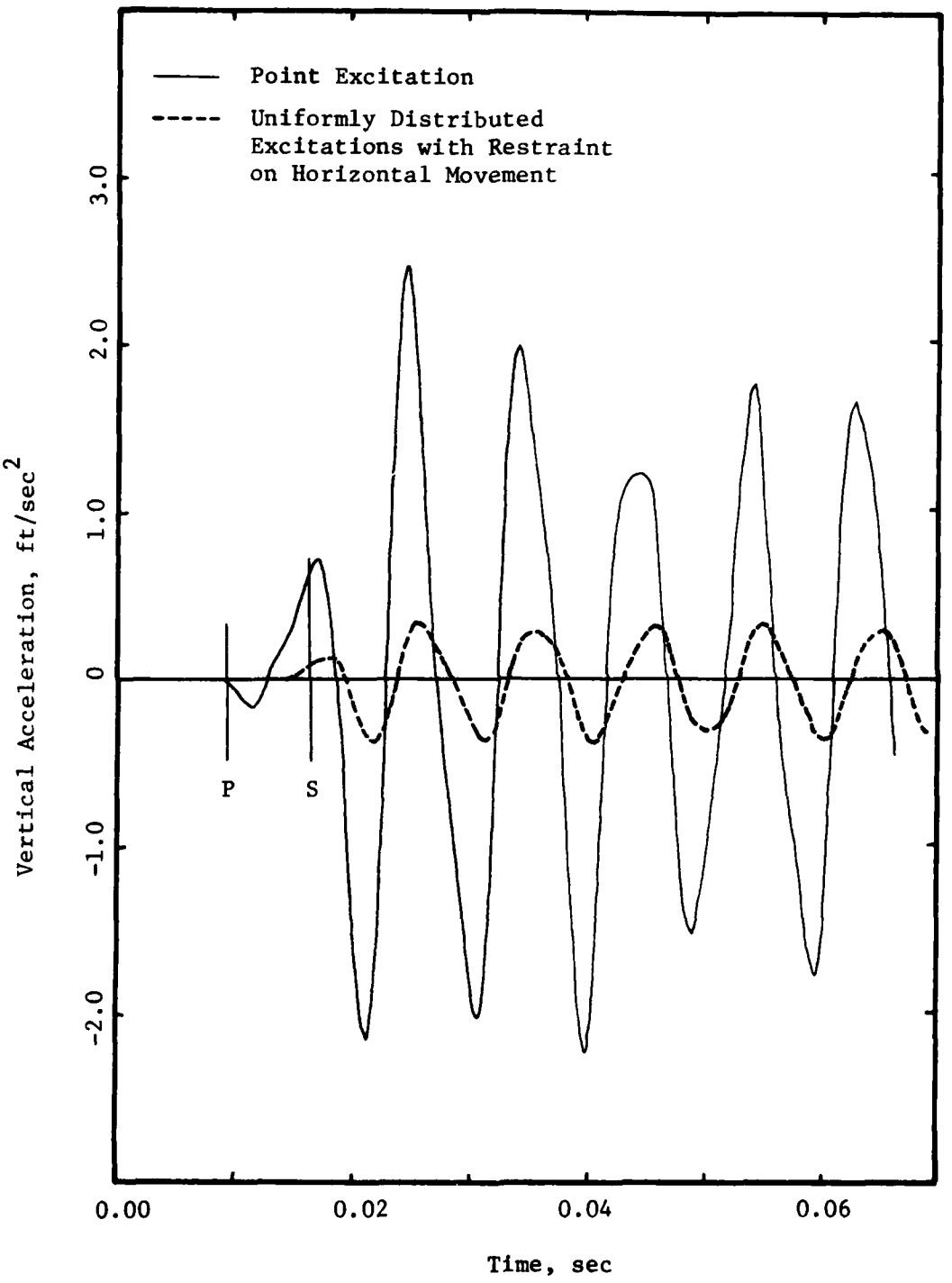

Fig. 3.5 - Vertical Accelerations at IX=14. Point Excitation and Uniformly Distributed Excitation with Restraints on Horizc tal Movement.

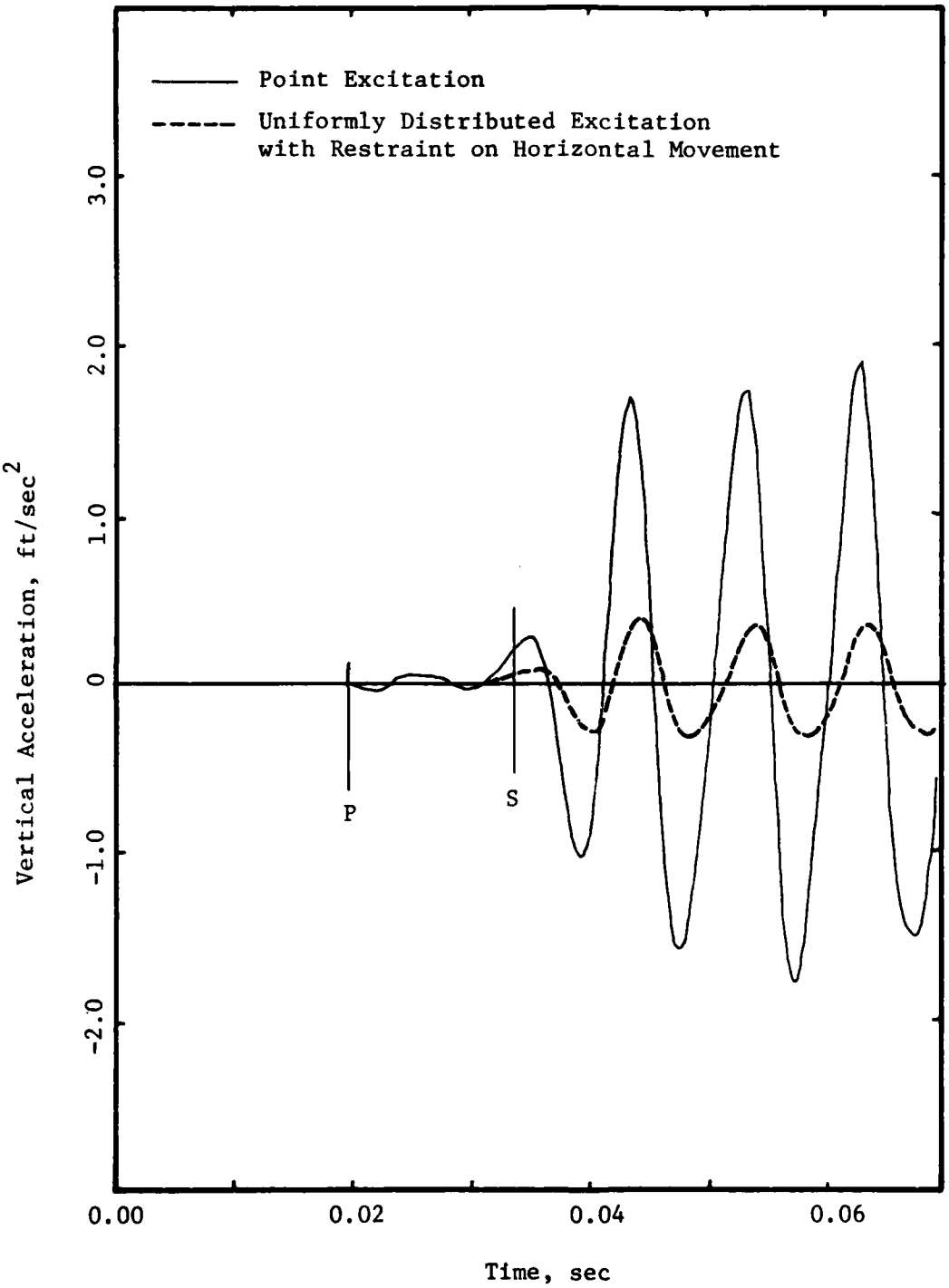

Fig. 3.6 - Vertical Accelerations at IX=28. Point Excitation and Uniformly Distributed Excitation with Restraints on Horizontal Movement.

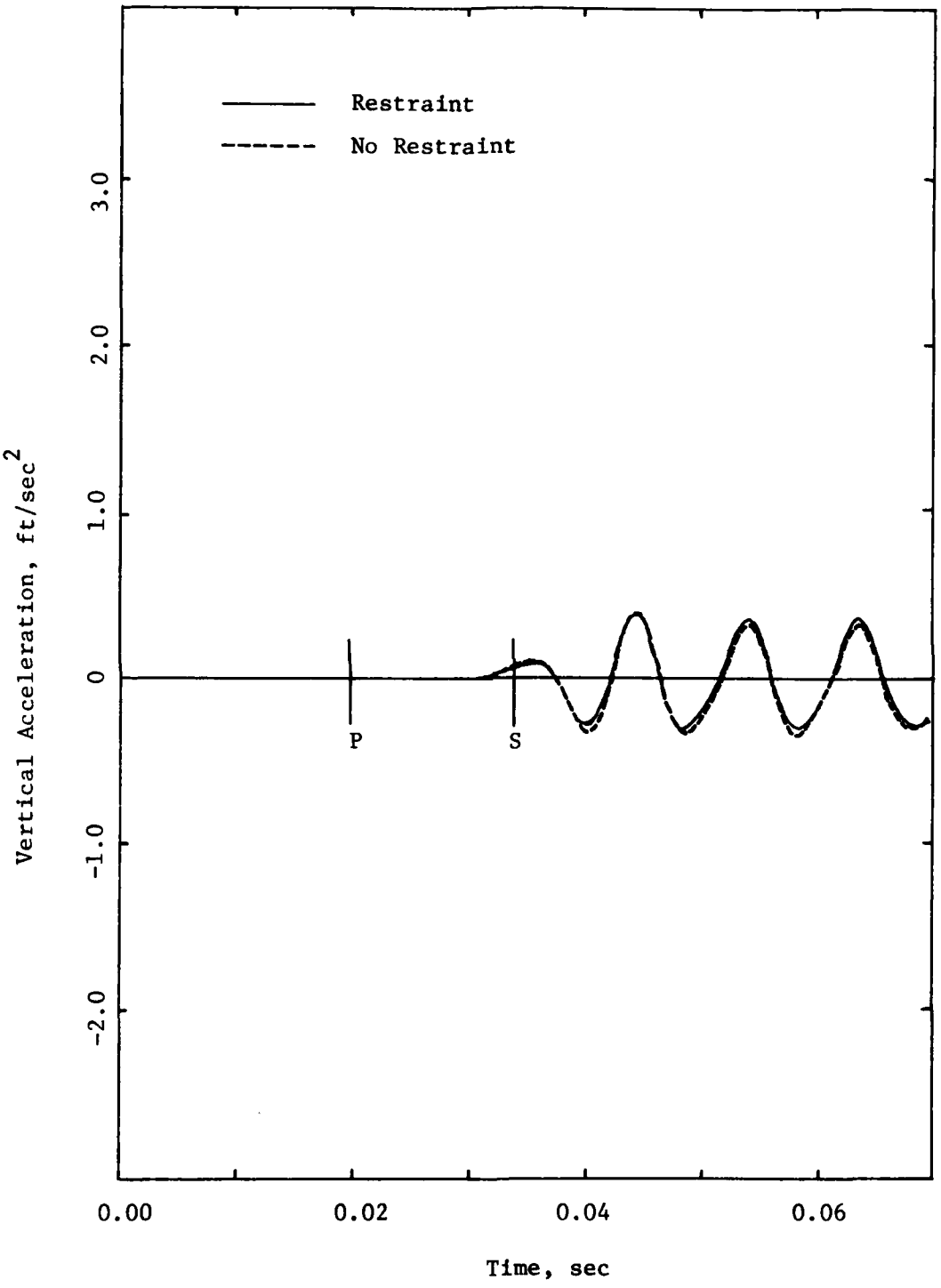

Fig. 3.7 - Vertical Accelerations at IX=28. Uniformly Distributed Excitations with and without Restrains on Horizontal Movement.

CHAPTER 4

EFFECT OF WAVELENGTH

4.1 INTRODUCTION

All studies described in the previous chapters and the first report were based on a sinusoidal excitation with a frequency of 650 rad/sec, corresponding to a wavelength of about one foot (1.03 ft actually). This value was selected because the wavelength is approximately eight times the size of the inclusion, and it was felt it would be the shortest wavelength used in the experiments. The effect of the inclusions should be even smaller for longer wavelengths (smaller frequencies) but the effect of the boundaries (finite dimensions of the cube) could be more pronounced. The size of the inclusions is also the size of each element in the finite element mesh. With eight elements per wavelength, the numerical results should still have good accuracy. It is commonly accepted that in dynamic analyses with fi ite elements the element size should be smaller than 1/4 to 1/6 of the wavelength to obtain reasonable answers. This implies that somewhat higher frequencies could be used with the model implemented, but a frequency of 1250 rad/sec would be a practical upper limit.

Additional analyses were conducted using two different frequencies of excitation: a frequency of 325 rad/sec, corresponding to a wavelength of approximately 2 ft (or 16 times the inclusion size), and a frequency of 975 rad/sec, corresponding to a wavelength of about 0.65 ft (about five times the size of the inclussion). In this chapter, these frequencies will be referred to as 'low' and 'high' frequencies, respectively.

The 650 rad/sec used in the other studies will be considered as the 'normal' frequency. For these new analyses only the case with free boundary conditions was considered.

4.2 AMPLITUDE AND SHAPE OF WAVES

Figures 4.1 and 4.2 show the displacement, velocity and acceleration records at the point of excitation for the low-frequency and high-frequency excitations, respectively. These results are directly comparable to those in Fig. 2.3 for the normal frequency. The shapes and the general characteristics of the motions are similar, and the observations made in Chapter 2 would seem to apply to all three frequencies. The acceleration trace for the low-frequency excitation shows, however, higher frequency components, which are particularly clear in the first cycles and appear to get smoothed out in the following ones.

The displacement, velocity and acceleration at the central target point IX28 are shown in Figs. 4.3 to 4.5 for all three frequencies. The amplitude of the first positive displacement peak increases markedly as the frequency decreases. This is still true for the velocity and even for the acceleration although the increase is smaller in each case. The first acceleration peak is poorly defined for the high-frequency excitation. For the following peaks the amplitude of the displacement seems to be largest for the normal frequency and smallest for the high frequency but there are not enough cycles of the low frequency response for a meaningful comparison (the displacement amplitude at low-frequency could in fact be larger). The normal frequency has clearly the largest amplitude of motion in the velocity

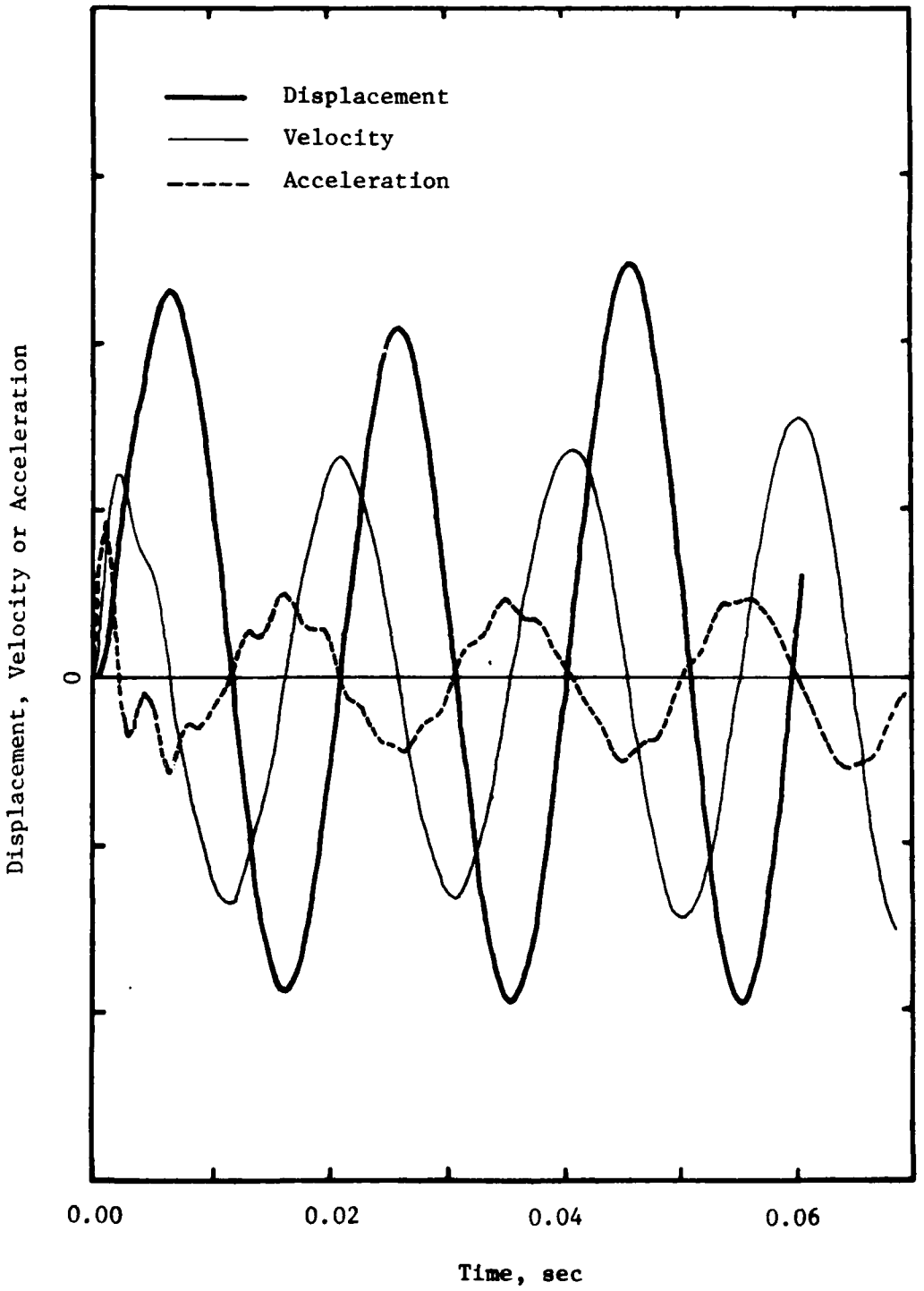

Fig. 4.1 - Displacement, Velocity and Acceleration at the Point of Excitation. Free Boundaries. No Rigid Inclusions. Low Frequency.

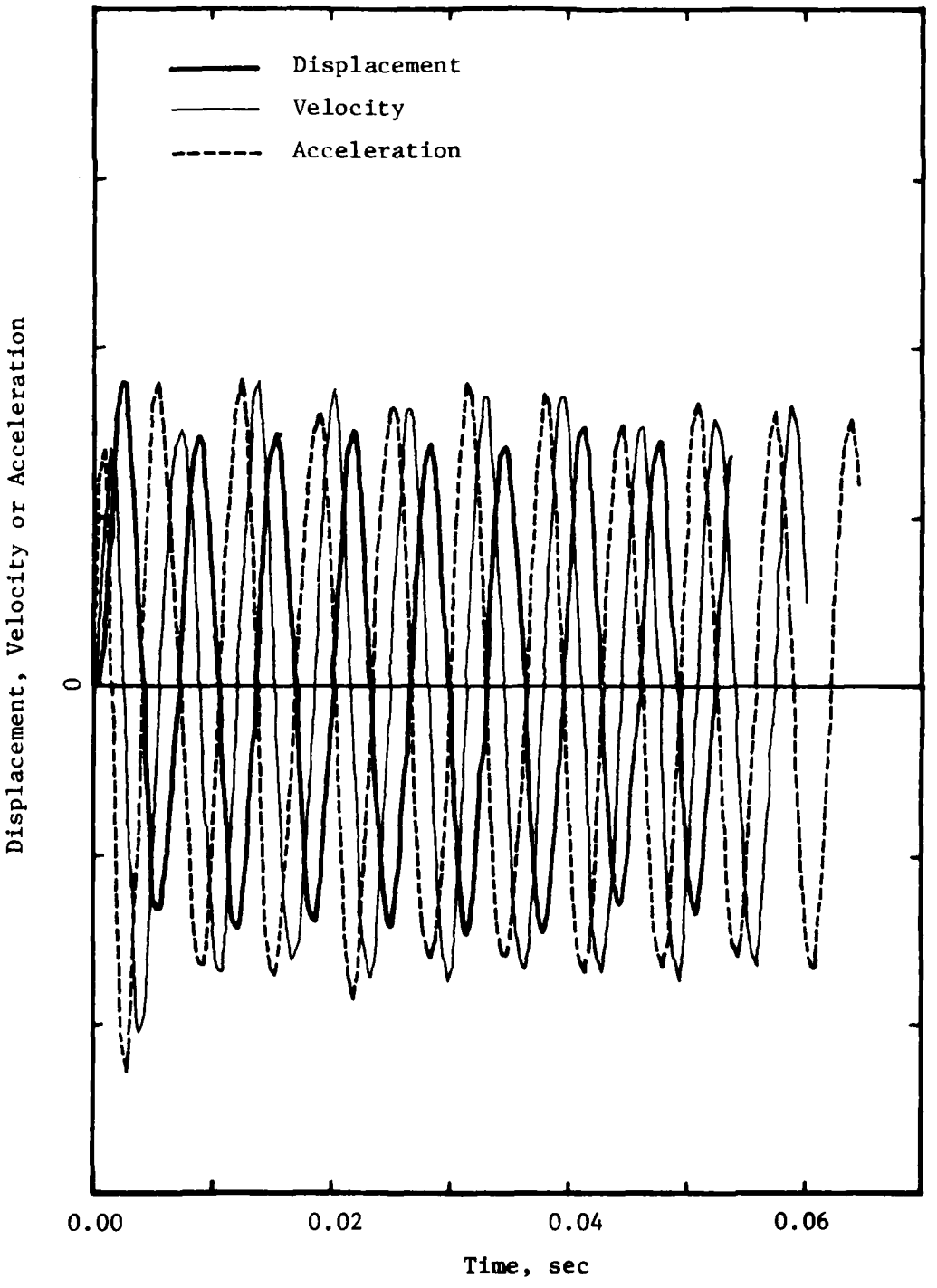

Fig. 4.2 - Displacement, Velocity and Acceleration at the Point of Excitation. Free Boundary. No Rigid Inclusions. High Frequency.

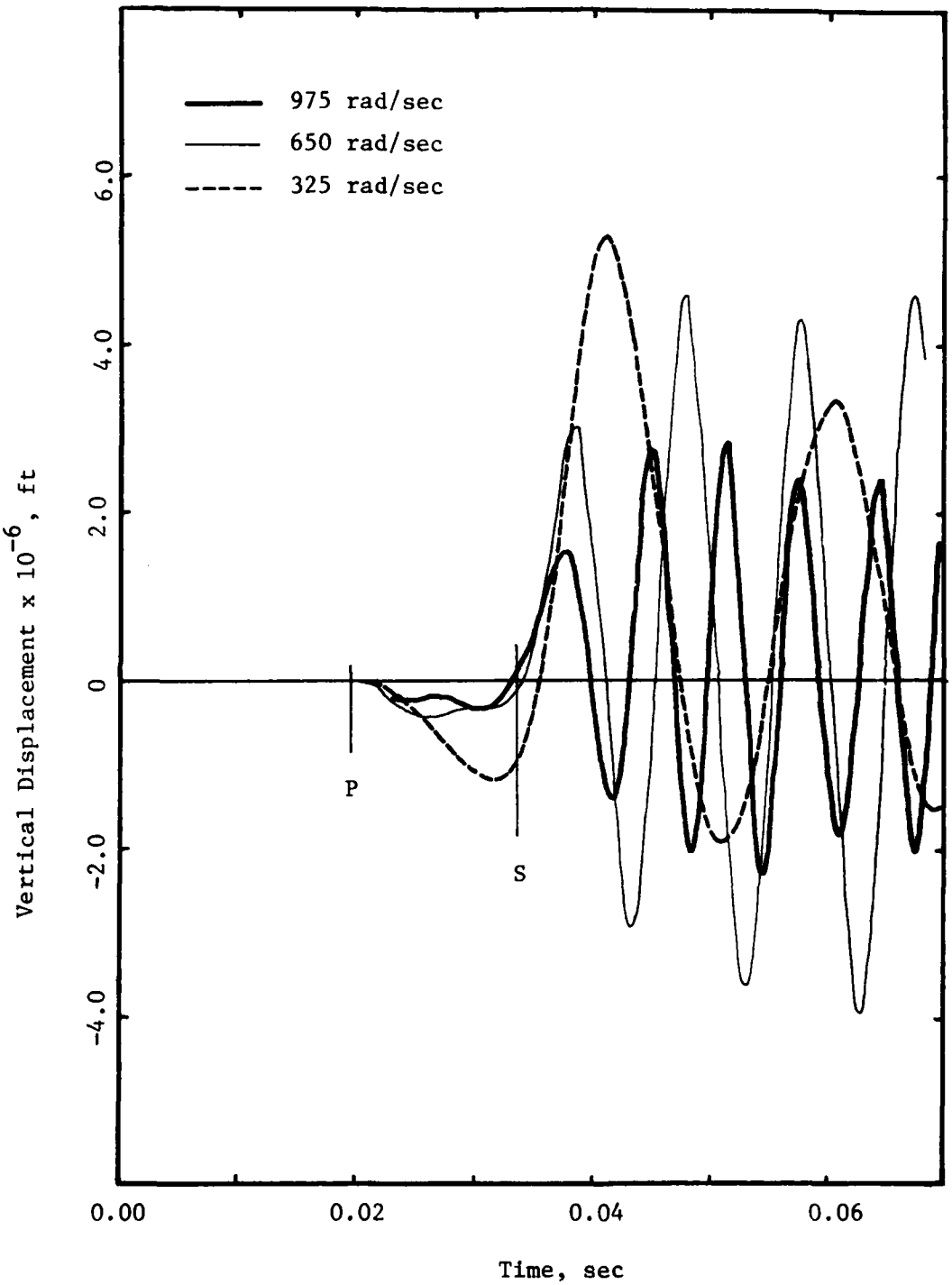

Fig. 4.3 - Vertical Displacements at IX=28 for Different Frequencies of Excitation.

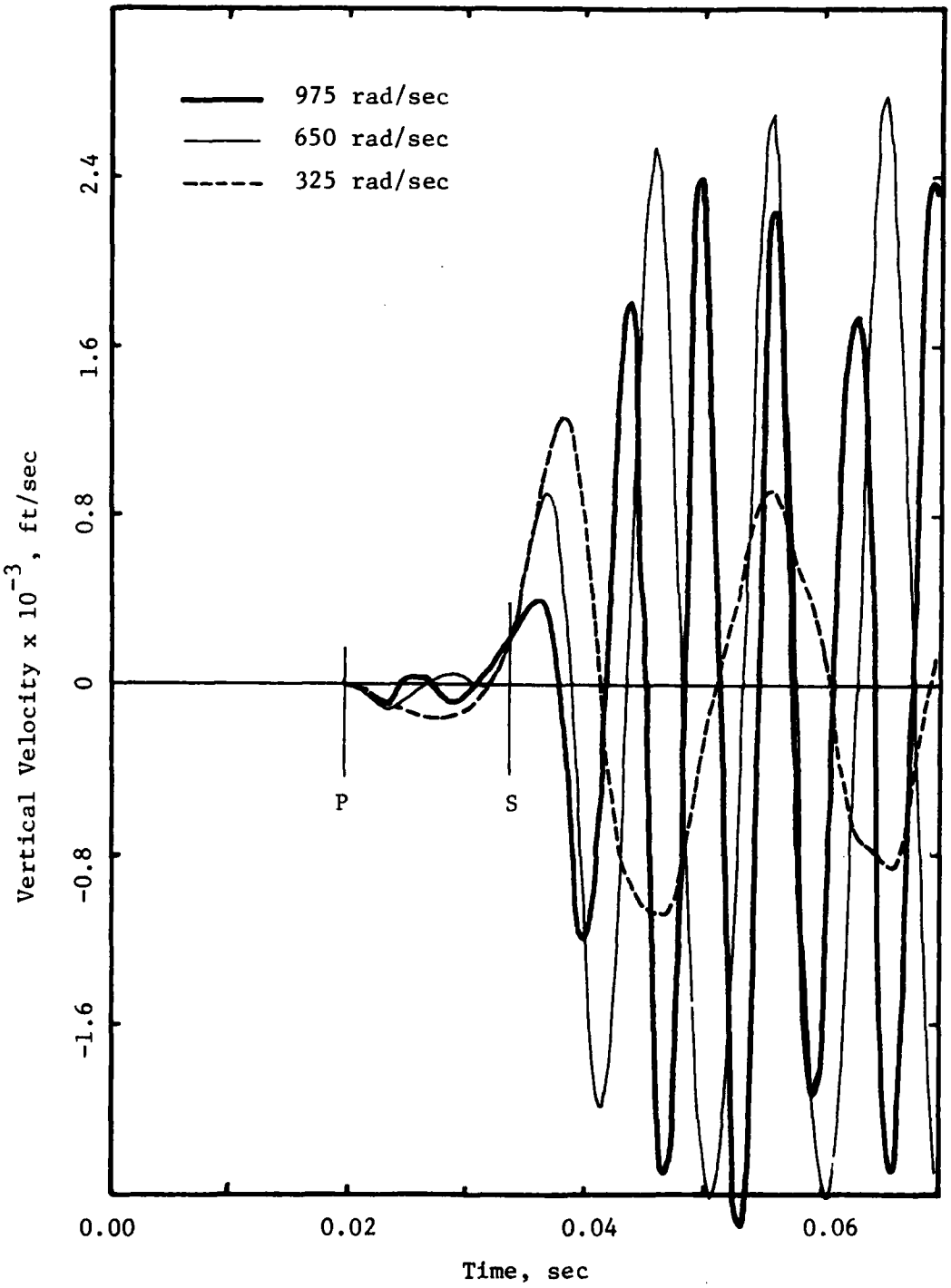

Fig. 4.4 - Vertical Velocities at IX=28 for Different Frequencies of Excitation.

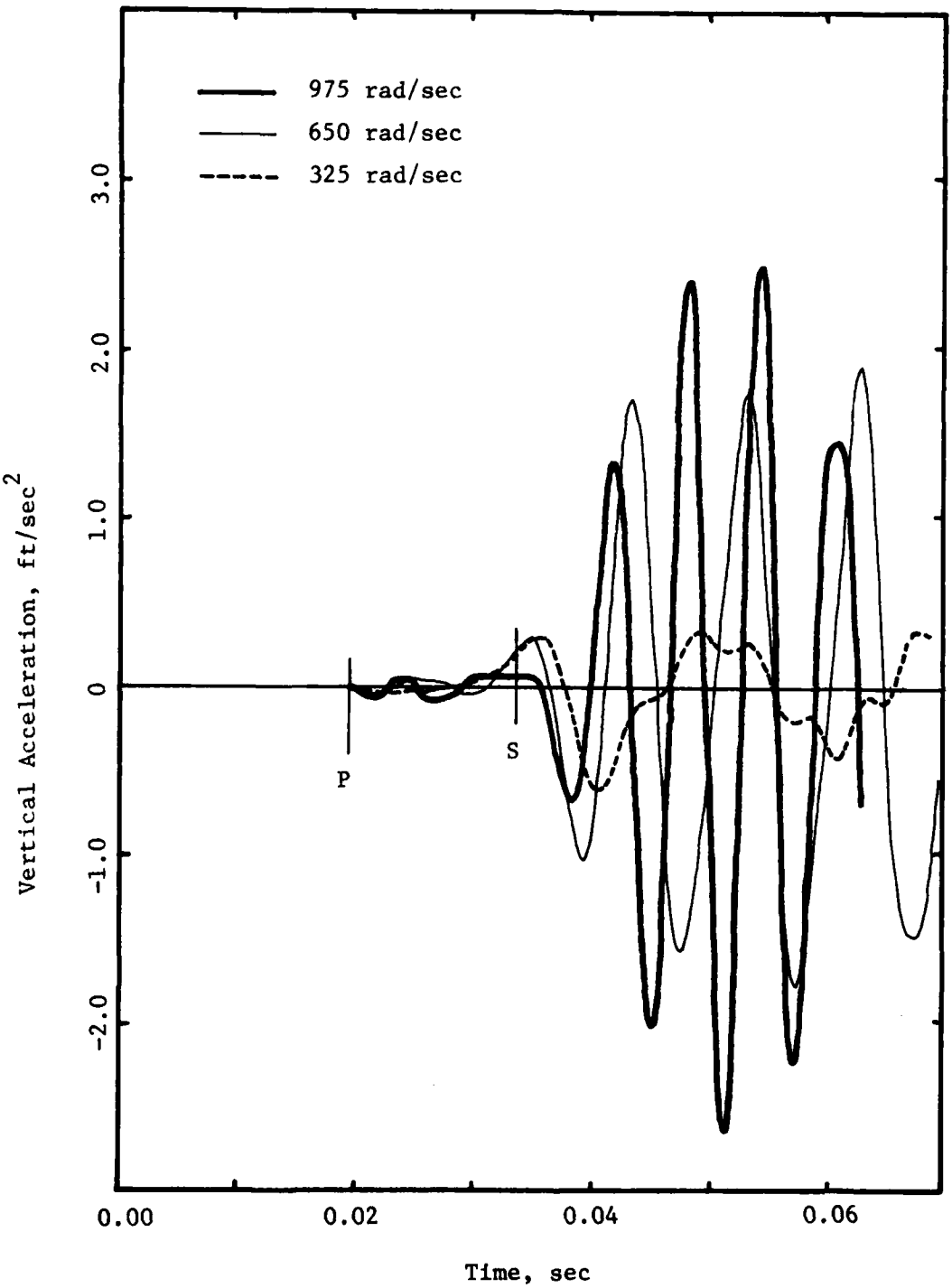

Fig. 4.5 - Vertical Accelerations at IX=28 for Different Frequencies of Excitation.

trace, and the low frequency the smallest. For the acceleration records the high frequency has the largest amplitude, followed by the normal and the low frequency. This is proper since the velocity for a steady state condition would be equal to the displacement multiplied by the circular frequency, while the acceleration would be the displacement multiplied by the square of the frequency. The acceleration trace for the low frequency at IX28 shows again higher frequency components.

The theoretical time of arrival of the S-wave coincides almost exactly with the zero crossing point of the displacement curve for the high frequency, is only slightly ahead of this point for the normal frequency and is further ahead for the low frequency. The estimate of the shear wave velocity based on the zero crossing point would be about five percent too small for the low frequency. This shift to the right of the curves with decreasing frequency is also apparent in the velocity and acceleration curves. The finite element model and the integration scheme would seem to result in a dispersive solution, with the measured shear wave velocity being a function of the frequency of excitation, if the velocity were determined from the estimate of the initial arrival.

To explore further this matter Figs. 4.6 to 4.8 show the corresponding results at the third target point, IX42. The sift in the curves is still apparent, but the theoretical time of arrival of the S-wave is now in between the zero crossing points for the high- (and normal) and low-frequency records. The shear wave velocity estimated from the displacement curves (Fig. 4.6) would be about three percent too

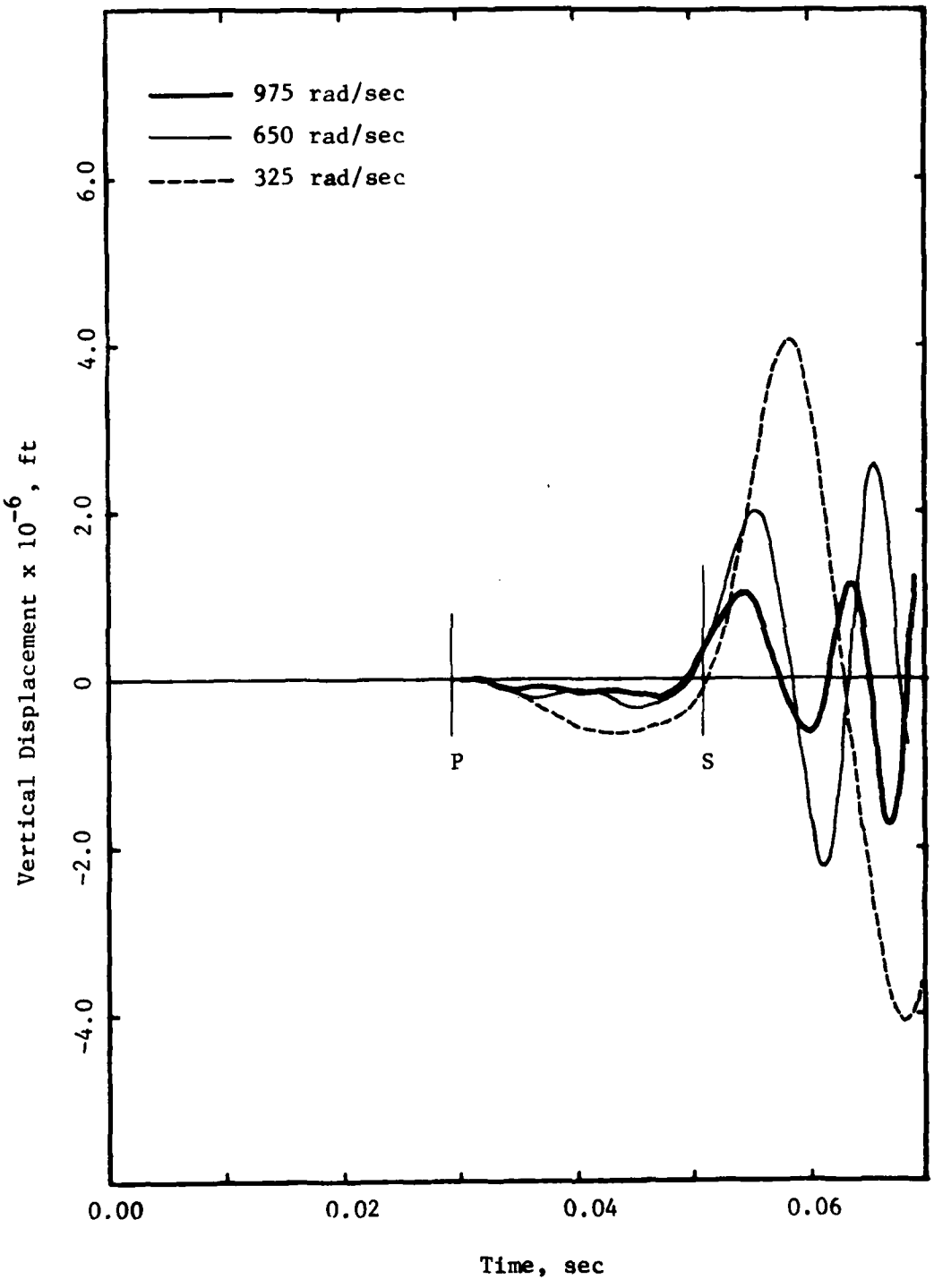

Fig. 4.6 - Vertical Displacements at IX=42 for Different Frequencies of Excitation.

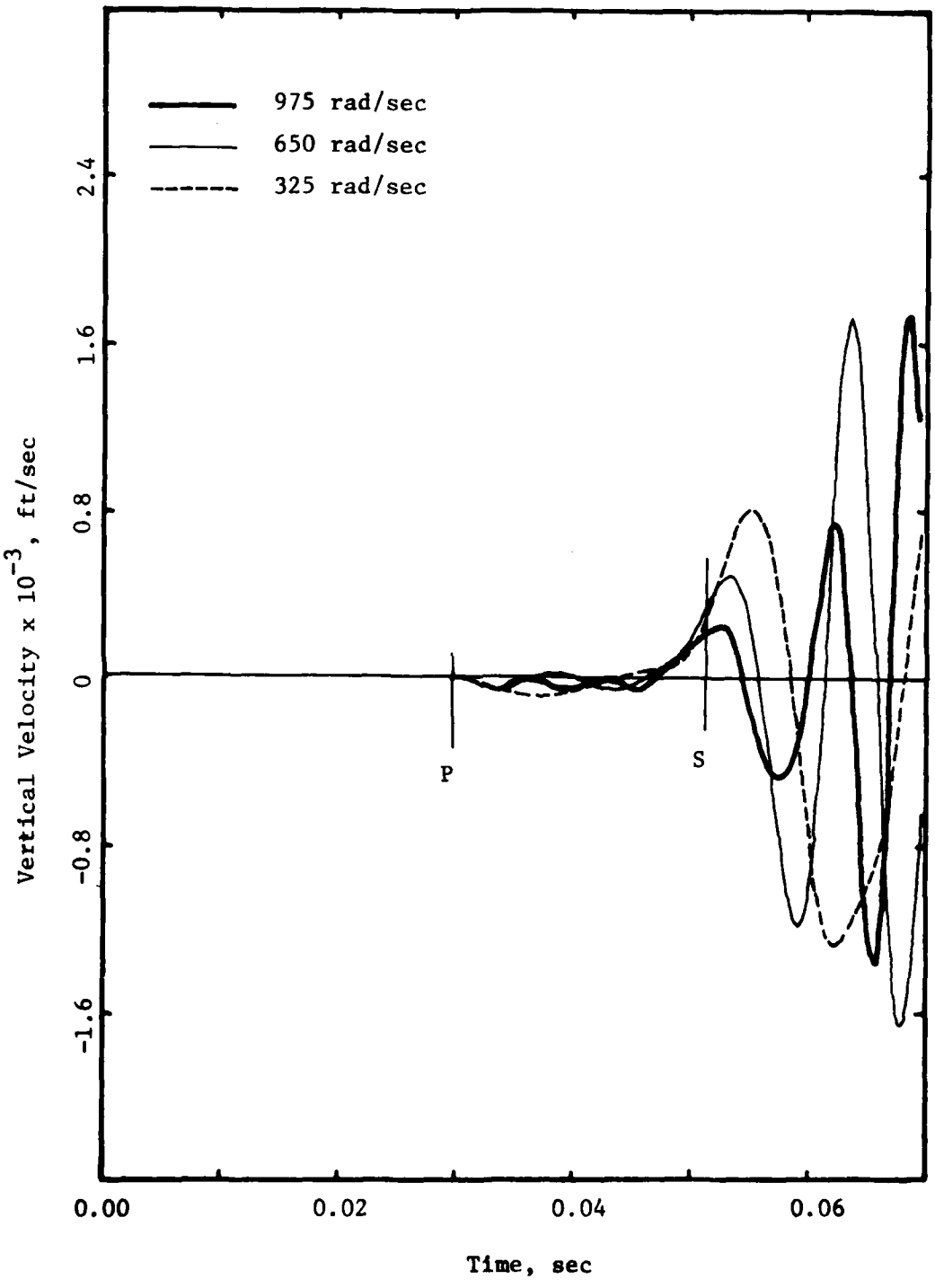

Fig. 4.7 - Vertical Velocities at IX=42 for Different Frequencies of Excitation.

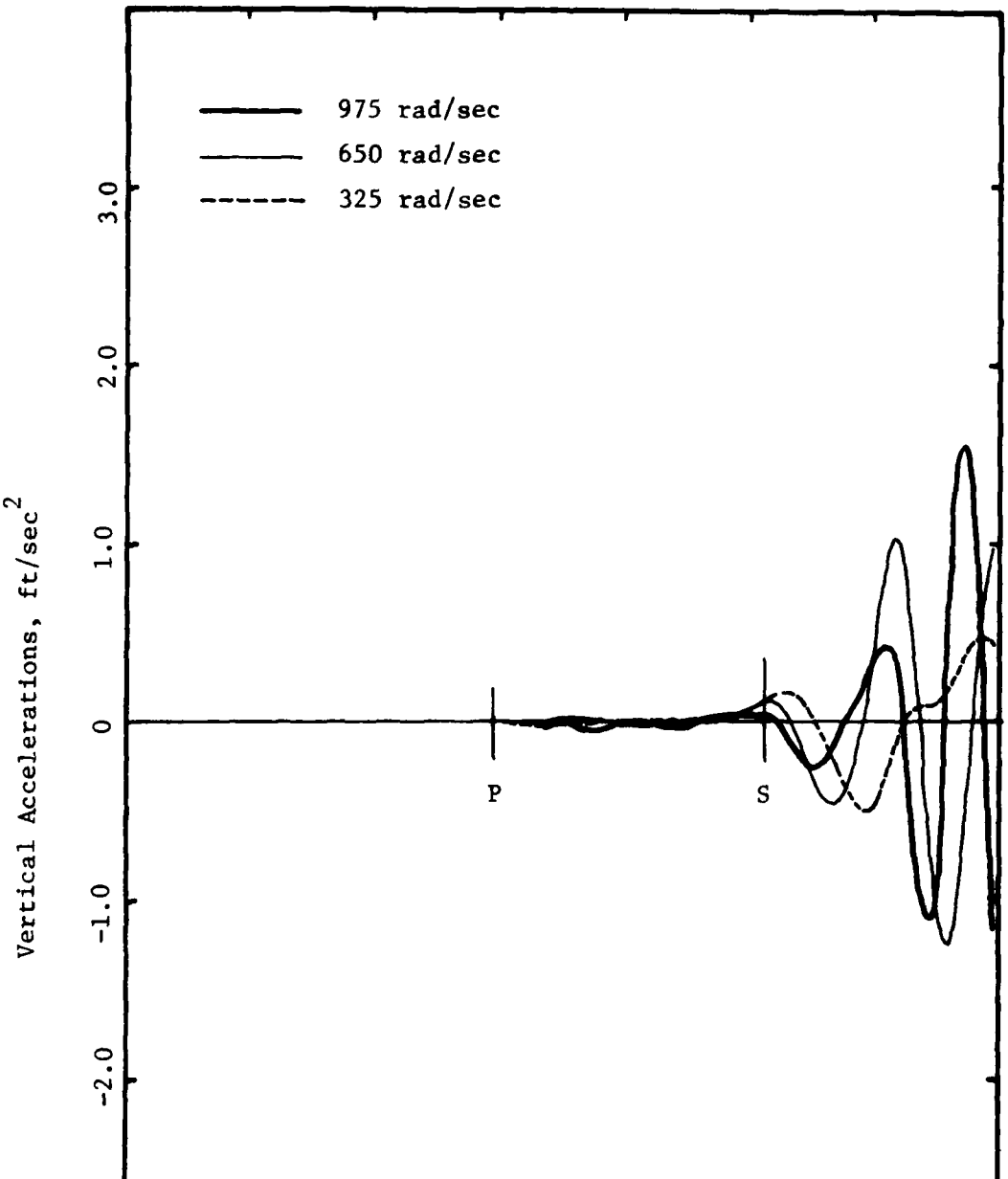

Fig. 4.8 - Vertical Accelerations at IX=42 for Different Frequencies of Excitation.

large for the high and normal frequency and about one percent (or less) too small for the low frequency. The same would be basically true for the velocity curves using the inflection point on the ascending branch to estimate the time of arrival. With the acceleration curve, using the first peak for the arrival time, determination is difficult for the high frequency excitation because the peak is not well defined. For the normal frequency the shear wave velocity would be underestimated by less than one percent, and for the low frequency it would be underestimated by about three percent.

Thus, while the shift in the curves with decreasing frequency occurs at all points for displacement, velocity and acceleration, whether it results in an underestimation of the shear wave velocity at low frequencies or an overestimation at high frequencies depends on the target point and the particular curve. For the range of frequencies considered, which is similar to the range of interest in the experimental work, the errors are, however, of the order of five percent or less.

Figures 4.9 to 4.11 illustrate the detemrination of the shear wave velocity using interval times for the high-frequency excitation and Figs 4.12 to 4.14 for the low-frequency case. Using the first peaks produces again better results than using the second. For the displacement curves and the high frequency, estimates of the wave velocity are 97.2 and 102.9 ft/sec (first to second target points and second to third target points, respectively), with an average of almost exactly 100 ft/sec. For the low frequency the corresponding values are 104.8 and 101.2 ft/sec, with an average of 103 ft/sec. Notice that this trend is opposite to

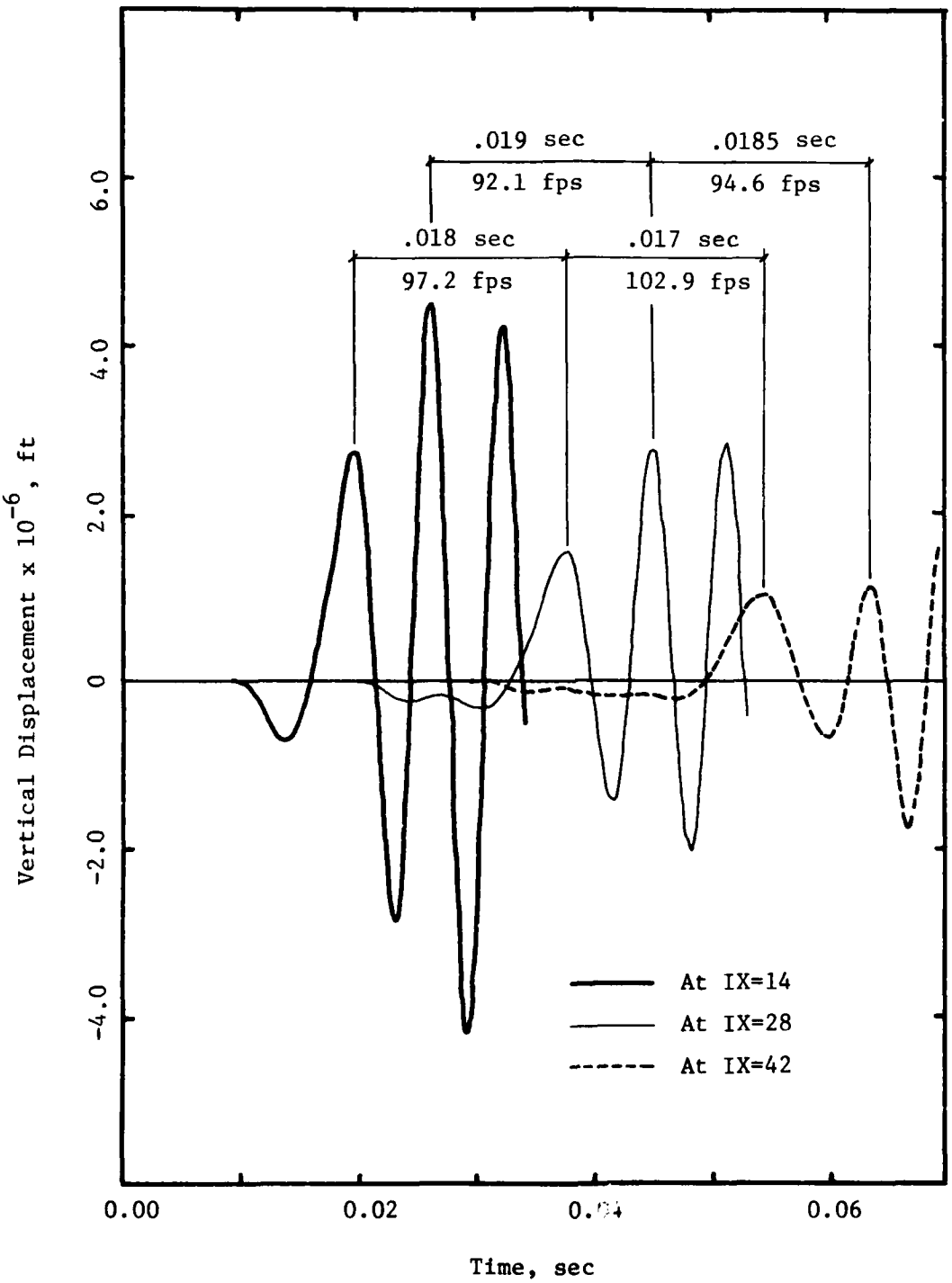

Fig. 4.9 - Inter-arrival Times and Corresponding Shear Wave Velocities from Displacement Curves. Free Boundaries. No Rigid Inclusions. High Frequency.

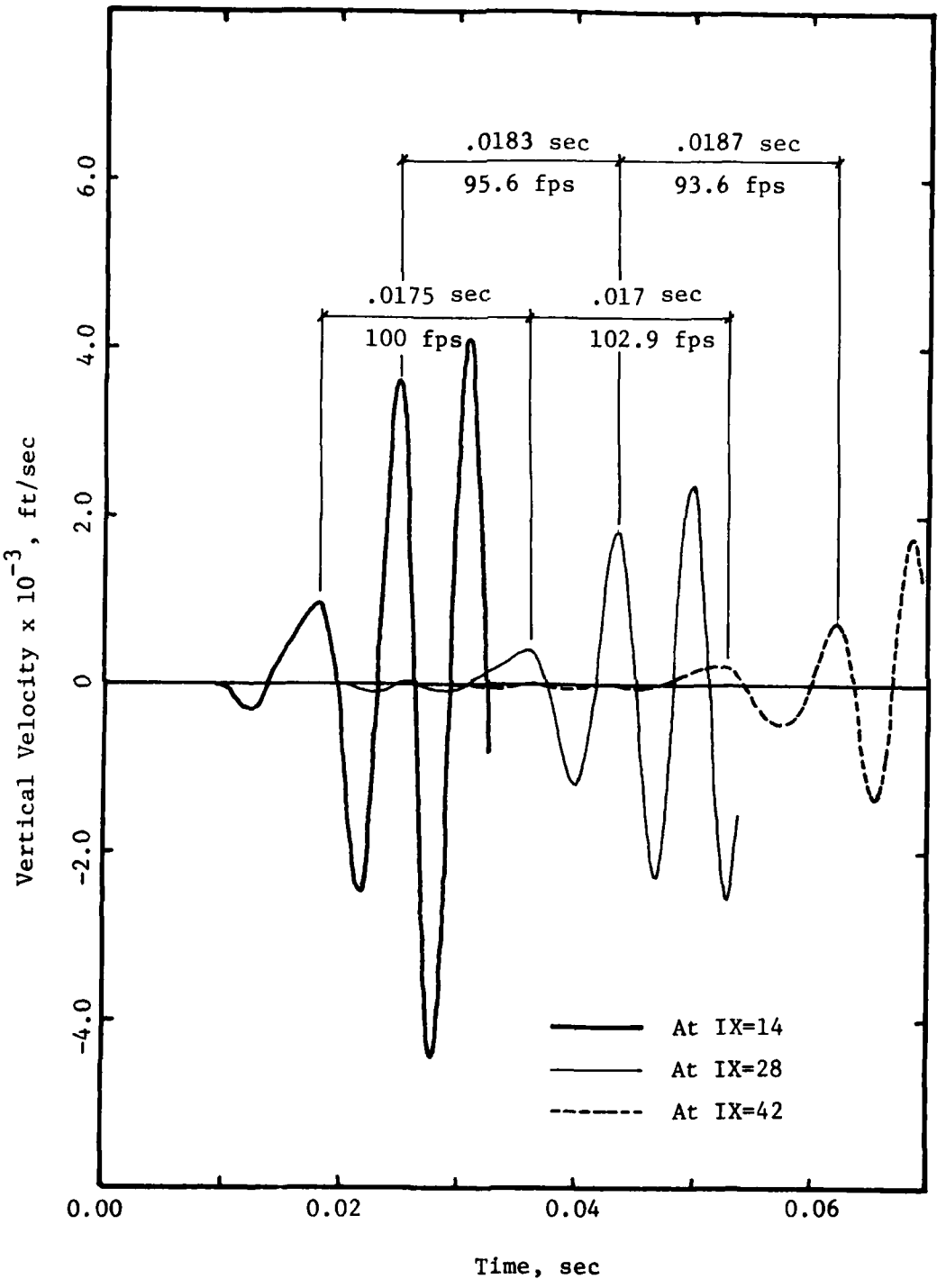

Fig. 4.10 - Inter-arrival Times and Corresponding Shear Wave Velocities from Velocity Curves. Free Boundaries. No Rigid Inclusions. High Frequency.

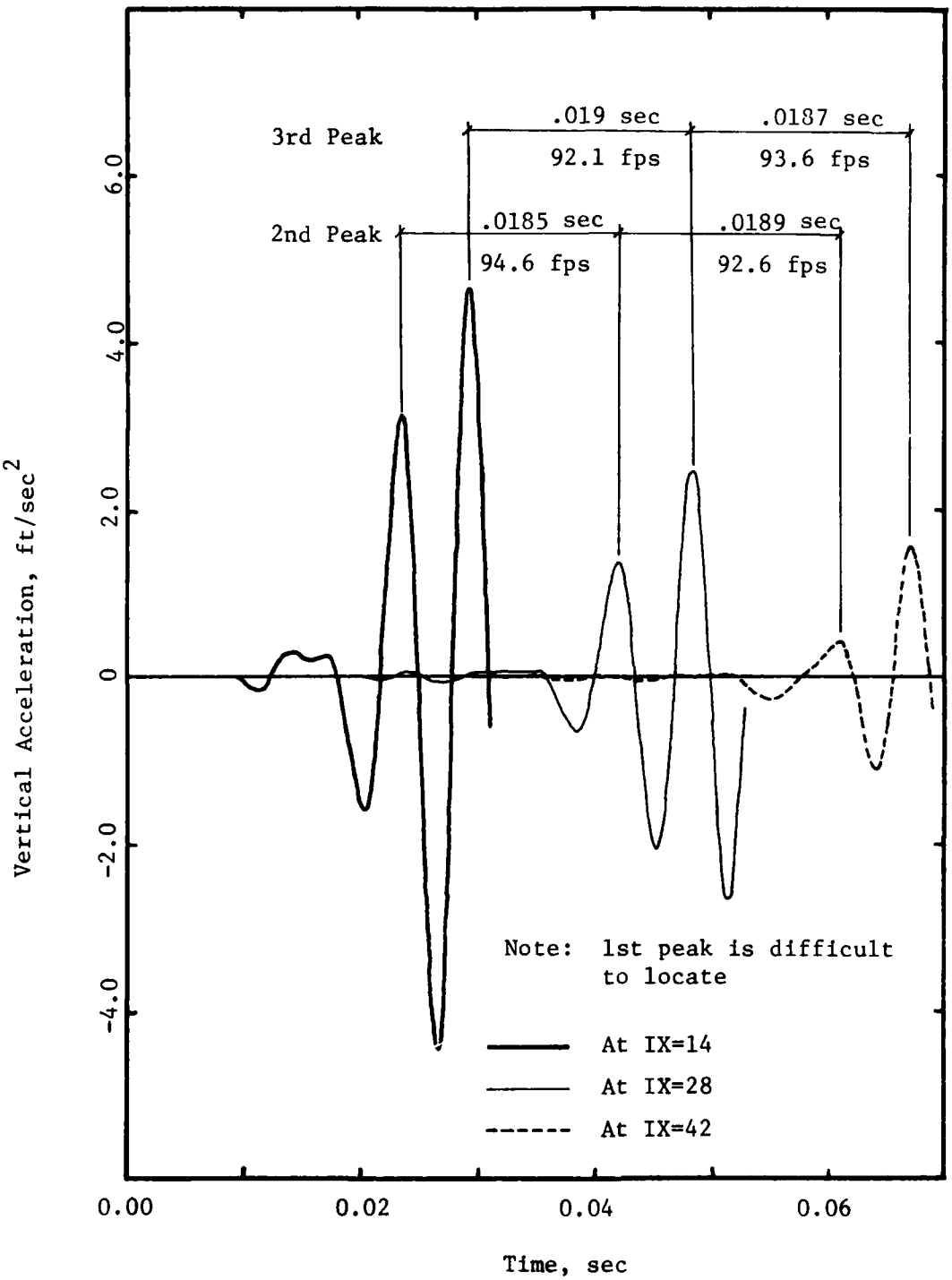

Fig. 4.11 - Inter-arrival Times and Corresponding Shear Wave Velocities from Acceleration Curves. Free Boundaries. No Rigid Inclusions. High Frequency.

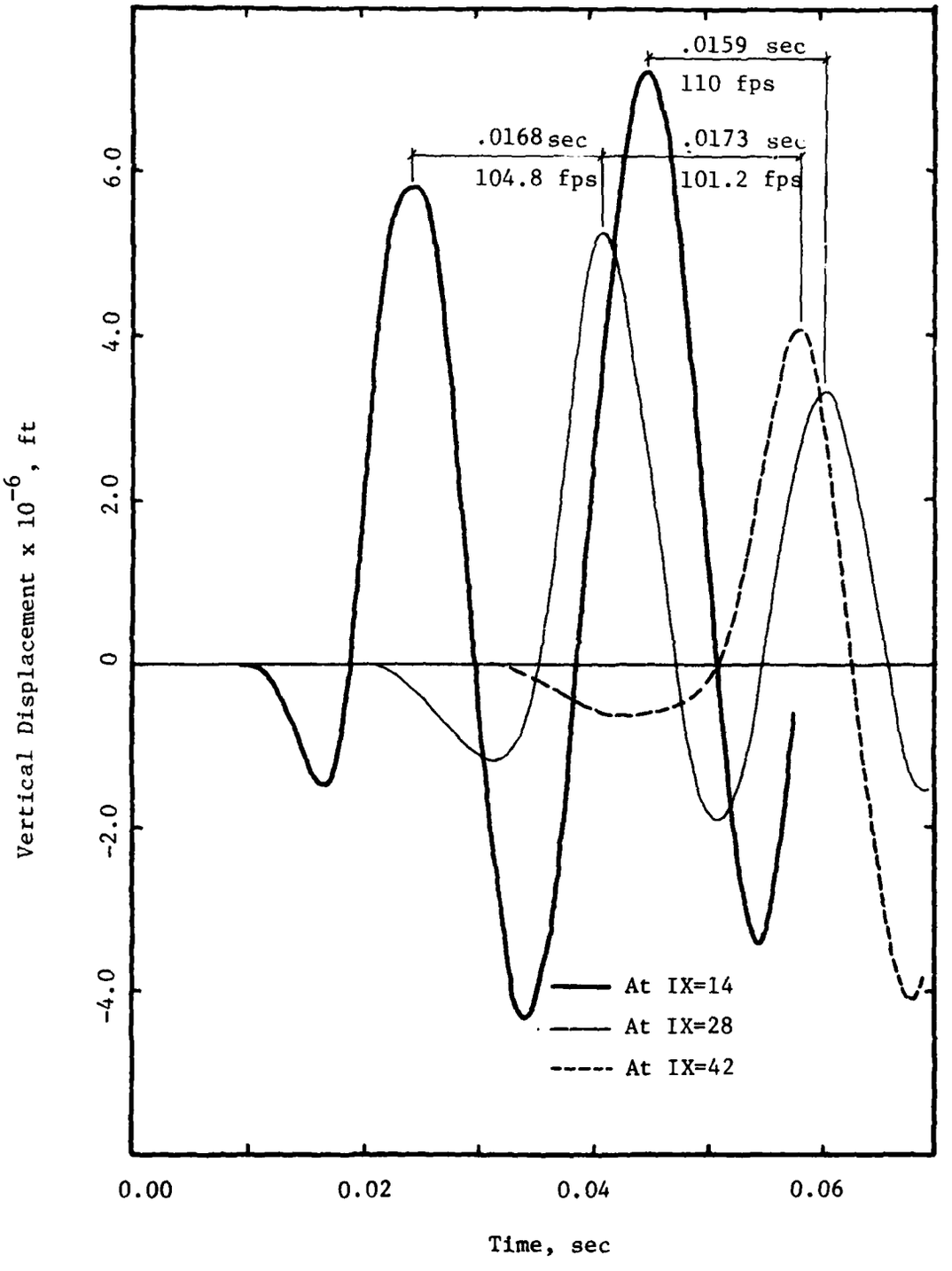

Fig. 4.12 - Inter-arrival Times and Corresponding Shear Wave Velocities from Displacement Curves. Free Boundaries. No Rigid Inclusions. Low Frequency.

AD-A131 366 EFFECTS OF RIGID INCLUSIONS ON WAVE PROPAGATION(U) 2/2
TEXAS UNIV AT AUSTIN GEOTECHNICAL ENGINEERING CENTER
C SUDDHIPRAKARN ET AL. MAR 83 GR83-3 AFOSR-TR-83-0656
UNCLASSIFIED AFOSR-80-0031 F/G 8/13 NL

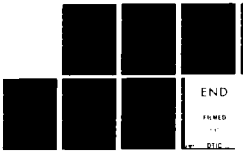

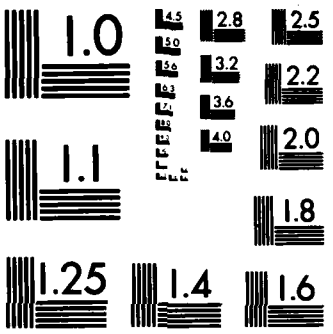

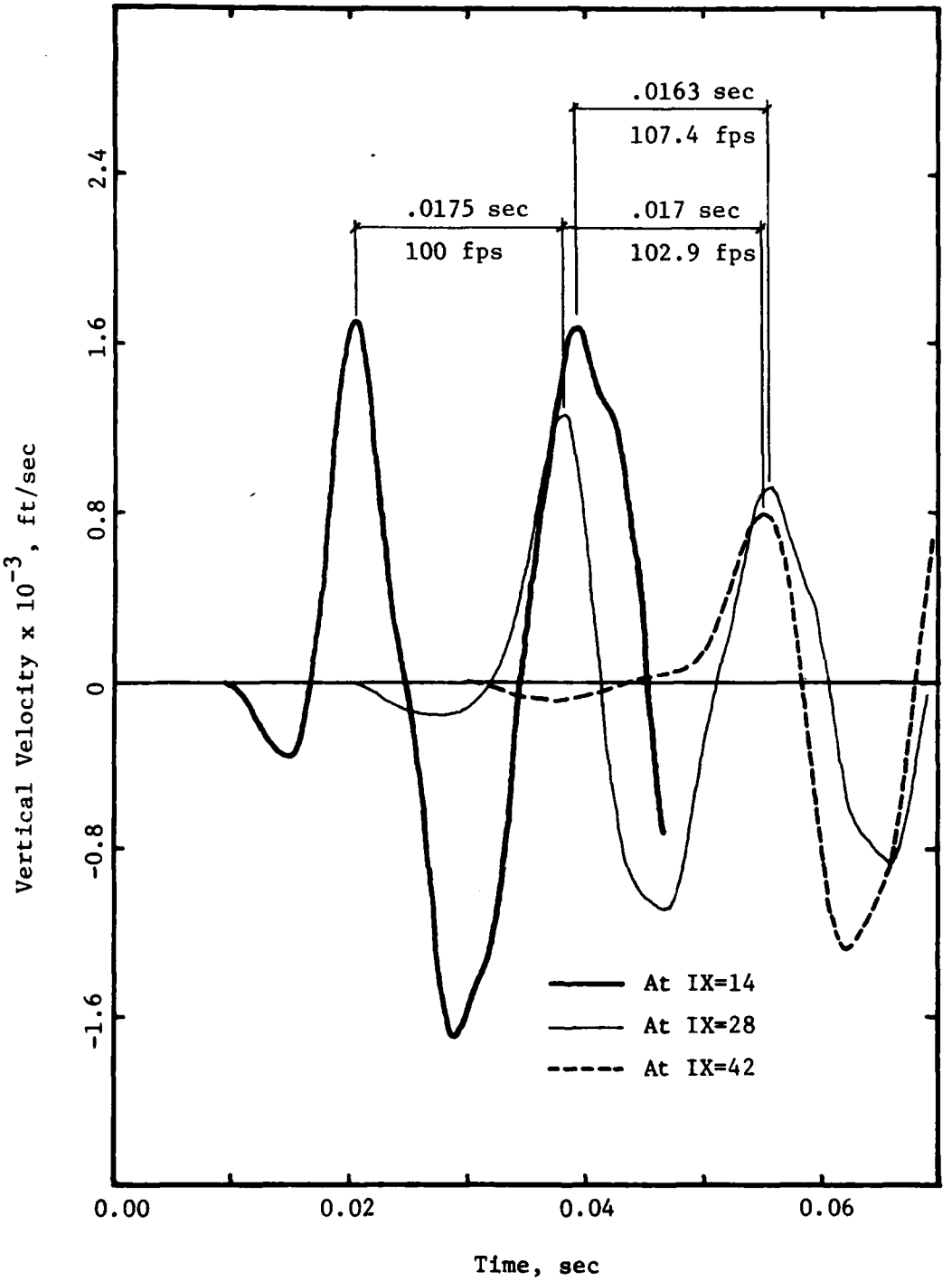

Fig. 4.13 - Inter-arrival Times and Corresponding Shear Wave Velocites from Velocity Curves. Free Boundaries. No Rigid Inclusions. Low Frequency.

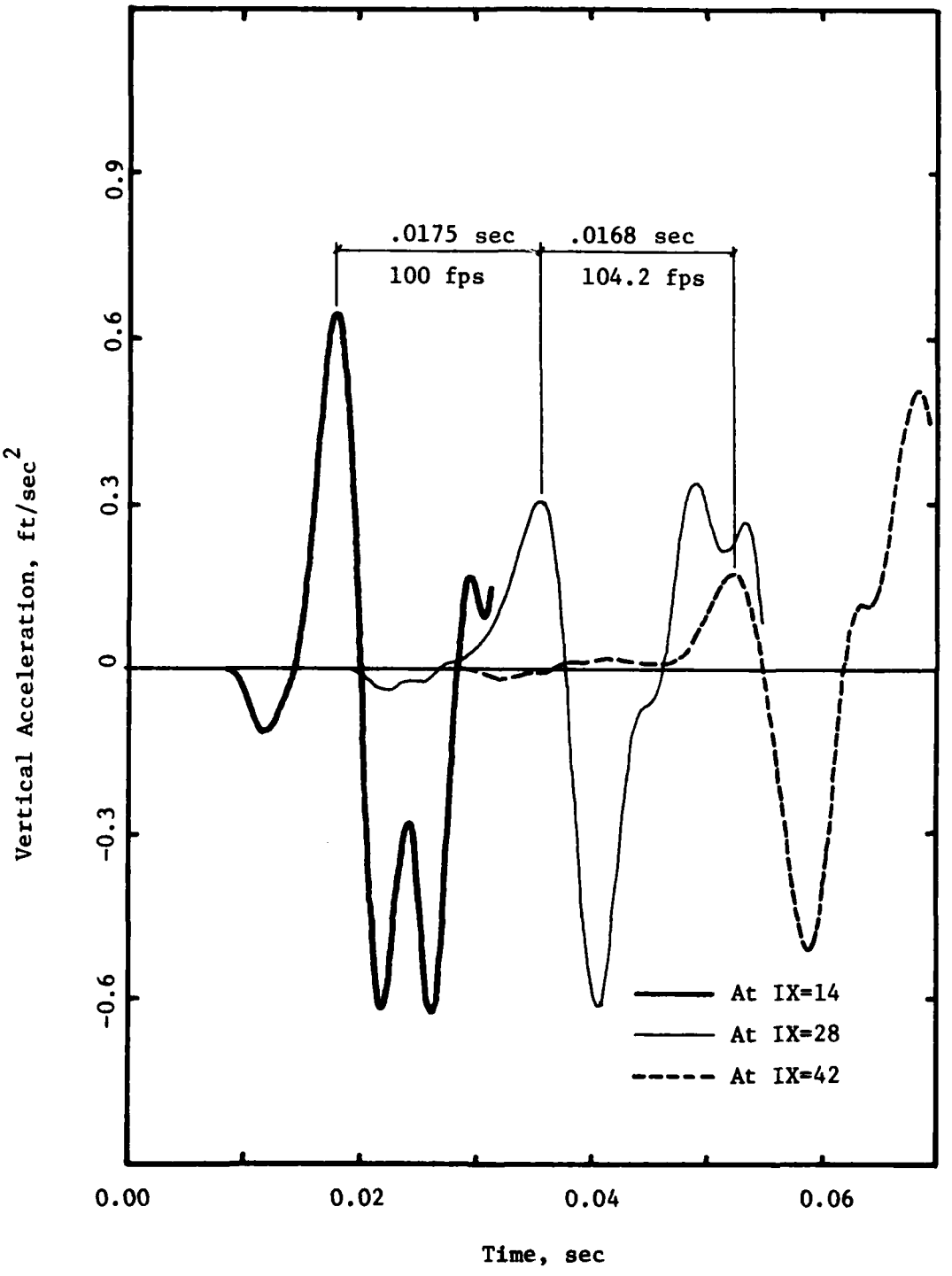

Fig. 4.14 - Inter-arrival Times and Corresponding Shear Wave Velocities from Acceleration Curves. Free Boundaries. No Rigid Inclusions. Low Frequency.

the one discussed above for first arrival times, where the results for the low frequency excitation would yield a slightly lower velocity. By using the velocity time histories, the estimates of wave velocity are 100 and 102.9 fts/ec (average of 101.5) for the high frequency, and the same for the low frequency. With the acceleration curves, no estimate can be obtained from the first peaks for high frequency because of their poor definition; for the low frequency the va ues are 100 and 104.2 ft/sec, with an average of 102.1 ft/sec.

4.3 EFFECT OF RIGID INCLUSIONS

Figures 4.15 to 4.17 compare the displacement, velocity and acceleration time histories at target point IX28 (left corner of the position of the cnetral inclusion) for the cases of no inclusions, one inclusion and three inclusions and the high-frequency excitation. Figures 4.18 to 4.20 show the corresponding results for the low-frequency case.

The presence of the inclusions produces again some very minor shifts in the curves, but the main effect is the filtering of the motion. The reduction in amplitude is significant for the high-frequency case and more pronounced than for the normal-frequency case (Figs. 2.34 to 2.39), as could be expected. It is very small for low-frequency excitation, although there is some smoothing of the high-frequency components in the acceleration trace.

The effect of the inclusions on the initial-arrival or interval travel times and on the estimates of the shear wave velocity is very small and independent of the frequency of the excitation (within the accuracy of

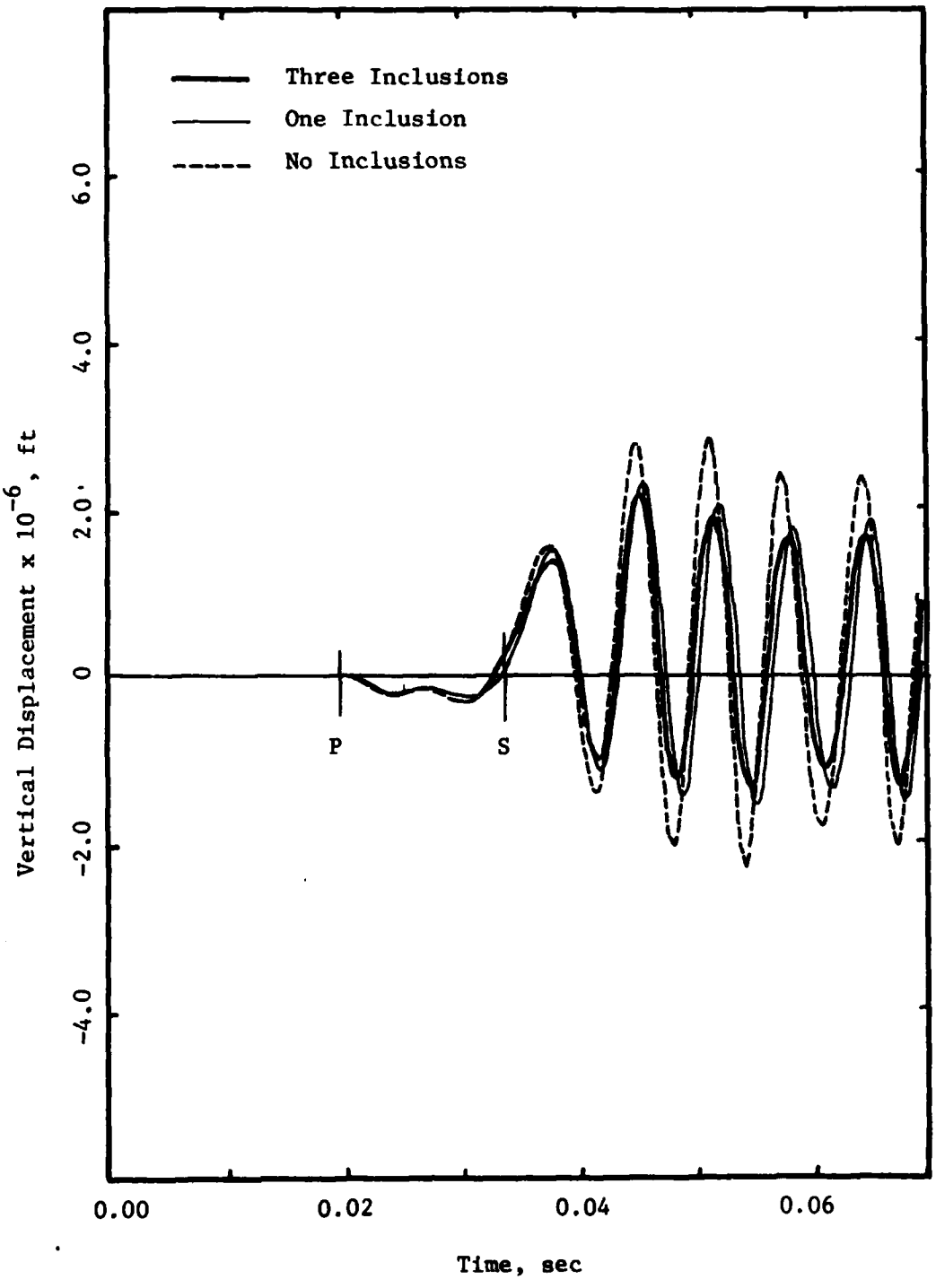

Fig. 4.15 - Free Field and Inclusion Displacements. Free Boundaries. High Frequency.

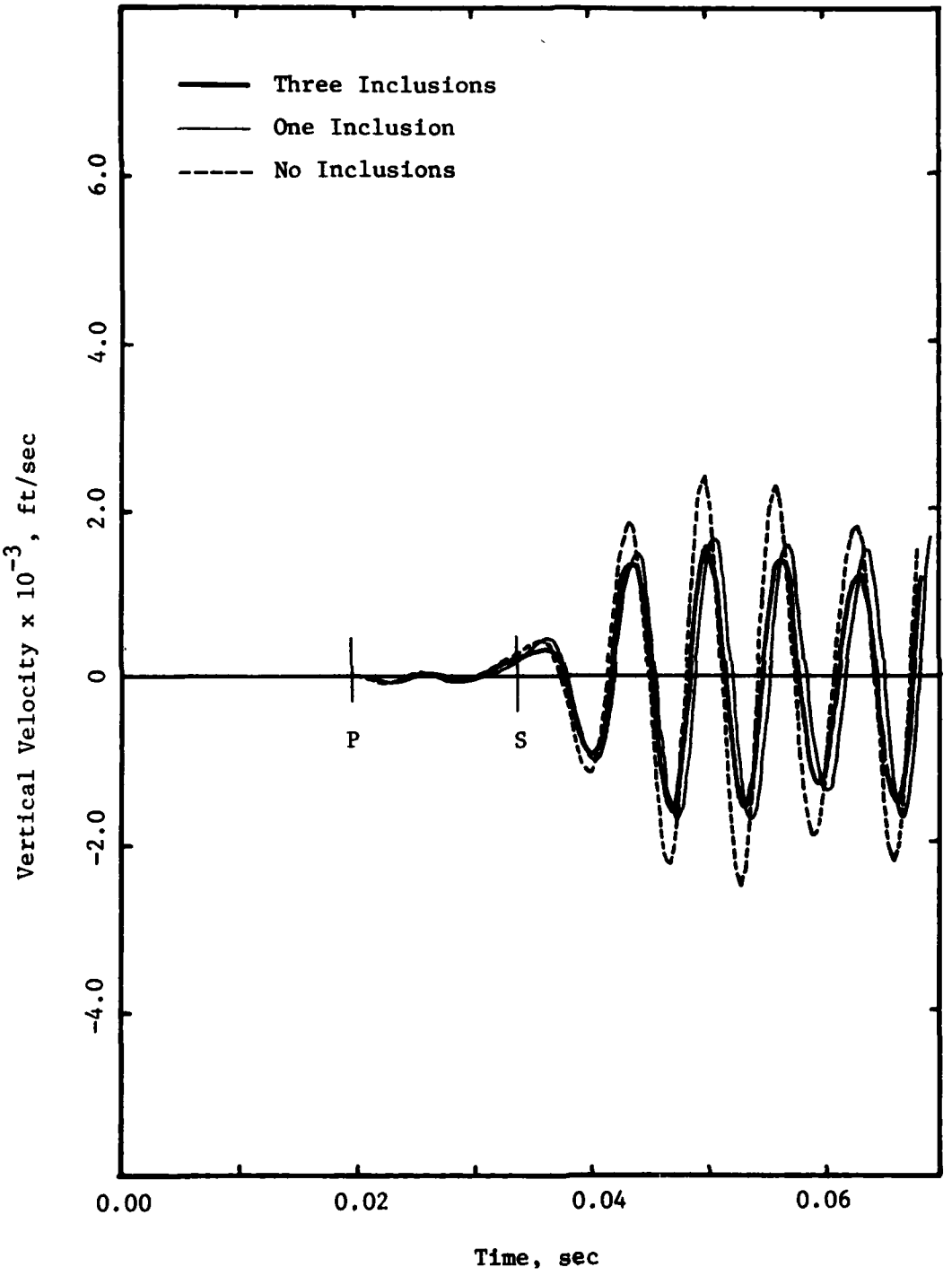

Fig. 4.16 - Free Field and Inclusion Velocities. Free Boundaries. High Frequency.

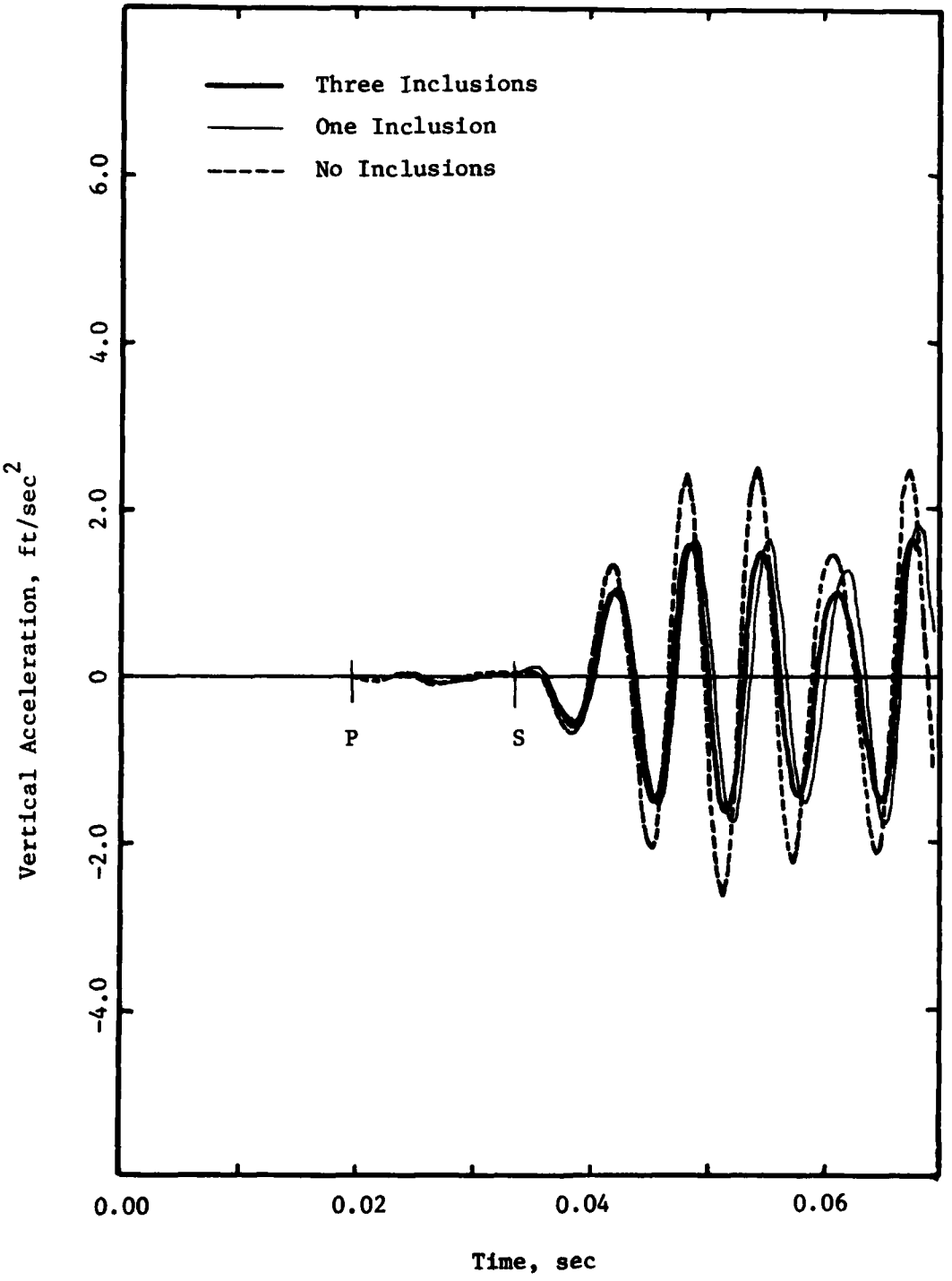

Fig. 4.17 - Free Field and Inclusion Accelerations. Free Boundaries. High Frequency.

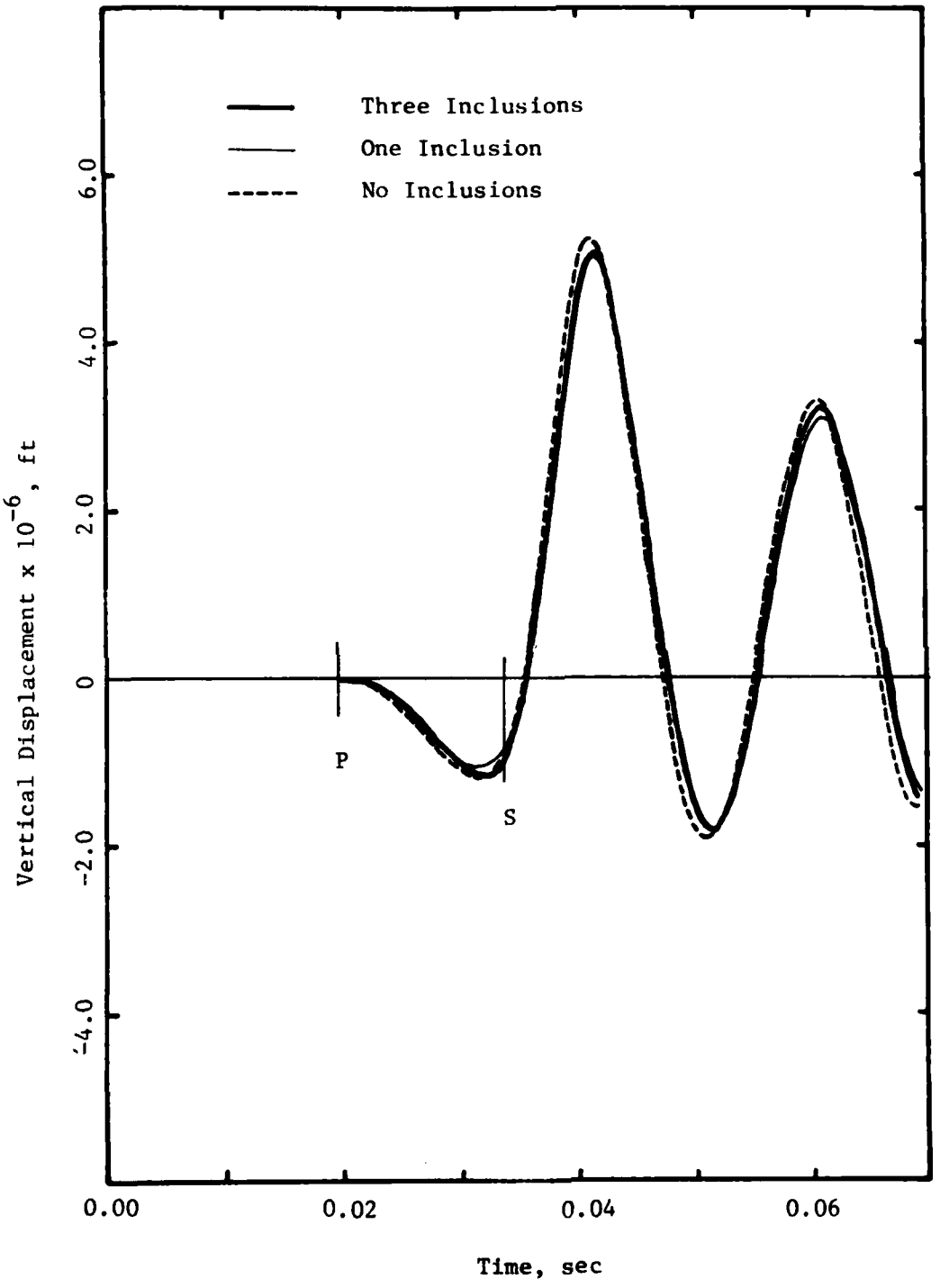

Fig. 4.18 - Free Field and Inclusion Displacements. Free Boundaries. Low Frequency.

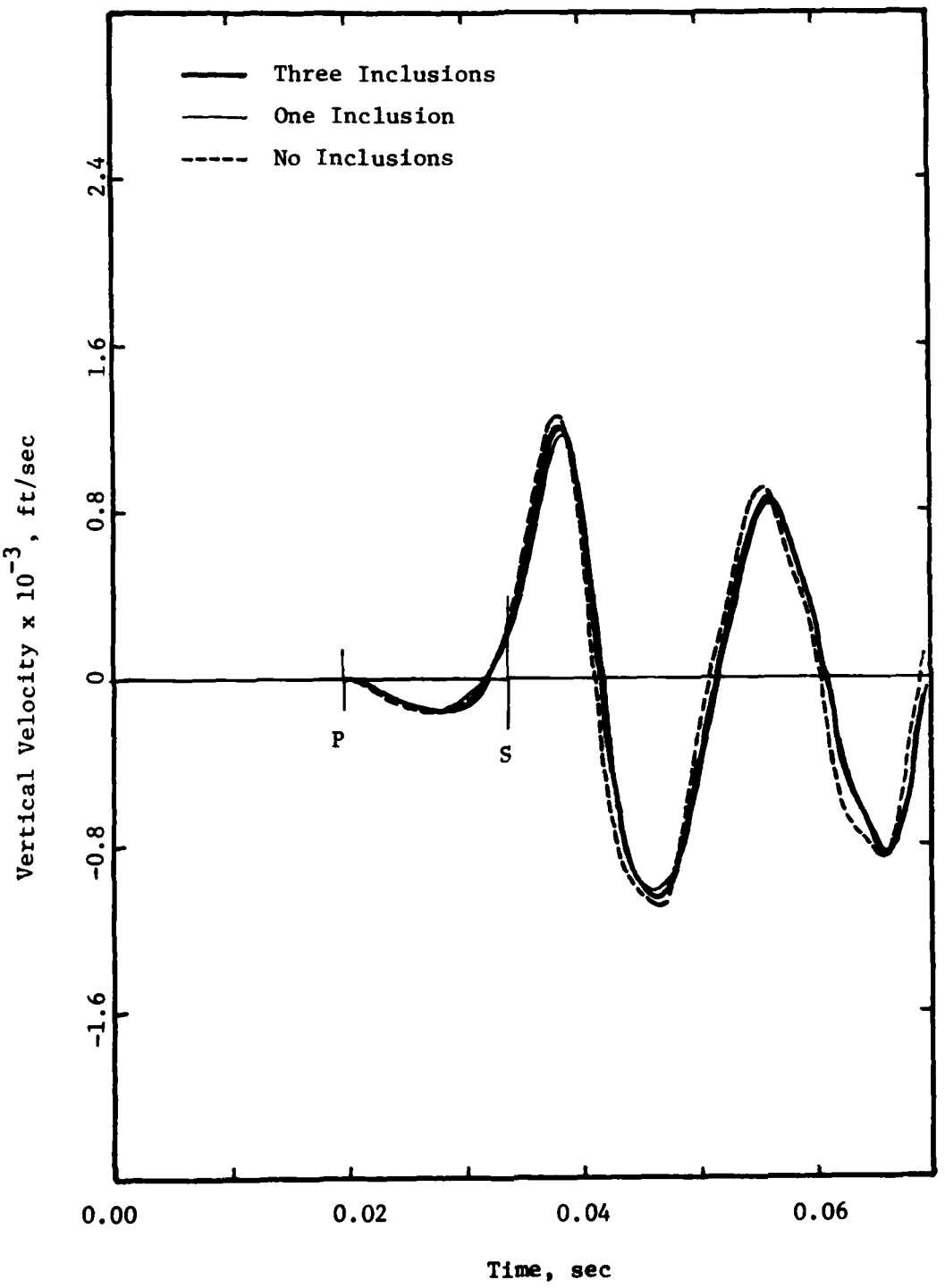

Fig. 4.19 - Free Field and Inclusion Velocities. Free Boundaries. Low Frequency.

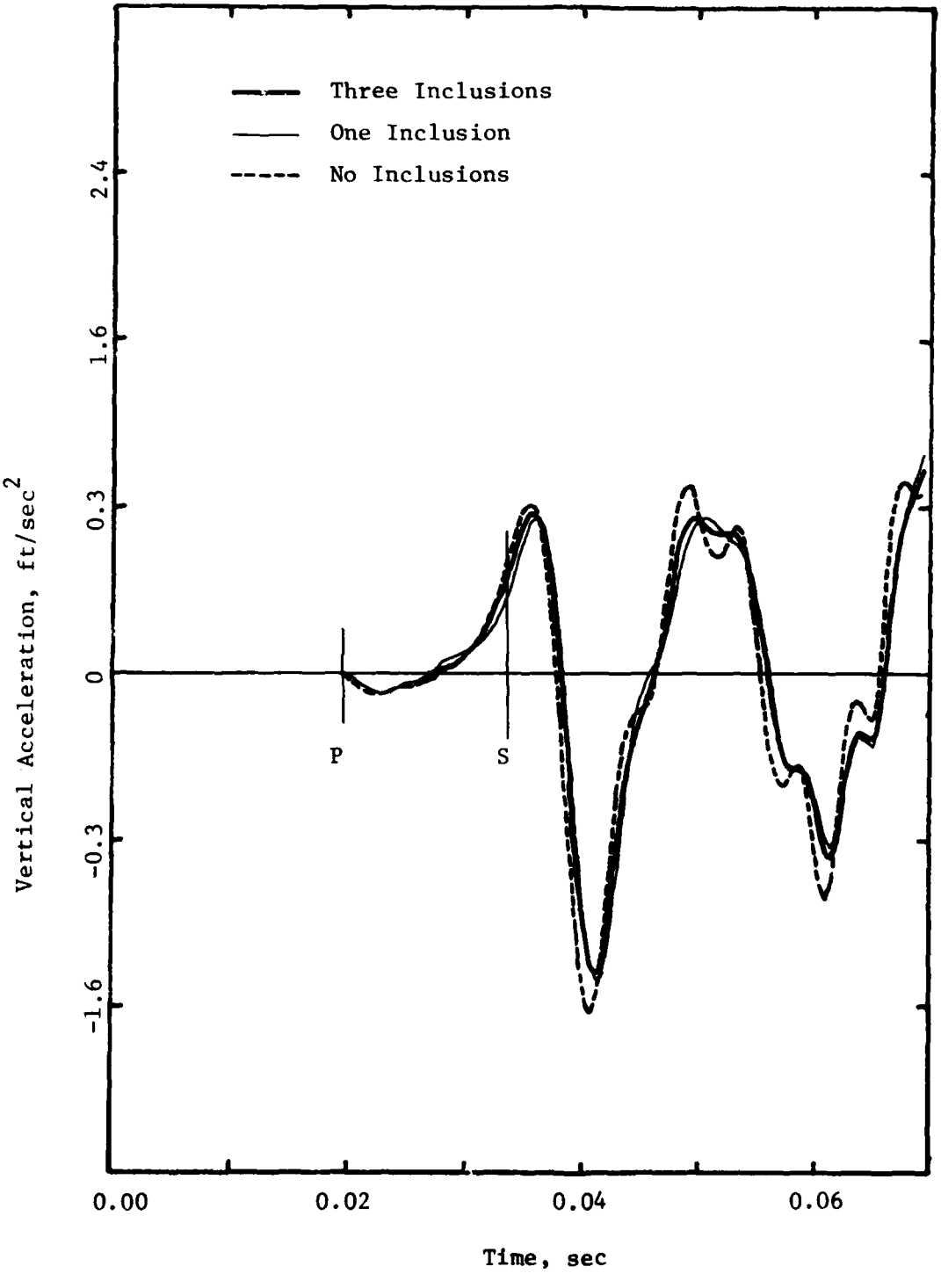

Fig. 4.20 - Free Field and Inclusion Accelerations. Free Boundaries. Low Frequency.

these estimates and for the range of parameters studied). The reduction in the amplitude of the waves increases, as expected, as the wavelength decreases and approaches the size of the inclusion, but this is not of importance for the studies conducted with the cube.

CHAPTER 5

CONCLUSIONS

The studies presented in this report were conducted to assess further the ability of a finite element model with an explicit integration scheme to reproduce the propagation of waves in a soil cube due to a harmonic excitation applied over a small area on one of the faces. Of particular interest was the study of the effect of the boundary conditions applied on the faces of the cube, the type of excitation, and the excitation frequency or wavelength, on the shape of the waves, their times of arrival and on estimates of wave velocity obtained form the results. Due to the cost of computation the analyses were performed with a two-dimensional, instead of a fully three-dimensional, model. It is believed, however, that the basic conclusions derived from these studies are applicable to both cases.

The results presented in the previous chapters indicate that:

1. When dealing with a shear type excitation applied over a small area, which could almost be considered a point load, the corresponding motions at various target points will start at the theoretical time of arrival of the P-wave and not at the arrival time of the S-wave. This early motion is more significant when the target point is relatively close to the point of excitation and tends to flatten out as the distance increases. When the excitation is a uniformly distributed force, simulating more closely a plane wave front, this early motion does not occur, and motion starts only slightly ahead of the theoretical time. This arrival time can be predicted very well by rounding the first half of the wave.

2. When dealing with a compressional type excitation applied over a small area, the above problem no longer exists, but the motion still starts slightly ahead of the thoeretical time.

3. For a point type excitation, if wave propagation velocity is to be estimated from the time of arrival of the first wave, selection of the arrival point depends on the type of trace used, displacement, velocity or acceleration. The arrival point should be selected as the zero crossing point or the starting point of the first wave for the displacement curve, the inflection point on the ascending branch of this wave for the velocity record, and a point close to the peak of this wave (and perhaps slightly before the peak) for the acceleration trace. The displacement time-history curve is the smoothest one and seems to provide the easiest reference point. The velocity curve is also useful, but the acceleration record may not have the first peak well defined, particularly for high frequencies.

4. Determination of the wave propagation velocity from the interval travel times between target points is somewhat easier and more reliable than from the first arrival. Taking three target points and averaging the values resulting from the travel times between the targets seems to provide the best results.

5. Boundary conditions applied on the faces of the model affect the shape and patterns of the waves but has only a small influence on arrival times. The motions for free boundary conditions lag slightly behind those obtained with fixed boundaries. This implies that if the wave propagation velocites are estimated from the first arrival time they would be somewhat smaller (about five percent) for the free boundary

model. On the other hand the velocities estimated from interarrival times are slightly larger with free boundary conditions.

6. As the frequency of the excitation decreases, within the range of frequencies studied, the arrival of the first wave seems to be delayed. Wave velocities determined from the first arrival time would decrease slightly with decreasing frequency (increasing wavelength). As in item 5 the opposite is true when measuring interval travel times.

7. The presence of rigid inclusions of the dimensions considered herein (one sixteenth to one fifth of the wavelength, at a distance equal to fourteen times their size) has only a very minor effect on the first-arrival and interval times. Estimated shear wave velocites with and without inclusions change by less than one percent. The inclusions smooth slightly the motions (particularly the acceleration traces) and reduce the amplitudes. This reduction is negligible for a wavelength sixteen times the inclusion size, small for half this wavelength and more significant when the wavelength is only five times the size of the inclusion.

8. While the numerical solution has some errors it appears that for the range of parameters studied, with some care, shear wave (or P-wave) velocities could be predicted from the results of the analyses within five percent. This should be sufficient accuracy for most practical applications.

It was intended in all these studies to simulate the wave patterns that would be generated inside the cube during the experimental work. This is the reason for the finite domain, the size and position of the inclusions and the range of frequencies used for the excitation. The

more general area of wave propagation in a nonhomogeneous medium, or a medium with inclusions of different properties (as might be an alluvial deposit), is one that has received relatively little attention and which deserves further research. By considering a full space, and thus eliminating the effect of the boundary conditions, the accuracy of the finite element solution can be better evaluated by comparing the results to those obtained with the boundary element (or boundary integral equation) method. The effects of size, position and properties of the inclusions for a more extensive range of frequencies should then be investigated.

REFERENCES

1. Knox, D.P., Stokoe, K.H., II, and Kopperman, S.E. (1982), "Effect of State of Stress on Velocity of Low-Amplitude Shear Waves Propagating along Principal Stress Directions in Dry Sand," Research Report GR82-23, Department of Civil Engineering, University of Texas at Austin.

2. Kopperman, S.E., Stokoe, K.H., II, and Knox, D.P. (1982), "Effect of State of Stress on Velocity of Low-Amplitude Compression Waves Propagating along Principal Stress Directions in Dry Sand," Research Report GR82-22, Department of Civil Engineering, University of Texas at Austin.

3. Stokoe, K.H., II, et al (1980), "Development of a Large-Scale Triaxial Testing Device for Wave Propagation Studies," Research Report GR80-10, Department of Civil Engineering, University of Texas at Austin.

No Rigid Inclusions. Low Frequency.

END

FILMED

9-83

DTIC